كلية العلوم و التقنيات فاس
ⵜⴰⵖⵉⵡⴰⵏⵜ ⵏ ⵜⵎⴰⵙⵙⴰⵏⵉⵏ ⴷ ⵜⵙⵏⵉⴳⵉⵜⵉⵏ
Faculté des Sciences et Techniques de Fès

جامعة سيدي محمد بن عبد الله
ⵜⴰⵙⴷⴰⵡⵉⵜ ⵙⵉⴷⵉ ⵎⵓⵃⵎⵎⴰⴷ ⴱⵏ ⵄⴱⴷⵓⵍⵍⴰⵀ
Université Sidi Mohamed Ben Abdellah

Centre d'Etudes Doctorales : Sciences et Techniques de l'Ingénieur

N° d'ordre : 60/2022

THESE DE DOCTORAT

Présentée par

Mr. Abdelilah CHALH

Spécialité : Génie électrique / Systèmes embarqués.

Sujet de la thèse

« Optimisation de la puissance soutirée d'un système photovoltaïque sous l'effet de l'ombre par un système embarqué »

Thèse présentée et soutenue le 01/10/2022 devant le jury composé de :

Nom Prénom	Titre	Etablissement	
Pr. MOSTAFA MRABTI	PES	Ecole Nationale des Sciences Appliquées de Fès	Président
Pr. HAJJI BEKKAY	PES	Ecole Nationale des Sciences Appliquées Oujda	Rapporteur
Pr. RACHID SAADANI	PES	Ecole Supérieure de Technologie de Meknès	Rapporteur
Pr. NAJIA ES-SBAI	PES	Faculté des Sciences et Techniques de Fès	Rapporteur
Pr. Amine ALLOUHI	PH	Ecole Supérieure de Technologie de Fès	Examinateur
Pr. Abdelaziz EL GHZIZAL Pr. Aziz DEROUICH	PES PES	Ecole Supérieure de Technologie de Fès Ecole Supérieure de Technologie de Fès	Directeurs de thèse

Laboratoire d'accueil : Technologies Innovantes.

Etablissement : Ecole Supérieure de Technologie de Fès.

كلية العلوم و التقنيات فاس
ⵜⴰⵖⵉⵡⴰⵏⵜ ⵏ ⵜⵎⴰⵙⵙⴰⵏⵉⵏ ⴷ ⵜⵙⵏⵉⴳⵉⵜⵉⵏ
Faculté des Sciences et Techniques de Fès

جامعة سيدي محمد بن عبد الله
ⵜⴰⵙⴷⴰⵡⵉⵜ ⵙⵉⴷⵉ ⵎⵓⵃⵎⵎⴰⴷ ⴱⵏ ⵄⴱⴷⵓⵍⵍⴰⵀ
Université Sidi Mohamed Ben Abdellah

Centre d'Etudes Doctorales : Sciences et Techniques de l'Ingénieur

DOCTORAL THESIS

Presented by

Abdelilah CHALH
ORCID ID: 0000-0002-8578-7732

With a view to obtaining the doctoral diploma
Specialty: **Electrical engineering / Embedded systems**

Topic
« Optimization of power withdrawn from PV system under partial shading conditions using an embedded system »

Copyright by
Abdelilah CHALH
2022

To my beloved parents

for their enduring love,

motivation and support.

ACKNOWLEDGEMENT

Alhamdulillah, I am greatly indebted to Allah SWT for His mercy and blessing for making this research successful.

I would like to take this opportunity to express my deepest gratitude and thanks to my project supervisors, Prof. Abdelaziz El ghzizal and Prof. Aziz Derouich for their constant guidance, assistance and support as well as all the knowledge they shared during the course of this research.

Mr. Mostafa MRABTI, professor of the National High School of Applied Sciences, for accepting to be the president of the reading committee of my thesis.

The rest of the reading committee members: Mr. HAJJI BEKKAY, Mr. RACHID SAADANI, Mrs. NAJIA ES-SBAI and Mr. Amine ALLOUHI for their helpful comments and their valuable suggestions.

Mr. Mustapaha IJJAALI the Dean of the Faculty of Sciences and Techniques of Fez and Mr. El Mestafa EL HADRAMI, the Director of Doctoral Studies Centre "Science and Engineering Techniques" for their efforts in ensuring the accomplishment of the these presentation in the best conditions.

I sincerely thank all the professors who have taught me, for the lesson that has been delivered. Not to mention, to my researchers friends, especially Mr. Saad Motahhir, Dr. Aboubakr El Hammoumi, Mr. Youssef Laaraj and Dr. Redouane chaibi thank you for helping me in my research, sharing useful ideas, information and moral support during the course of study.

To my closer friends, especially Hdioud Mohammed, Nhili Mohammed, Salah Eddine Farhanne and Othmane El-Morabit, I express my gratitude for their unconditional friendship, support and patience throughout these years.

Last but not least I would like to express my appreciation and gratitude to my parents Rkia and Abdeletif, sisters and Brother Mohammed and my entire family for all the supports and encouragements they provide during my studies.

ABSTRACT

Partial shading is one of the main factors that significantly affect the maximum power that can be harvested from a PV array. Indeed, partial shading decreases the efficiency of the PV array and causes multiple local peaks in its power-voltage characteristic, which makes tracking the maximum power point (MPP) more difficult. The objective of this thesis is to contribute to the improvement of the performance of PV arrays, by optimizing the energy extracted from PV arrays operating under the effect of partial shading.

First, a simple method to track the global maximum power point (GMPP) under the partial shading conditions (PSCs) of the PV system is proposed in this thesis. This method scans the P–V curve and memorizes all the peaks to get the global peak which is the GMPP. This method takes a long processing time, because this scan is started from the point of the short-circuit current (I_{CC}) to the open-circuit voltage (V_{OC}) of the P-V characteristic. Hence, this technique interrupts the system operation when scanning the entire control range between the V_{OC} and I_{CC}, which yields power losses. Therefore, an improved scanning method is also proposed in this thesis to reduce and limit the scan interval, which eliminates the passage through the short-circuit point of the P-V characteristics. In addition, it avoided the open-circuit of the PV string during the scan interval to prevent disconnection of the PV system. All these modifications allow this method to track the GMPP with good response time and high efficiency under dynamic PSCs. The improved scanning method is simulated using a proposed PV simulator designed under Proteus software. The obtained results show that the improved scanning method efficiently tracks the GMPP under different PSCs and has a good response time (1.4 s), which improves the response time of the PV system by 0.55 s compared to the conventional scanning method.

On the other hand, if cost minimization is not more important than ensuring a very high level of robustness and efficiency of our PV system, a powerful method is required. Therefore, this thesis introduces a novel SOA-based metaheuristic MPPT method to track the GMPP to maximize PV power generation in PV systems operating under both uniform and PSCs. This method is considered best suitable for real engineering problems compared to another metaheuristic algorithm. The obtained results clearly highlight the superiority of the proposed method; it gives an efficiency of 98.85%, which is almost 1.05% higher than the PSO-MPPT method.

Finally, a Processor In the Loop (PIL)" test is done to validate the efficiency of the proposed SOA-MPPT. It should be mentioned that the PIL is tested using the MKRZERO board. Therefore, the PIL test can be used as a low-cost option to test the hardware implementation of the MPPT algorithm.

Key words: PV array, Proteus, Scanning method, Partial shading, MKRZERO board, low-cost PV system, SOA based MPPT, PV simulator, PIL.

RÉSUMÉ

L'ombrage partiel est l'un des facteurs de l'environnement affectant considérablement la puissance maximale obtenue à partir d'un champ photovoltaïque. En effet, l'ombrage partiel réduit l'efficacité du champ photovoltaïque (PV) et provoque de multiples pics locaux dans la caractéristique Puissance-tension du champ, rendant ainsi difficile le suivi du point maximum de puissance. Face à cette difficulté, il est nécessaire de procéder à des solutions permettant de mieux extraire la puissance produite par un générateur PV. L'objectif des travaux présentés dans cette thèse s'inscrit pleinement dans cette optique. En effet, il consiste à améliorer les performances des panneaux photovoltaïques, en contribuant à l'optimisation de l'énergie soutirée des panneaux photovoltaïques fonctionnant sous l'effet d'ombrage partiel.

Tout d'abord, une méthode simple pour suivre le point de puissance maximale globale (GMPP) du système PV sous des conditions d'ombrage partiel (PSCs) dynamiques a été proposée dans cette thèse. Cette méthode balaie la courbe P-V et mémorise tous les pics pour obtenir le pic global qui est le GMPP. Elle prend un long temps de traitement étant donné que ce balayage commence à partir du point du courant de court-circuit (I_{CC}) jusqu'à la tension de circuit ouvert (V_{OC}) de la caractéristique P-V. Par conséquent, cette technique interrompt le fonctionnement du système PV lors du balayage total de la plage de contrôle (entre la valeur de V_{OC} et I_{CC}), ce qui entraîne des pertes de puissance. À ce propos, une amélioration de la méthode de balayage a été également proposée dans cette thèse pour réduire et limiter l'intervalle de balayage, ce qui élimine le passage par le point de court-circuit des caractéristiques P-V. De plus, elle évite le circuit ouvert de la chaîne PV pendant le balayage afin de prévenir la déconnexion du système PV. Pour pallier à ces deux obstacles posés par les deux limites extrêmes de la courbe I-V, et pour un choix judicieux de la zone de balayage afin d'améliorer le temps de réponse du système, nous avons fait une étude basé sur la simulation de l'impact de différents scénarios d'ombrage partiel sur les caractéristiques des panneaux PV. Cette étude nous a permet le suivi du GMPP avec un bon temps de réponse et une efficacité élevée sous des PSCs dynamiques. De surcroît, la méthode de balayage améliorée a été simulée à l'aide d'un simulateur PV, conçu sous le logiciel Proteus. Ce simulateur PV peut être utilisé pour vérifier et évaluer les performances des algorithmes avec une approximation plus proche de la mise en œuvre réelle. Les résultats obtenus démontrent que la méthode de balayage améliorée suit efficacement le GMPP sous différents PSCs

avec un bon temps de réponse (1,4 s), ce qui améliore le temps de réponse du système PV de 0,55 s par rapport à la méthode de balayage conventionnelle.

Ensuite, cette thèse introduit une nouvelle commande MPPT basée sur une approche métaheuristique (l'algorithme d'optimisation des mouettes (SOA)) pour maximiser la production d'énergie des systèmes PV fonctionnant à des conditions d'ombrage partiel. Cette méthode est considérée comme une solution plus adaptée aux problèmes d'ingénierie réels par rapport à d'autres algorithmes métaheuristiques. La vitesse et l'efficacité du SOA-MPPT ont été considérablement améliorées. Les résultats obtenus mettent clairement en évidence la supériorité de la méthode proposée; elle donne une performance de 98,85%, dépassant celle de la méthode PSO-MPPT de presque 1,05%.

Enfin, un test (Processor In the Loop) a été réalisé avec la carte MKRZERO et Matlab/Simulink pour valider nos résultats de simulation.

Mots clés: Champ PV, Proteus, méthode de balayage, d'ombrage partiel, carte MKRZERO, système PV à faible coût, SOA-MPPT, simulateur PV, PSO, PIL.

TABLE OF CONTENTS

List of Figures 4
List of Tables 6
NOMENCLATURES 7
GREEK LETTERS 7
ABBREVIATIONS 7
Introduction 9
Chapter 1 Overview of the PV System and effect of partial shading on maximum power point 15
1. Introduction 16
2. An overview of PV solar energy: from material to use 16
2.1. Photovoltaic effect 16
2.2. PV technologies 17
2.3. Photovoltaic generator 18
2.3.1. PV cell and module modelling 18
2.3.2. Irradiance and cell temperature effect 21
2.3.3. Effect of partial shadow on maximum power point 23
2.3.4. Effect of shading and bypass diode impacts 23
2.3.4.1. Mathematical modeling 24
2.3.4.2. Hotspot problem 25
2.3.4.3. Bypass diode impacts 25
2.3.5. Effect of load on power Point operating 26
2.3.6. The adaptation stage between the PVG and Load 27
2.3.7. DC-DC Converter 27
2.3.7.1. Structure of boost converter 28
2.3.7.2. The operating of boost converter 28
2.3.7.3. Electrical circuit analysis 30
2.3.7.4. Inductor selection 33
2.3.7.5. Output capacitor selection 33
2.3.7.6. Input capacitor selection 34
2.3.8. Maximize the transfer of power from the PV panel to the load 34
3. Summary 35
Chapter 2 State of the art of the MPPT algorithms 36
1. Introduction 37
2. Maximum Power Point Tracking: Literature review 37
2.1. Group 1: Conventional Techniques 38
2.1.1. Perturb and observe (P&O) 38

2.1.2. Incremental Conductance (INC) 38
2.2. Group 2: MPPT based on PV model and PV characteristics 40
2.2.1. Fractional Open-Circuit Voltage (FOCV) 40
2.2.2. Fractional Short-Circuit Current (FSCC) 41
2.2.3. MPPT based curve fitting 41
2.3. Group 3: Soft computing Approach 42
2.3.1. Fuzzy Logic Control (FLC) 42
2.3.2. Artificial Neural Network (ANN) based MPPT 45
2.3.3. Metaheuristic approach (Evolutionary computation) 46
A. Particle Swarm Optimization based MPPT 46
B. Artificial Bee Colony (ABC) based MPPT 48
C. Whales Optimization Algorithm (WOA) based MPPT 50
D. Grey Wolf Optimization (GWO) based MPPT 52
E. Ant Colony Optimization (ACO) based MPPT 54
2.4. Group 4: Soft computing Approach 55
2.4.1. Hybrid DEPSO method 55
2.4.2. Artificial Bee Colony and P&O algorithm 55
2.4.3. Hybrid GWO and FLC method 55
3. Recapitulation 56
4. Summary 57
Chapter 3 Development of an improved GMPPT based on Scanning method for PV system operating under a dynamic partial shading conditio 59
1. Introduction 60
2. Investigation of partial shading conditions on a photovoltaic array's characteristics 61
3. Scanning method based MPPT 66
3.1. Classical scanning method 66
3.2. Improved scanning method 67
4. Development of First PV simulator : Using Proteus software environment 68
4.1. Description of the Entire PV System 69
4.2. Proteus PV panel model 69
4.3. PV system design in Proteus Software 71
5. Results and discussions 73
5.1. Tests under a dynamic partial shading conditions 75
5.2. Tests under a change of the solar irradiance value during the scanning loop 76
6. Summary 77
Chapter 4 Development of a Novel MPPT Design Based on the Seagull Optimization Algorithm for Photovoltaic Systems Operating Under Partial Shading 78
1. Introduction 79

2. Seagull optimization algorithm (SOA) 79
2.1. The basics of the SOA 79
2.2. Mathematical model of SOA 81
2.3. Application of SOA to the MPPT 83
3. Results and discussions 84
4. Processor In the Loop (PIL) testing 88
5. Recapitulation 90
6. Summary 92
Conclusion and future work 93
REFERENCES 96

List of Figures

Chapter 1

Figure 1.1 Semiconductor subjected to illumination 17
Figure 1.2 The most used PV cells for solar energy harvesting 17
Figure 1.3 Photovoltaic array architecture. 18
Figure 1.4 The equivalent circuit of the solar cell for the single diode model 19
Figure 1.5 The equivalent circuit of the PV module....21
Figure 1.6 I-V characteristics of the module for various values of irradiance G and fixed temperature. 22
Figure 1.7 I-V characteristics of the module for various values of temperature T and fixed irradiance. 22
Figure 1.8 P-V characteristics of the module for various values of irradiance G and fixed temperature. 22
Figure 1.9 PV array under partial shadow caused by a tree 23
Figure 1.10 Equivalent circuit of shading PV panel consists of 38 cells in series. 23
Figure 1.11 I-V curves for PV panel under partial shading condition 25
Figure 1.12 Hot spot phenomenon....25
Figure 1.13 Bypass diode activation scheme (a) Uniform conditions, (b) Mismatching conditions without bypass diode activation, (c) Mismatching conditions with bypass diode activation. 26
Figure 1.14 PV array functionality: (a) Unshaded condition of PV array, (b) shaded condition of PV array, and (c) I-V and P-V curves resulting from different scenarios (a) and (b). 26
Figure 1.15 Effect of resistive Load on PV system operating point 27
Figure 1.16 Block diagram of the PV system adapted by the DC-DC converter 27
Figure 1.17 DC-DC boot converter 28
Figure 1.18 The equivalent scheme of DC-DC boot converter, (a) ON, (b) OFF state 28
Figure 1.19 Waveforms of current and voltage in a boost converter operating in continuous mode. 29
Figure 1.20 Waveforms of current and voltage in a boost converter operating in discontinuous mode. 29
Figure 1.21 Inductor's current variation....31

Chapter 2

Figure 1.22 Block diagram of MPPT controller....35
Figure 2.1 Flowchart of conventional Perturb and Observe (P&O) method. 38
Figure 2.2 P-V characteristics for the basis of INC method. 39
Figure 2.3 The basic flow chart of the voltage based INC method. 40
Figure 2.4 Block diagram of Fuzzy logic control (FLC) 43
Figure 2.5 Fuzzy membership functions (a) of the error variation CE, (b) of the error C, (c) of the duty cycle D. 43
Figure 2.6 A typical three layer feed-forward ANN structure. 45
Figure 2.7 The particles movement in PSO 46
Figure 2.8 Flowchart of the PSO algorithm. 48
Figure 2.9 Flowchart of the ABC algorithm. 50
Figure 2.10 Flowchart of the WOA algorithm. 51
Figure 2.11 Hunting behavior of grey wolves: (a)–(c) chasing and tracking prey; (d) encircling prey; and (e) attacking prey method. 53
Figure 2.12 Flowchart of GOW algorithm. 53
Figure 2.13 Block diagram of the GWO-MPPT method. 54
Figure 2.14 Flowchart of ABC-P&O algorithm. 56

Chapter 3

Figure 3.1 PV array with three PV panels exposed to shade. 61
Figure 3.2 P-V curves of PV array for STC and for two shading scenarios. 62
Figure 3.3 The current flow direction of the PV array (a) in area 1 and (b) in area 2. 62
Figure 3.4 Experimental set-up of the measurement system. 63
Figure 3.5 The variation in irradiance levels during a day in shaded and unshaded places. 63
Figure 3.6 The P-V characteristic of the PV array for different shading scenario tests: (a) Test 1, (b) Test 2, (c) Test 3, (d) Test 4, (e) Test 5. 65
Figure 3.7 The scan points on the P-V curves Under PSC3 using the classical scanning method. 66
Figure 3.8 Diagram of the proposed scanning method 67
Figure 3.9 The output power of the PV string under PSC3 by using the classical scanning method. 67
Figure 3.10 The scan points on the P-V curves under PSC3 using the classical and Improved scanning method. 68
Figure 3.11 The output power of the PV string under PSC3 by using the improved scanning method 68
Figure 3.12 Steps to develop a circuit board in Proteus tool: (a) compared to those for developing it in traditional design tools, (b) such as Matlab/Simulink or PSIM. 69
Figure 3.13 . Schematic diagram of the entire photovoltaic (PV) system. 69
Figure 3.14 Equivalent circuit for single diode model of solar cell. 70
Figure 3.15 The equivalent circuit of panel model under Proteus [100]. 71
Figure 3.16 (a): Measurement setup, (b): I-V and P-V characteristics for simulation and experimental data [100]. 71
Figure 3.17 Schematic of PV system design in Proteus software. 72
Figure 3.18 The global schematic of the PV system designed in the proteus environment. 74
Figure 3.19 The P-V curves characteristics of a PV String under diverse irradiation. 75
Figure 3.20 The output power of the PV string Under Various PSCs. 75
Figure 3.21 The output power under a change of the insolation value during the scanning loop. 76

Chapter 4

Figure 4.1 Migration and attacking behaviors of seagulls [12]. 80
Figure 4.2 Flowchart of the SOA based MPPT algorithm 84
Figure 4.3 PV system configuration with the SOA based MPPT controller. 85
Figure 4.4 PV characteristics under different PSCs. 86
Figure 4.5 Output power under PSC1 using: P&O, PSO and SOA. 87
Figure 4.6 Output power obtained under PSC2 using: P&O, PSO and SOA. 87
Figure 4.7 Output power obtained under PSC3 using: P&O, PSO and SOA. 87
Figure 4.8 Output power obtained under STC to PSCs variations using: P&O, PSO and SOA. 88
Figure 4.9 Diagram of PV generation using PIL block 89
Figure 4.10 PIL results of output power obtained under STC to PSCs variation using SOA algorithms 89
Figure 4.11 Diagram comparative of the tracking efficiency obtained using P&O, PSO and SOA methods 91
Figure 4.12 Extracted output power of PV system from different uniform irradiation using P&O, PSO and SOA. 91

List of Tables

Chapter 1

Table 1-1 Comparison of photovoltaic technologies 18
Table 1-2 Characteristics of the PV panel TDC-M20-36 at STC [33]....21

Chapter 2

Table 2-1 Fuzzy rule table....44
Table 2-2 Review of the most used MPPT algorithms. 57

Chapter 3

Table 3-1 Tests applied to the simulation set-up 64
Table 3-2 Characteristics of the used PV model at Standard Test Conditions (STC)....70
Table 3-3 the value of the irradiation taken for all simulation tests. 74
Table 3-4 Comparisons of classical and modified scanning methods under various PSCs 76

Chapter 4

Table 4-1 The electrical parameters of the used PV system 85
Table 4-2 Irradiation values considered in the simulation tests....85
Table 4-3 Performance comparison of the SOA, PSO, and P&O based MPPT methods. 90

NOMENCLATURES

- A : is the diode's ideality factor
- F : is switching frequency [Hz]
- I_D : is the diode current [A]
- I : is the panel output current [A]
- I_s : is the panel reverse saturation current [A]
- I_{ph} : is the panel photocurrent [A]
- Io : is the output current of the Boost converter [A]
- K : is the constant of Boltzmann [$J.K^{-1}$]
- N_s : is the number of cells connected in series
- q : is the electron charge [C]
- R_s : is the series resistance [Ω]
- R_{sh} : is the shunt resistance [Ω]
- R : is the load [Ω]
- T: is the junction temperature [K]
- V_D : is the diode voltage [V]
- V : is the panel output voltage [V]
- V_t : is thermal voltage [V]
- Vo : is the output voltage of the Boost converter [V]
- ΔV: input voltage ripple of the Boost converter [V]
- ΔV_o: output voltage ripple of the Boost converter [V]
- ΔI_L: inductor current ripple [A]

GREEK LETTERS

- α : is the duty cycle

ABBREVIATIONS

- ABC : Artificial Bee Colony
- ACO : Ant Colony Optimization
- CCM : Continuous-Conduction Mode
- DCM : Discontinuous-Conduction Mode
- DSP : Digital Signal Processor
- FLC: Fuzzy Logic Control
- FSCC: Fractional Short-Circuit Current
- FOCV: Fractional Open-Circuit Voltage
- FPGA : Fied-Programmabe Gate Array
- FPU : Floting Point Unit
- GWO : Grey Wolf Optimization
- GMPPT: global MPPT
- INC : Incremental Conductance
- LCD: Liquid Crystal Display
- MBD : Model-Based Design
- MPP : Maximum Power Point
- MPPT : Maximum Power Point Tracking
- PSC : Partial Shading Condition
- PIC : Programmable Interface Controllers
- PSO : Particle Swarm Optimization
- PCB : Printed Circuit Board
- P&O : Perturb and observe

- PIL : Processor In the Loop
- PV : Photovoltaic
- PWM : Pulse Width Modulation
- RE : Renewable Energy
- STC : Standard Test Conditions
- SOA : Seagull Optimization Algorithm
- USB : Universal Serial Bus
- WOA : Whales Optimization Algorithm

Introduction

Today, more than ever before, climate change is affecting us and, its harmful effects are constantly increasing. This is, in part, due to human activity. In fact, a large part of the world's energy production is provided by fossil fuels. To reduce the negative impact of fossil fuels on the environment, and to satisfy the increasing energy demand, we are witnessing the development of renewable energies (wind, solar, hydroelectric and biomass) worldwide. Among all these sources of energy, Photovoltaic (PV) generators play an important role and are widely developed in sunny countries.

However, the development of PV systems has brought to light some factors that have a direct impact on the performance of these renewable energy sources. Several studies have found that factors like increased cell temperature and partial shading have an impact on the performance of solar PV systems. For instance, partial shading phenomena generate high power losses, which can lead to the destruction of solar panels. From an economic standpoint, these drawbacks affect the profitability of the production of PV systems, both for sale and for autonomy, with a return on investment time and a too-long life span of the non-optimized equipment. Many works have proposed technical solutions to eliminate or reduce these phenomena. The objective is to maximize the power extraction of PV panels whatever the environmental conditions.

The high initial cost and low efficiency of generating electricity using PV systems are the main limiting factors. For this reason, it is required that the PV system operates at its maximum power point (MPP) to minimize costs and maximize efficiency. In addition, the I-V and P-V characteristics of the PV array are affected by irradiation and temperature, which have a nonlinear relationship. The issue becomes more complicated when the entire PV array does not receive uniform insolation, which is called partial shading [1]. Maximum power point tracking (MPPT) control techniques are appropriate for obtaining the maximum possible power extracted from the PV systems. Traditional approaches such as perturb and observe (P&O) and incremental conductance (IC) are routinely used to estimate maximum power under uniform irradiance conditions [2, 3]. These systems employ a set step to determine the ideal duty cycle value, which may result in incorrect or sluggish tracking during abrupt changes in temperature or irradiance. Fuzzy logic, neural networks, and neuro-fuzzy are examples of intelligent algorithms. These algorithms use a variable step to determine the ideal duty cycle value, resulting in a quicker time response and greater stability under varied operating circumstances.

However, PV arrays are frequently subjected to partial shading conditions (PSCs), which are the root cause of the majority of output power decrease and mismatch [4]. When the PV array is operating under these conditions, the P-V curves are characterized by the appearance of many local peaks, which are caused by the activation of bypass diodes, which protect shaded cells [5]. In such

partial shading conditions, standard MPPT algorithms may miss the target by converging to a local, rather than a global, maximum, resulting in a large loss in output power and, as a result, a poor overall system yield. A variety of enhancements to traditional MPPT algorithms have been developed to deal with the impact of shading on the P–V curves. Some are topology-based and require extra power circuits to accomplish global MPPT (GMPPT) [6]. As a result, overall efficiency is lowered. Others are algorithm-based strategies such as fuzzy logic with polar controller and sequential extremum searching control [7]. These approaches are expensive, time-consuming operations that necessitate the use of complicated technology. However, this solution can increase the cost of the PV system due to the high number of used sensors. In addition, the application of the metaheuristic algorithm for MPPT has attracted the interest of many researchers due to its ability to handle nonlinear functions without requiring derivative information. Since metaheuristic MPPT approaches are an efficient search and optimization method for real-valued multi-modal objective functions, it is envisaged to be very effective to deal with MPPT problems. Various metaheuristic approaches are found in the literature but the more popular ones are particle swarm optimization (PSO), grey wolf optimization (GWO), ant colony (ACO), Artificial Bee Colony (ABC), and Whales Optimization Algorithm (WOA). Sarvi et al. in [8] proposed the PSO-based MPPT for PV systems under PSC to find the GMPP. Nevertheless, this solution presented oscillations around the steady-state. Hence, some researchers have attempted to improve the PSO to reduce oscillations [9, 10]. However, their improved method cannot follow the dynamic GMPP under various shading patterns. Furthermore, Jang et al. in [11] proposed an ACO algorithm and showed that this method has a faster convergence speed compared to the Basic PSO. ACO and PSO methods present a major disadvantage in terms of convergence linked to the initial placement of the agents into the research space. In addition, both PSO and ACO need the determination of many parameters, making them rigid and complicated.

To overcome these complexities, a simple method to find the global maximum power point (GMPP) under the PSCs of the PV system is proposed in this thesis. This method scans the P–V curve and memorizes all the peaks to get the global peak which is the GMPP. This method is simple and easy to implement in low-cost microcontrollers. But, under storing all the possible MPPs, this method takes a long processing time, because the scan is started from the point of the short-circuit current (I_{CC}) to the open-circuit voltage (V_{OC}) of the P-V characteristic. Hence, this technique interrupts the system operation when scanning the entire control range between the V_{OC} and I_{CC}, which yields power losses. Therefore, an improved scanning method is also proposed in this thesis to reduce and limit the scan interval, which eliminates the passage through the short-circuit point of the P-V characteristics. In addition, it avoided the open-circuit of the PV string during the scan interval to prevent disconnection of the PV system. All these modifications allow this method to track the GMPP with good response time and high efficiency under dynamic PSCs. Moreover, the simple scheme of the

proposed method will ensure reduced complexity of implementation, which reduces the cost of the PV system. Although the proposed method is simple and easy to implement in low-cost microcontrollers, it has a limitation in terms of tracking the actual GMPP when a change in the insolation value during the scan operation occurs.

Moreover, to overcome the complexity found in the PSO and ACO methods, the authors of [12] established a comprehensive bio-inspired approach for addressing computationally costly issues called the seagull optimization algorithm (SOA), which mimics the search and attack behaviors of seagulls in nature. This algorithm is one of the latest effective optimization methods, which is gradient-free and applicable to optimize all engineering problems occurring in real life. Additionally, compared to other evolutionary algorithms, SOA requires fewer variables for adjustment and fewer operators, which is advantageous when considering a speedy design process [12]. However, to the best of the authors' knowledge, no research has been done on MPPT based on SOA so far, which motivates us to study this method and to enrich the scientific references with the developed version of the SOA for MPPT controllers. Therefore, this thesis introduces a new SOA-based metaheuristic MPPT method for tracking the GMPP to maximize the PV power output in PV systems operating under both uniform and partial shading conditions. This method is considered best suited for real engineering problems compared to another metaheuristic algorithm. The MPPT's speed and efficiency will be considerably improved.

On the other hand, to validate the performance of MPPT algorithms, it is necessary to test them before implementation. For this reason, researchers often use simulation tools such as Matlab-Simulink or PSIM to model PV systems and then test the performance of their MPPT algorithms. However, the main disadvantage of these tools is that they do not contain microcontrollers or embedded boards (such as Digital Signal Processor (DSP), Field-Programmable Gate Array FPGA, Arduino, Programmable Interface Controllers (PIC)…) in which the MPPT algorithm can be implemented and tested as it is done in an actual prototype. Therefore, once we start the actual implementation of the MPPT algorithm for a real PV system, several problems may occur due to the disparities that can appear between the software development and the requirements during the development process. Moreover, as all the components used (DC/DC converter, sensors, actuators and microcontroller) are real, unlike those designed in the simulation tool, it is difficult to know the component responsible in the event of a bug. That can increase the time spent debugging runtime errors. Against this, these problems can be avoided by using the Proteus tool as an alternative for modelization and simulation.

Proteus is an electronic circuit design software that includes diagrammatic capture, PROSPICE simulation, and printed circuit board (PCB) layout modules. It provides in its libraries embedded

boards such as PIC and Arduino, where we can implement our controller by uploading the hex code to the microcontroller as it happens in reality. In addition, this tool has been developed to contain components or models that are close to reality, which can give more accurate results. However, using Proteus, software development can begin as soon as the schematic is drawn, and the combination of hardware and software can be thoroughly tested before physical prototyping. In addition, the same algorithm's code implemented in the microcontroller on Proteus will be used in the real experiment. For these reasons, researchers and engineers can benefit from Proteus to test and evaluate the performances of their MPPT algorithm before the real implementation. However, to the authors' best knowledge, there is no simulation found in the literature of an entire PV system under Proteus software. Hence in this thesis, a PV simulator is designed under Proteus software. This PV simulator can be used to verify and evaluate the performance of MPPT algorithms with a closer approximation to the real implementation. Therefore, by using Proteus, the MPPT algorithm can be implemented on the electronic boards, and consequently, this solution can be used as a low-cost PV simulator.

Finally, a Processor In the Loop (PIL) test is done to validate the efficiency of the proposed SOA-MPPT. It should be mentioned that the PIL is tested using the MKRZERO board. Therefore, the PIL test can be used as a low-cost option to test the hardware implementation of the MPPT algorithm.

The main objectives of this research are:

(i) Propose a trusted simulation of a PV system designed under Proteus software. The proposed PV simulator can be used to verify and evaluate the performance of MPPT algorithms with a closer approximation to the real implementation. The main advantage of this model is that it contains a real microcontroller, as can be found in reality, so that the same code for the MPPT algorithm used in the simulation will be used in real implementation.

(ii) Develop an MPPT controller based on the scanning method. For this purpose, the proposed scanning algorithm is based on simple instructions that do not require extensive computation. Therefore, we can integrate the proposed method with low-cost microcontrollers.

(iii) Propose and design a new MPPT based on a metaheuristic algorithm (SOA-based MPPT) through the "Processor In the Loop" test. The expected outcome of this proposal is an efficient MPPT method that presents a very high level of robustness, reliability, and accuracy.

The content of this thesis is organized as follows:

(i) Chapter 1 provides a brief reminder of the principle of PV conversion, the main characteristics of a PV cell and its modeling, and the different components of a PV system.

(ii) Chapter 2 introduces an extensive review of MPPT algorithms that have been prominently used in PV systems. They are classified into four groups, namely the traditional or conventional techniques, MPPT that exploits the characteristics of PV model, soft computing techniques and hybrid techniques. The advantages, limitations and drawbacks of each method are highlighted.

(iii) Chapter 3 presents the proposed scanning method for tracking the GMPP of the PV system. The effectiveness of the improved scanning method is verified using a PV simulator design in Proteus software.

(iv) Chapter 4 describes the design and simulation of the Seagull Optimization Algorithm (SOA) based MPPT to track GMPP during partial shading with high efficiency. The performance of the SOA-based MPPT method is verified by comparing its performance with P&O and PSO based MPPT methods under different shading scenarios.

(v) Chapter 5 concludes the work carried out in this thesis. Some suggestions and perspectives of the present work are given at the end of this chapter.

Chapter 1

Overview of the PV System and effect of partial shading on maximum power point

1. Introduction

Solar energy is a clean energy, it does not present serious environmental problems as the conventional sources (fossil fuels), namely global warming. In addition, compared to other renewable energy sources, solar energy has a low impact on the environment, which does not occur with hydroelectric and wind power. For the construction of a hydroelectric plant, the course of the river is changed and large areas of forest are flooded [13]. Compared to wind energy, solar energy is silent and can be installed on the roof in urban areas. In general, the solar energy is exploited in two approaches: (i) photovoltaic (PV) technology and (ii) solar thermal technology. These approaches are already proven and widely practiced worldwide [14].

In this chapter, we briefly recall the principle of PV conversion, the main characteristics of a PV cell, its modeling and the different components of a PV system. Then, we will examine the effect of different partial shading scenarios on PV array characteristics to provide a simple and easily applicable method for GMPP tracking.

2. An overview of PV solar energy: from material to use

2.1. Photovoltaic effect

The photoelectric effect was first introduced by the French physicist, Edmund Becquerel, in 1839, who found that certain materials would produce small amounts of electric current when exposed to light. In 1905, Albert Einstein described the nature of light and the photoelectric effect on which PV technology is based. The first PV module was built by Bell Laboratories in 1954. It was billed as a solar battery and was mostly just a curiosity as it was too expensive and with a relatively low efficiency of around 4.5% [15]. In the 1960s, space industry began to make the first serious use of this technology to provide power aboard space crafts, and during the energy crisis in the 1970s, PV technology gained recognition as a source of power for non-space applications.

By definition, the PV effect is the direct conversion of light into electricity at the atomic level. Some materials exhibit a property known as the photoelectric effect that causes them to absorb photons of light and release electrons. When light shines on a PV cell, it may be reflected, absorbed, or pass right through; but only the absorbed light generates electricity. The energy of the absorbed light is transferred to electrons in the atoms of the PV cell. With their new found energy, these electrons escape from their normal positions in the atoms of the semiconductor PV material and become part of the electrical flow, or current, in an electrical circuit. To induce the built-in electric field within a PV cell, two layers of somewhat differing semiconductor materials are placed in contact with one another. One layer is an n-type semiconductor with an abundance of electrons, which have a negative electrical charge. The other layer is a p-type semiconductor with an abundance of holes,

which have a positive electrical charge. Sandwiching these together creates a p/n junction at their interface, thereby creating an electric field (see Figure 1.1).

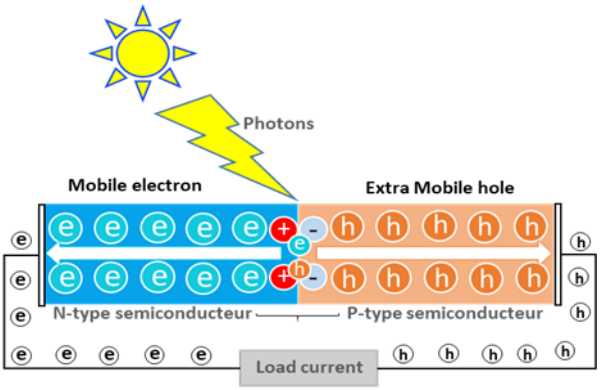

Figure 1.1 Semiconductor subjected to illumination

2.2. PV technologies

Many different solar cells are now available, yet more are under development. The range of solar cells spans different materials and structures in the quest to extract maximum power from the device while keeping the cost to a minimum. Devices with efficiencies exceeding 30% have been demonstrated in the laboratory; however, the efficiency of commercial devices is still less than half this value. There are two main PV technologies, Crystalline Silicon (C-Si) technology and thin-film technology [16, 17]. Crystalline silicon PV cells, known as the first generation technology are currently the most common solar cells in use (about 90% of the world market share in 2013 [18]), mainly because C-Si is stable and it operates at a good efficiency [19, 20]. Despite gaining more favour, C-Si based PV cells are relatively expensive because of difficulties in the industrial preparation of the high-grade silicon. As the second generation PV cells technology, thin-film PV cells use very thin layers of semiconducting materials, so they can be manufactured in large quantity at low cost, but with low efficiency. However, both technologies have advantages and disadvantages. It is important to take a variety of factors into account, when making a choice. Figure 1.2 presents pictures of the most commonly used PV cells.

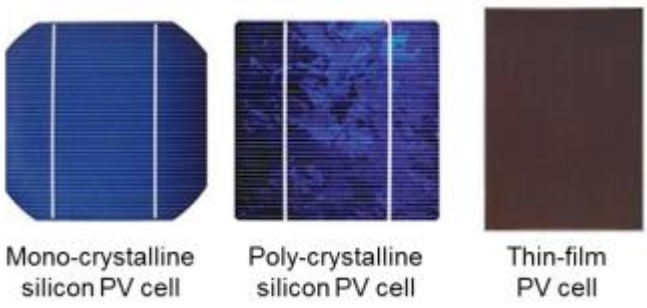

Figure 1.2 The most used PV cells for solar energy harvesting.

The classification of PV technologies is divided into three generations such as: crystalline silicon technology, thin-film technology and multi-junction technology [21, 22]. The comparative table below can serve as a basis for a quick comparison:

Table 1-1 Comparison of photovoltaic technologies

	1st Generation Silicon technology	**2nd Generation** Thin-film technology	**3rd Generation** multi-junction technology
Types	Mono-crystalline cell Poly-crystalline cell	Amorphous silicon cell Cadmium telluride cell Copper indium gallium selenide cell	Organic solar cell Copper Zinc tin sulfide cell Dye-sentitized cell Perovskite cell Quantum cell
Efficiency	16% - 26%	10% - 16%	~ 45%
Price/W	Higher	Lower	Higher

2.3. Photovoltaic generator

A typical PV cell produces a voltage of approximately 0.5V and a current that depends on the intensity of the sunlight and the area of the cell. To increase the output power, PV cells are connected in series (to increase the output voltage) and in parallel (to increase the output current) [23]. Many cells are packaged together to form a PV module. In turn, these modules can be wired together in a series–parallel combination to form an array that best meets the needs of the application, as shown in Figure 1.3.

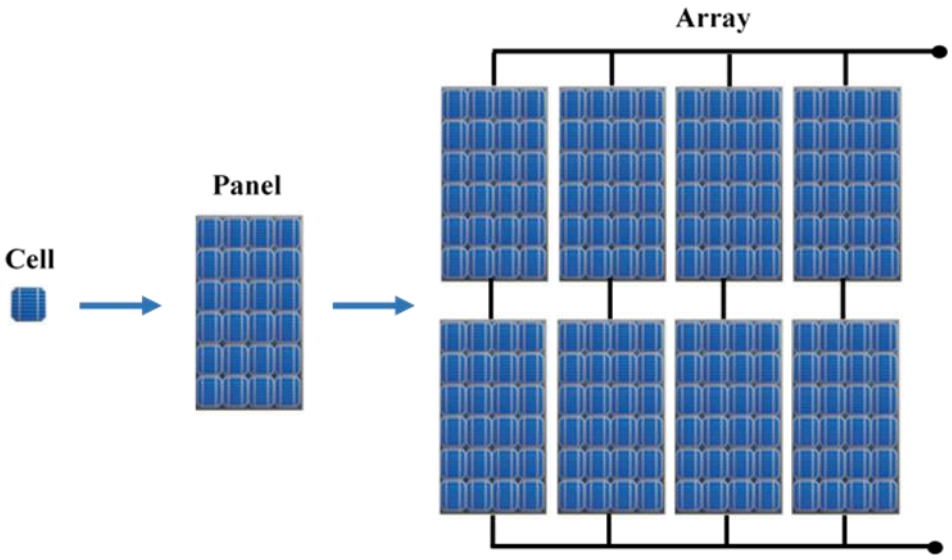

Figure 1.3 Photovoltaic array architecture.

2.3.1. PV cell and module modelling

The electrical model of the PV cell, as illustrated in Figure 1.4, consists of a current source, a diode, and a resistor $R_{sh,c}$ linked in parallel, as well as a series resistor $R_{s,c}$.

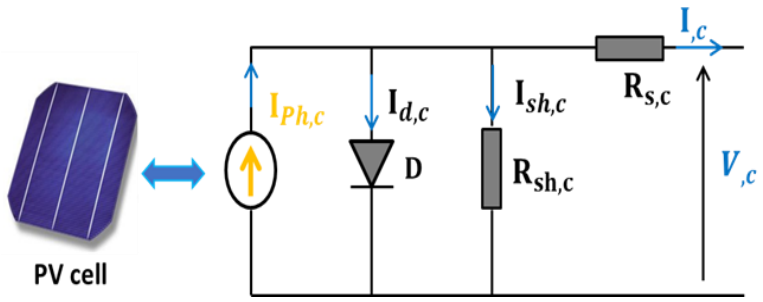

Figure 1.4 The equivalent circuit of the solar cell for the single diode model

where the current source is proportional to sun irradiation. The $R_{s,c}$ is primarily determined by the metal base's contact resistance with the p semiconductor layer, the p and n bodies' resistances, the n layer's contact resistance with the top metal grid, and the grid's resistance. The $R_{sh,c}$ resistance is mostly influenced by the leakage current of the p–n junction and is affected by the PV cell production procedure [24].

Based on the Figure 1.4, the following equation (1.1) gives the output current [25]:

$$I_{,c} = I_{ph,c} - I_0\left(e^{\frac{q(V_{,c}+I_{,c}R_{s,c})}{AV_t}} - 1\right) - \frac{V_{,c} + I_{,c}R_{s,c}}{R_{sh,c}} \qquad (1.1)$$

where $I_{ph,c}$ I and I_0 are denoted the photocurrent, the output cell current, and the reverse saturation current respectively. V represents the output cell voltage. $R_{s,c}$ and $R_{sh,c}$ present a series resistance and parallel resistance respectively. A is the diode ideality factor.

The value of the termal voltage is given by equation (1.2).

$$V_t = \frac{KT}{q} \qquad (1.2)$$

Where K, q and T are denoted the Boltzmann constant (1.38×10-23 (J/K)), the charge of electron (1.6×10-19 (C)), and the solar cell temperature (K) respectively.

The photocurrent $I_{ph,c}$ of a solar cell depends on many material characteristics. However, it can be approximated as linear-dependent on irradiance and temperature with sufficient accuracy as follow [30]:

$$I_{ph,c} = \frac{G}{G_{ref}}\left[I_{sc,ref} + \mu_{sc}(T - T_{ref})\right] \qquad (1.3)$$

Where $I_{sc,ref}$ is solar cell short-circuit current at standard test conditions (STC): G_{ref}=1000 W/m^2, T_{ref}=25°C.

μ_{sc} is the solar cell short-circuit temperature coefficient, normally provided by the manufacturer (A/K).

G is the actual irradiance intensity (W/m^2);

The well-known diode saturation current estimation equation is given by [26]:

$$I_0 = I_{0,ref}\left(\frac{T_{ref}}{T}\right)^3 exp\left[\frac{qE_g}{nk}\left(\frac{1}{T_{ref}} - \frac{1}{T}\right)\right] \quad (1.4)$$

Where, the nominal saturation current $I_{0,ref}$ at STC is given by:

$$I_{0,ref} = \frac{I_{sc,ref}}{exp\left(\left(V_{oc,ref}/nV_t\right) - 1\right)} \quad (1.5)$$

$V_{oc,ref}$ is solar cell open-circuit voltage at reference condition.
E_g is band-gap energy in the solar cell, (1.12-1.15eV).

To achieve the desired voltage and current levels, *Ns* cells are connected in series and N_P cells are connected in parallel respectively, thus forming a PV module. There for the PV module parameters are scaled according to N_S and N_P as given bellow [27]:

$$I_{ph\_Total} = N_p * I_{ph,c} \quad (1.6)$$

$$I_{0\_Total} = N_p * I_0 \quad (1.7)$$

$$A_{Total} = N_s * A \quad (1.8)$$

$$R_{s\_Total} = \frac{N_s}{N_p} * R_{s,c} \quad (1.9)$$

$$R_{sh\_Total} = \frac{N_s}{N_p} * R_{sh,c} \quad (1.10)$$

The overall PV module model can then be represented by the following Figure 1.5.

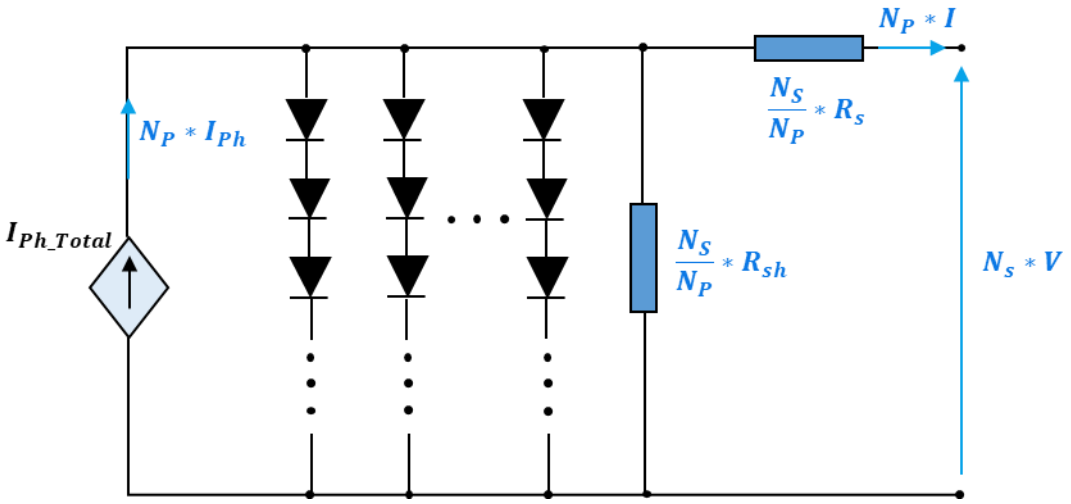

Figure 1.5 The equivalent circuit of the PV module

Current-voltage characteristic equation of equivalent circuit for the PV module arranged in N_P parallel and N_S series cells is given by [25]:

$$I^M = N_p I_{ph} - N_p I_0 \left(exp \frac{q\left(V^M/N_s + I^M R_s/N_p\right)}{AV_t} - 1 \right) - \frac{\left((N_p/N_s)V^M + I^M R_s\right)}{R_{sh}} \qquad (1.11)$$

The characteristics of the PV panel used in this work are shown in Table 1.2.

Table 1-2 Characteristics of the PV panel TDC-M20-36 at STC [28].

TDC-M20-36 PV Panel at STC	
Maximum power	20 W
Maximum voltage	18.76 V
Maximum current	1.07 A
Short-circuit current	1.17 A
Open-circuit voltage	22.70 V
Temperature coefficient of open-circuit voltage	−0.35%/°C
Temperature coefficient of short-circuit current	−0.043%/°C
Number of cells	36
Type of cells	Monocrystalline

2.3.2. Irradiance and cell temperature effect

The I-V characteristics of a photovoltaic module strongly depend on irradiance and temperature (equation (1.3)). This becomes very apparent when evaluating equation (1.11) for selected values of temperature and irradiance. Figure 1.6 shows that the output current I is mainly influenced by the change in irradiance G, whereas the open-circuit voltage V_{oc} remains approximately unchanged. In contrast, for a changing temperature one can see that the voltage varies widely while the short-circuit current remains unchanged Figure 1.7.

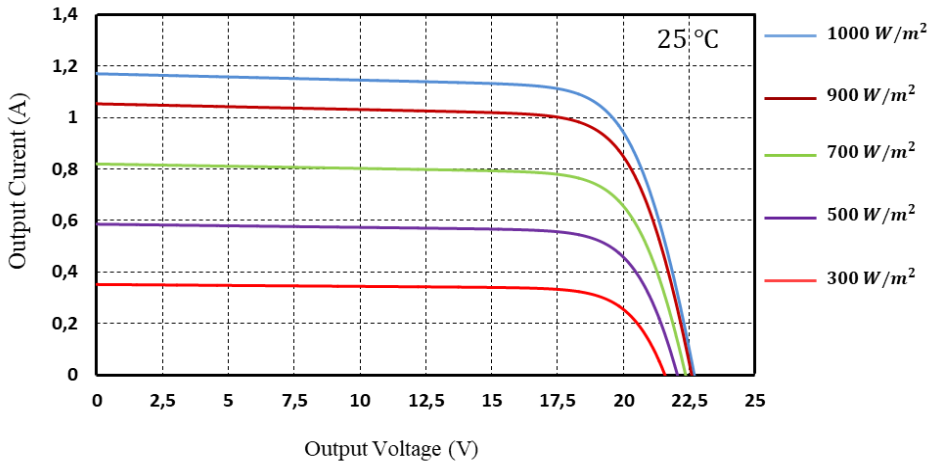

Figure 1.6 I-V characteristics of the module for various values of irradiance G and fixed temperature.

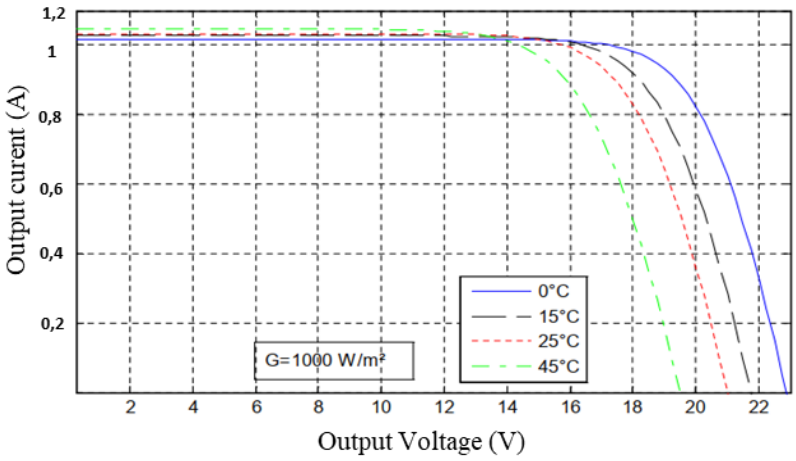

Figure 1.7 I-V characteristics of the module for various values of temperature T and fixed irradiance.

The corresponding power-voltage (P-V) characteristics for variable irradiance and fixed temperature are shown in Figure 1.8 respectively. Which shows clearly the dependence of the output power of the PV module on both irradiance.

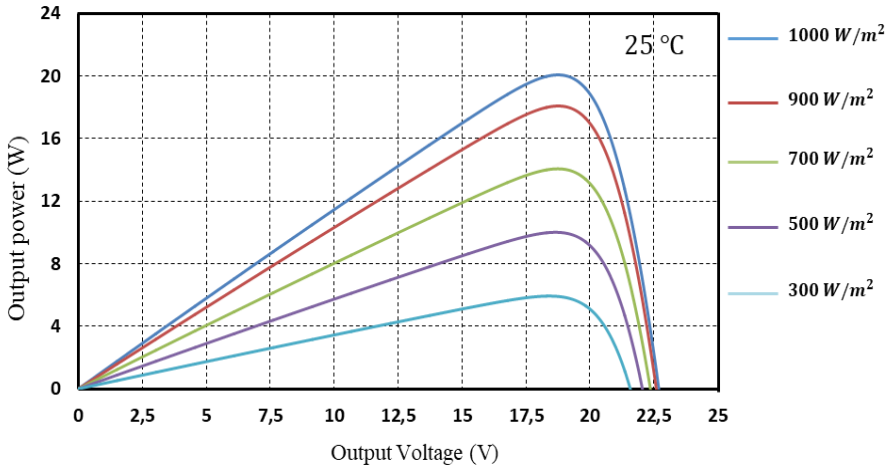

Figure 1.8 P-V characteristics of the module for various values of irradiance G and fixed temperature.

2.3.3. Effect of partial shadow on maximum power point

The phenomenon of partial shading on solar panels is generally caused by obstacles close to PV systems such as trees and bird sloping walls, etc. Most of these obstacles are permanent, predictable and detected at certain times of the year thanks to the path of the sun. There are also temporary and unpredictable partial shadows due to the cloudy passage, bird droppings, snow, dust etc. A typical partial shading example is shown in Figure 1.9.



Figure 1.9 PV array under partial shadow caused by a tree.

2.3.4. Effect of shading and bypass diode impacts

In Figure 1.10, a set of illuminated cells is connected in series with another set of shaded cells. The photon current I_{phs} of shaded cells is lower than the photon current I_{phi} of illuminated cells. Therefore, if the module current I_{ms} is low compared with I_{phs}, the diode D_s is forward biased and there is no risk. But if I_{ms} is high compared with I_{phs}, the diode current $I_{Ds} = I_{phs} - I_{ms} < 0$. As a result, the diode is reverse biased; meaning that the whole current flowing through the module must travel through both the R_{shs} and R_{ss} resistors of the shaded cells [29].

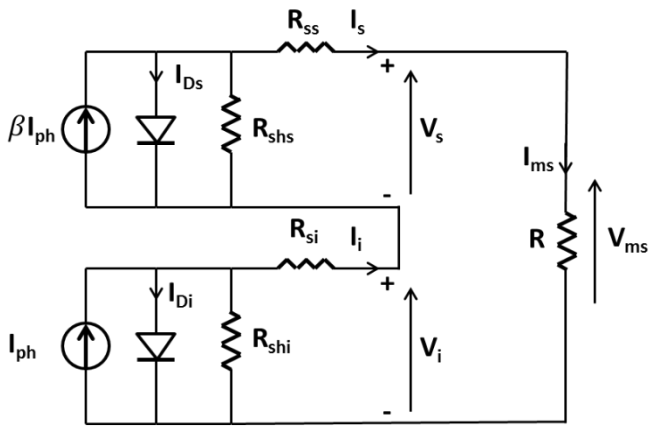

Figure 1.10 Equivalent circuit of shading PV panel consists of 36 cells in series.

2.3.4.1. Mathematical modeling

In Figure 1.10, when a solar cell in a series assembly is in the shade, their output current is given by [29]:

$$I_s = \beta I_{ph} - I_0\left(e^{\frac{V_{Ds}}{V_{ts}}} - 1\right) - \frac{V_{Ds}}{R_{shs}} \quad (1.12)$$

$$\text{Where, } V_{Ds} = V_s + I_s R_{ss} \quad (1.13)$$

βI_{ph} is the photon current generated by the shaded cells as shown in Figure 1.10, where β is the ratio of the photo current generated by the shaded cells and the current generated by the illuminated cells. β = 1 means all cells are illuminated and β = 0 means all cells are shaded.

In the same way the current generated by the illuminated cells is given by the equation:

$$I_i = I_{ph} - I_0\left(e^{\frac{V_{Di}}{V_{ti}}} - 1\right) - \frac{V_{Di}}{R_{shi}} \quad (1.14)$$

$$\text{Where, } V_{Di} = V_i + I_i R_{si} \quad (1.15)$$

Since the shaded and the illuminated cells are connected in series, the same current is forced to cross them both. So in the equations (1.12), (1.13), (1.14) and (1.15), I_i and I_s replaced by the same current I_{ms} Consequently:

$$I_{ms} = \beta I_{ph} - I_0\left(e^{\frac{V_{Ds}}{V_{ts}}} - 1\right) - \frac{V_{Ds}}{R_{shs}} \quad (1.16)$$

$$I_{mi} = I_{ph} - I_0\left(e^{\frac{V_{Di}}{V_{ti}}} - 1\right) - \frac{V_{Di}}{R_{shi}} \quad (1.17)$$

Since the diode D_s is reverse biased, V_{Ds} tends to negative infinity. As a result, $e^{\frac{V_{Ds}}{V_{ts}}}$ tends to zero. So, the equation can be simplified as:

$$I_{ms} = \beta I_{ph} + I_0 - \frac{V_s + I_{ms} R_{ss}}{R_{shs}} \quad (1.18)$$

In order to prove the theory presented by (1.18), the simulation of the PV panel under shading is made and presented in Figure 1.11.

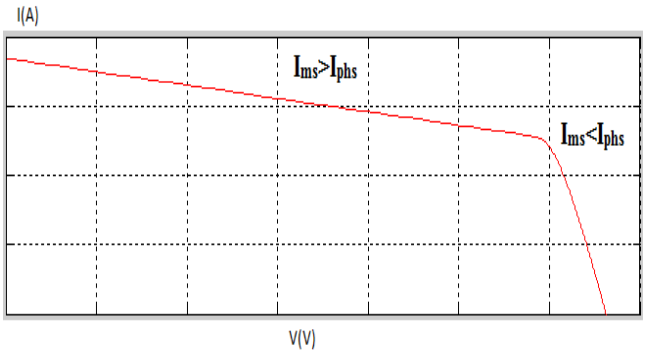

Figure 1.11 I-V curves for PV panel under partial shading condition

As shown in Figure 1.11, once I_{ms} is lower than I_{phs}, the curve I-V loses its exponential characteristic like it is presented in the equation (1.18).

2.3.4.2. Hotspot problem

Once partial shading occurs, the short circuit current of the shaded cells drops considerably. Since they are connected in series, the cells are required to drain all, the same current. However, they are incapable of it; this is due to the fact that some PV cells receive partial shade. This leads the shaded cells to function in reverse polarization [30]. In this region of reverse polarization, the PV solar cell will dissipate power in the form of heat. This has the consequence of creating a hot spot capable of damaging the shaded PV solar cells as shown in Figure 1.12.

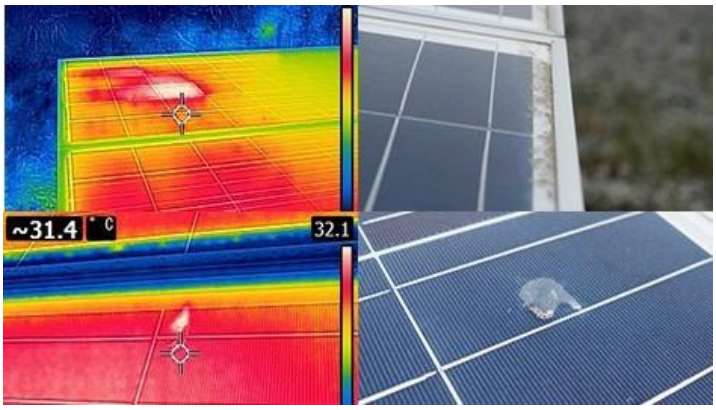

Figure 1.12 Hot spot phenomenon.

2.3.4.3. Bypass diode impacts

One method to protect the module from hot-spot problem is when the bypass diodes are connected in parallel with PV cells [31, 32]. In order to represent the operation of a bypass diode connected to a module in a string, Figure 1.13 (a) shows two modules connected in series. In Figure 1.13 (a) the modules are under the same irradiance conditions, the bypass diodes are inactive. In Figure 1.13 (b) the upper module is shaded; its level of irradiate is, therefore, lower than that of the PV module at the top, but its bypass diode stays inactive since the string current $I_{str} \leq I_{PV's}$. In Figure 1.13 (c) the bypass diode active since the string current $I_{str} > I_{PV's}$. When PV cells (or modules) are

partially shaded, they work as a load on other cells/modules and become reverse biased. As a result, instead of generating energy, they will dissipate it, resulting in a rise in cell temperature. The cell/module can be damaged and influence the entire PV module/array if the temperature becomes too high, which is called the hot spot issue.

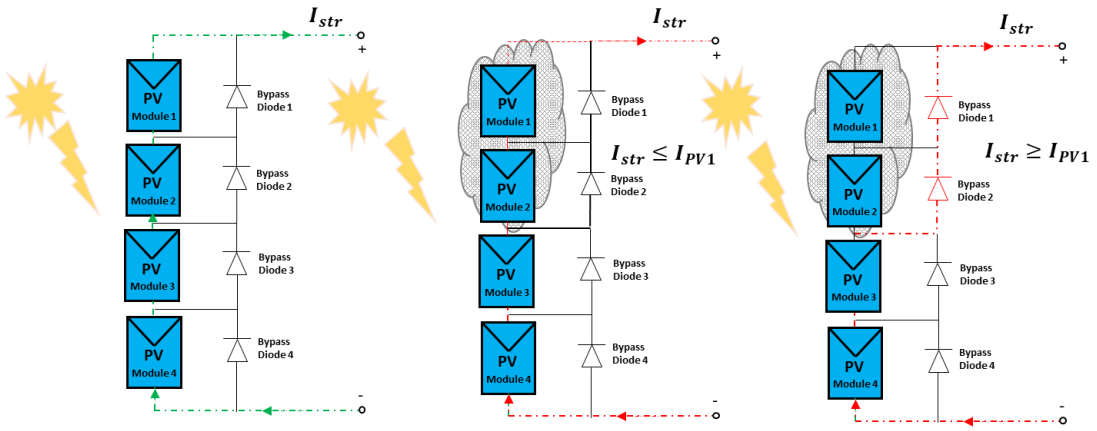

Figure 1.13 Bypass diode activation scheme (a) Uniform conditions, (b) Mismatching conditions without bypass diode activation, (c) Mismatching conditions with bypass diode activation.

To apprehend the current flow direction of the PV array under PSC, consider the PV array in figure 1.14. The PV array consists of four PV modules where two PV panels are unshaded and the other are shaded, as illustrated in Figure 1.14 (b). The P–V curve of the PV array under PSC can be divided into two phases. During uniform solar irradiance, the bypass diodes are reverse biased and therefore have no effect (Figure 1.14 (a)). In the other phase, when the PV panels are shaded, the bypass diodes are forward biased, and the current flows through them instead of the PV panels as can be seen in Figure 1.14 (b).

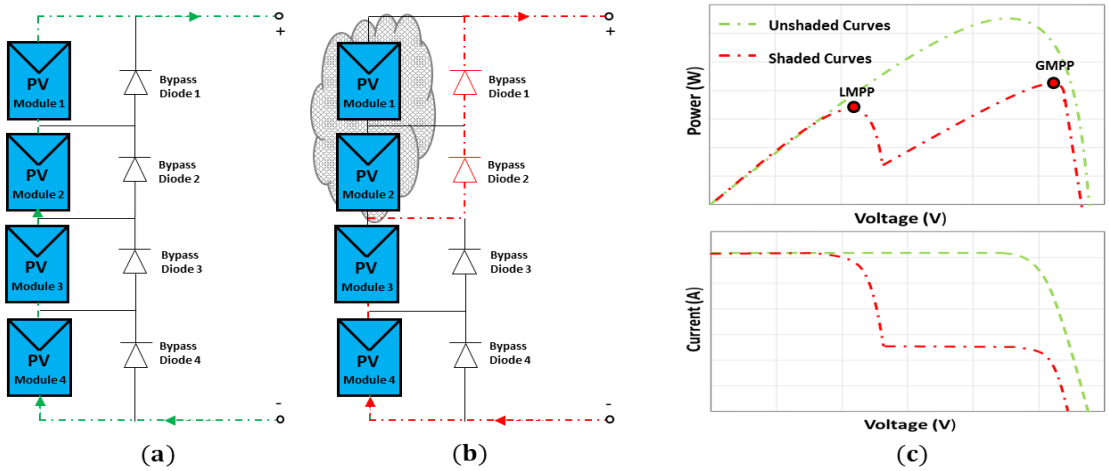

Figure 1.14 PV array functionality: (a) Unshaded condition of PV array, (b) shaded condition of PV array, and (c) I-V and P-V curves resulting from different scenarios (a) and (b).

2.3.5. Effect of load on power Point operating

When a load is connected to a photovoltaic generator (PVG), the operating point (current and voltage), is obtained by the intersection of the I–V characteristics curve of the PVG and the I–V

characteristics of the load, as shown in Figure 1.15. The slope of this curve is 1/R and the operating point will depend on the value of R. For maximum efficiency purpose, the desired operating point should be located at the Maximum Power Point (MPP). The corresponding values for voltage and current are denoted by V_{mpp} and I_{mpp}, respectively. It is important to keep the operating voltage as close as possible to V_{mpp}.

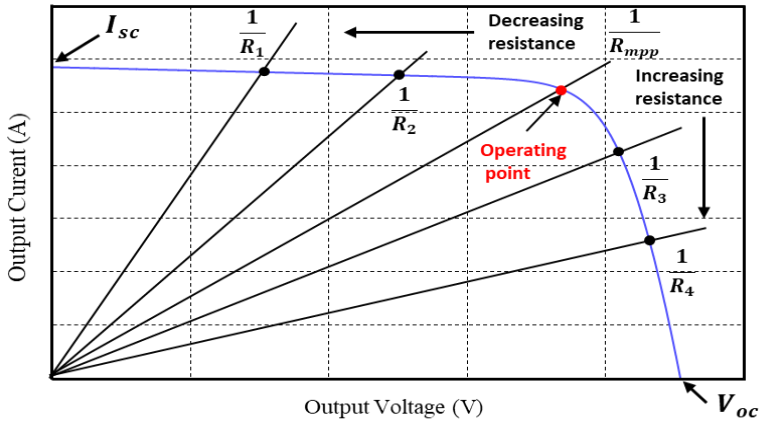

Figure 1.15 Effect of resistive Load on PV system operating point.

2.3.6. The adaptation stage between the PVG and Load

As we have seen previously, the operating point of PVG depends on the value of load connected. To keep the operating point as close as possible to MPP for various values of load, an adaptation stage between the generator and the load is necessary. This stage acts as an interface between the PV generator and the load (refer to Figure 1.16) which ensure the transfer of the maximum power supplied by the generator. The adaptation of the PVG is ensured by a command and control device to force the system to operate at its maximum power. The approach of the problem consists in interposing between the generator and the receiver a static converter [33, 34].

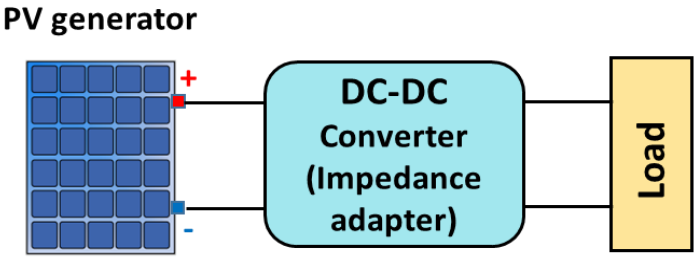

Figure 1.16 Block diagram of the PV system adapted by the DC-DC converter.

2.3.7. DC-DC Converter

The DC-DC converters are used in order to provide impedance matching between the PV array and load. These converters are generally employed as a power-processing unit with MPPT algorithms by adjusting the duty cycle. This duty cycle is calculated by the MPPT algorithm and varies between 0 and 1. There are several topologies of DC-DC converters such as DC-DC converter Boost, Buck,

Buck-Boost, and SEPIC [35-37]. Subsequently, we will only study choppers and as an example the DC-DC Boost converter.

2.3.7.1. Structure of boost converter

A boost converter (step-up converter) is a power converter with an output DC voltage greater than its input DC voltage [38]. It is a class of switching-mode power supply (SMPS). A simple boost converter consists of an inductor L boost, a controlled switch S and a diode D, filters made of a capacitors are normally added to the output and the input of the converter to reduce voltage ripples (see Figure 1.17).

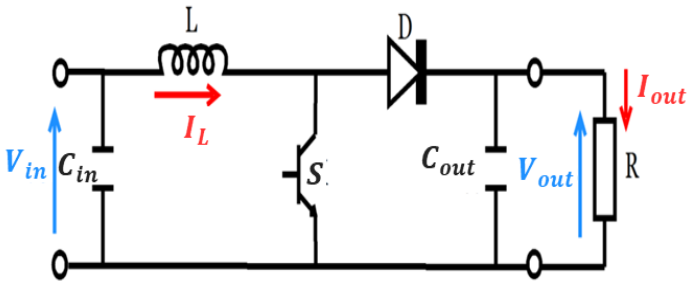

Figure 1.17 DC-DC boot converter.

2.3.7.2. The operating of boost converter

The operation of a boost converter is to boost or step-up a certain input voltage to a higher level, at the same time the boost converter steps-down the current as a natural result of the energy conservation principle, which implies that power, being the product of voltage and current, must be conserved.

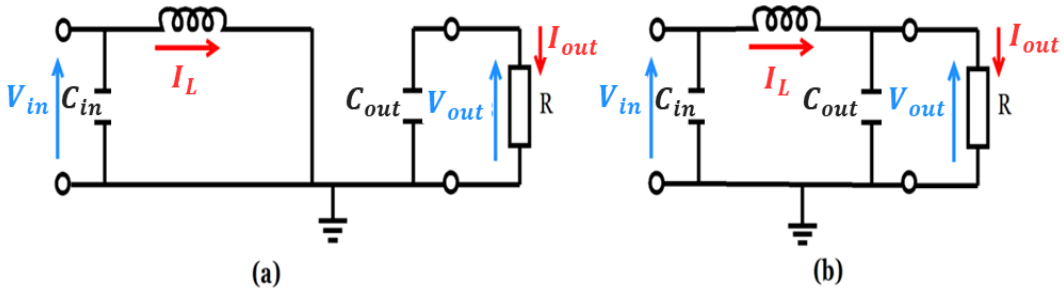

Figure 1.18 The equivalent scheme of DC-DC boot converter, (a) ON, (b) OFF state.

The operation of the boost converter is essentially based on the inductor charge and discharge. When an inductor is charged, it behaves like a load as it absorbs energy. On the other hand, when it is discharged, it behaves as an energy source. The fundamental idea behind the boost effect is the fact that the inductor's voltage during a discharging process depends only on the rate of change of its current with respect to time, and this voltage is independent of the source voltage by which the inductor was charged. This independency gives the possibility of having an output voltage greater

than the input voltage. The Boost converter circuit operation can be divided into two phases: Phase one begins when the switch S is turned on at $t=T_{on}$ as shown in Figure 1.18(a). The input current which rises flows through inductor L boost and switch S. During this mode, energy is stored in the inductor. Phase 2 begins when the switch is turned off at $t=T_{off}$; the energy stored in the inductor is released through the diode to the output Load, as shown in Figure 1.18(b).

The boost converter as all others DC-DC converters has two fundamentally different modes of operation: Continuous-Conduction Mode (CCM) and Discontinuous-Conduction Mode (DCM). The boost converter and its control are designed based on both modes of operation. In the continuous conduction mode, the inductor current flows continuously that is the inductor current is always above zero throughout the switching period as shown in Figure 1.19.

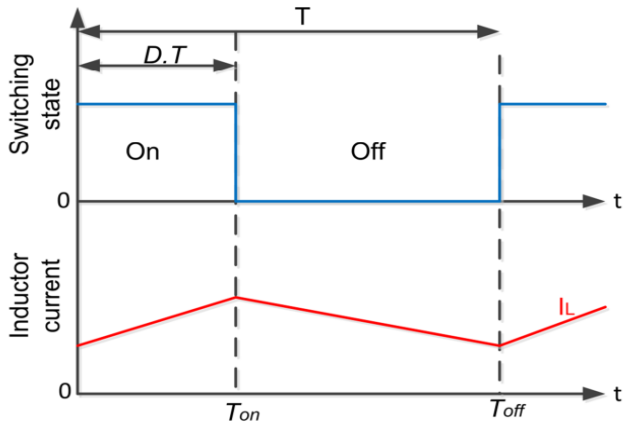

Figure 1.19 Waveforms of current and voltage in a boost converter operating in continuous mode.

In the discontinuous conduction mode, the inductor current is discontinuous; that is, inductor current reaches zero before the end of each switching period, as shown in Figure 1.20.

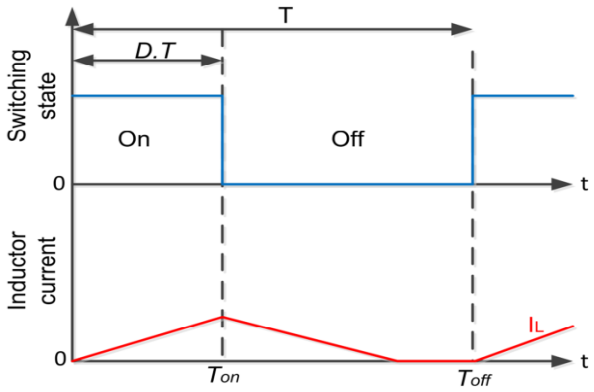

Figure 1.20 Waveforms of current and voltage in a boost converter operating in discontinuous mode.

The advantages of CCM over DCM include the DC conversion ratio is independent of the load, which makes DC analysis of converters operating in CCM easier. While operating in DCM, the output voltage depends on the load and the duty ratio of the switch, which makes DC analysis of converters operating in DCM more complicated. Also, to deliver the same power in DCM as in CCM, the peak

currents are higher, resulting in greater losses in the conduction paths leads to reduced efficiency and higher peak current can also cause switch stress and greater input and output current ripple that adversely affects EMC noise issues.

On this basis, the electrical analysis is dictated by the choice of operating the converter "boost" in continuous conduction mode (CCM) and under the below assumptions:

- ✓ The circuit is operating in the steady state.
- ✓ The components are ideal.

2.3.7.3. Electrical circuit analysis

A. Current flows through the inductor

During the On-state, the switch S is closed, which makes the input voltage Vin appear across the inductor, which causes a change in current I_L flowing through the inductor during a time period t to be as in (1.12):

$$\frac{dI_L}{dt} = \frac{V_L}{L} = \frac{V_{in}}{L} \tag{1.19}$$

By integrating the two parts of the equality, we find that:

$$I_{LI}(t) = \frac{V_{in}}{L} t + I_{Lmin} \tag{1.20}$$

We can see that $I_L(t)$ has a positive slope, which proves that in this phase, the inductor is charging.

At the end of the On-state, the increase of I_L is therefore:

$$\Delta I_{Lon} = \frac{1}{L} \int_0^{DT} V_{in}\, dt = \frac{DT}{L} V_{in} \tag{1.21}$$

D is the duty cycle. It represents the fraction of the commutation period T during which the switch is on. Therefore D ranges between 0 (S is never on) and 1 (S is always on).

During the Off-state, the switch S is open, so the inductor current flows through the load. If we consider zero voltage drop in the diode, and a capacitor large enough for its voltage to remain constant, the evolution of I_L is:

$$\frac{dI_L}{dt} = \frac{V_{in} - V_{out}}{L} \tag{1.22}$$

By integrating the two parts of the equality, we find that:

$$I_{L2}(\mathrm{t}) = \frac{V_{in} - V_{out}}{L} t + I_{Lmax} \tag{1.23}$$

In the case of boost converter V_{out} is always greater than V_{in}. Thus, $I_L(t)$ has a negative slope, which proves that in this phase, the inductor is discharging.

Therefore, the variation of I_L during the Off-period is:

$$\Delta I_{Loff} = \int_0^{(1-D)T} T\frac{V_{in} - V_{out}}{L}dt = \frac{(V_{in} - V_{out})(1-D)T}{L} \quad (1.24)$$

It should be noted that during the two conduction phases (on/off), I_L varies (increases/decreases) in a ΔI_L bandwidth around a mean value $I_{Lmean} = I_{in}$ (See Figure 1.21).

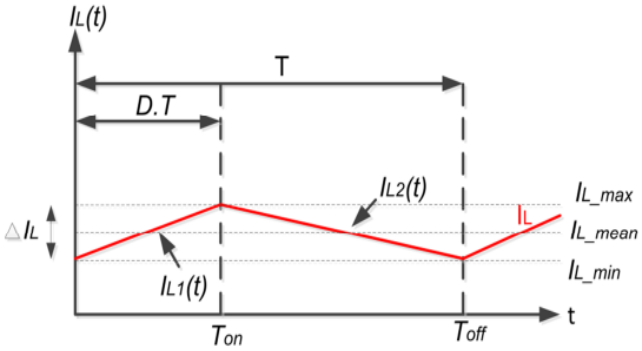

Figure 1.21 Inductor's current variation.

B. Current flows through the diode

During the On-state, the switch S is closed, the diode becomes reverse-biased and the average current passing through it is zero.

$$I_D(t) = 0 \quad (1.25)$$

During the Off-state, the switch S is open. According to the circuit diagram in Figure 1.18(b) and according to the Kirchhoff's circuit law, we can write:

$$I_D(t) = I_{L2}(t) = \frac{V_{in} - V_{out}}{L}t + I_{Lmax} \quad (1.26)$$

C. Current flows through the switch

During the On-state, the switch S is closed, and if we assume that the switching resistance R_{DS_ON} is zero; the current flows through the switch can be given by:

$$I_s(t) = I_{L1}(t) = \frac{V_{in}}{L}t + I_{Lmin} \quad (1.27)$$

During the Off-state, the switch S is open, and if we assume that the switching resistance R_{DS_Off} is infinite; the current flows through the switch can be given by:

$$I_s(t) = 0 \quad (1.28)$$

D. Current flows through the input capacitor

During the On-state, the switch S is closed. According to the circuit diagram in Figure 1.18(a) and according to the Kirchhoff's circuit law, the current flows through the input capacitor can be given by:

$$I_{Cin}(t) = I_{in} - I_{L1}(t) = I_{L\_mean} - I_{L1}(t) \quad (1.29)$$

Following the same reasoning as that adopted during the On-state. During the Off-state, the current flows through the switch can be given by:

$$I_{Cin}(t) = I_{in} - I_{L2}(t) = I_{L\_mean} - I_{L2}(t) \quad (1.30)$$

E. Current flows through the output capacitor

Referring to the diagram in Figure 1.18(a), it is clearly shown that the output capacitor feeds the load R_L during the On-state with a constant current I_{out} given by:

$$I_{Cout}(t) = I_{out}(t) = \frac{V_{out}}{V_{Load}} \quad (1.31)$$

During the Off-state, the output capacitor is connected to the source supply via the inductor L. According to the Kirchhoff's circuit law, the current flows through the output capacitor can be given by:

$$I_{Cout}(t) = I_{L2}(t) - I_{out} \quad (1.32)$$

Thus,

$$I_{Cout}(t) = \frac{V_{in} - V_{out}}{L} t - I_{Lmax} - \frac{V_{out}}{R_{Load}} \quad (1.33)$$

F. Boost converter gain

As we consider that the converter operates in steady-state conditions, the amount of energy stored in each of its components has to be the same at the beginning and at the end of a commutation cycle. In particular, the energy stored in the inductor is given by (1.27).

$$E = \frac{1}{2} L I_L^2 \quad (1.34)$$

Therefore, the inductor current has to be the same at the beginning and the end of the commutation cycle. This can be written as:

$$\Delta I_{Lon} + \Delta I_{Loff} = 0 \quad (1.35)$$

Substituting $\Delta I_{L\,on}$ and $\Delta I_{L\,off}$ by their expressions yields:

$$\Delta I_{Lon} + \Delta I_{Loff} = \frac{DT}{L} V_{in} + \frac{(V_{in} - V_{out})(1-D)T}{L} = 0 \tag{1.36}$$

This can be written as:

$$\frac{V_{out}}{V_{in}} = \frac{1}{1-D} \tag{1.37}$$

This in turns reveals the duty cycle to be:

$$D = 1 - \frac{V_{in}}{V_{out}} \tag{1.38}$$

From the expression (1.30) it can be seen that the output voltage is always higher than the input voltage (as the duty cycle goes from 0 to 1), and that it increases with D, theoretically to infinity as D approaches 1.

2.3.7.4. Inductor selection

Estimate the inductor ripple current is 20% to 40% :

$$\Delta I_L = I_{out\_max} \times (0.2\ to\ 0.4) \times \frac{V_{out}}{V_{in}} \tag{1.39}$$

The critical inductance value of the boost converter is given by the equation (1.33):

$$L = \frac{V_{in}(V_{out} - V_{in})}{\Delta I_L \times f_{sw} \times V_{out}} \tag{1.40}$$

where:

- V_{in} is the input voltage;
- V_{out} is the desired output voltage;
- f_{sw} is the designed switching frequency;
- ΔI_L is inductor ripple current;

2.3.7.5. Output capacitor selection

The current store to the output circuit is discontinuous. Therefore, to limit the output voltage ripple, a big filter capacitor must be used. When the diode is off, the filter capacitor should supply the output DC to the load.

$$C_{out\_min} = \frac{D \times I_{out\_max}}{\Delta I_{out} \times f_{sw}} \tag{1.41}$$

where

- C_{out_min} is the output capacitance(minimum);
- ΔV_{out} is the ripple of output voltage;
- f_{sw} is switching frequency in kHz;
- I_{out_Max} is maximum output current;
- D is the duty cycle;

The selection of C_{min} must be higher than the calculated value to make sure that the converter's output voltage ripple remains within the specific range and its equivalent series resistance (ESR) should be low. ESR can be minimized by connecting many capacitors in parallel. Therefore, it can be assumed that the ESR is as in equation (1.35):

$$\Delta V_{out\_ESR} = ESR\left(\frac{I_{out\_max}}{1-D} + \frac{\Delta I_L}{2}\right) \approx 0.05\, V_{out} \tag{1.42}$$

2.3.7.6. Input capacitor selection

As stated earlier, the output of the PV voltage has ripples due to the change in temperature and irradiation. Therefore, it is necessary to replace the input capacitor in parallel with the voltage supply to minimize ripples produced by the solar panel. The ripples have an adverse effect on the output as the input voltage is proportional to the output current. Similarly, the output capacitor, ESR on the input capacitor should be considered by selecting a greater capacitor value than the calculated one. Equation (1.44) computes the value of the input capacitor while considering the ripples limit.

$$C_{in} = \frac{\Delta I_L}{8 \times f_{sw} \times \Delta V_{in}} \tag{1.43}$$

where:

$$\Delta V_{in} = ESR \times V_{in} \approx 0.05\, V_{in} \tag{1.44}$$

2.3.8. Maximize the transfer of power from the PV panel to the load

The maximum power point tracking (MPPT) controllers are ensured the optimal operation of a PVG. These controllers are designed to extract and maintain the maximum power from the PV panel at any environmental condition, by matching its I-V operating point with the load characteristic through a DC/DC converter. The maximization of the delivered power can be attained by regulating the PV panel's outputs, voltage or current, to make the converter works at (or near) the maximum

power point (MPP) on the P-V characteristic. Figure 1.22 presents a typical MPPT controller in conjunction with the DC-DC converter.

To make an MPPT analysis, we must know the optimal resistance (R_{mpp}) seen from the PV array, which is defined as the ratio of voltage and current at MPP. Next, the choice of load resistance value depends on the selection of a DC-DC converter. For example, if a Buck converter is used, the impedance of load must be lower than R_{mpp}. Contrary to using a Boost converter, the impedance of load must be bigger than R_{mpp}. In this thesis, a Boost DC-DC converter is used.

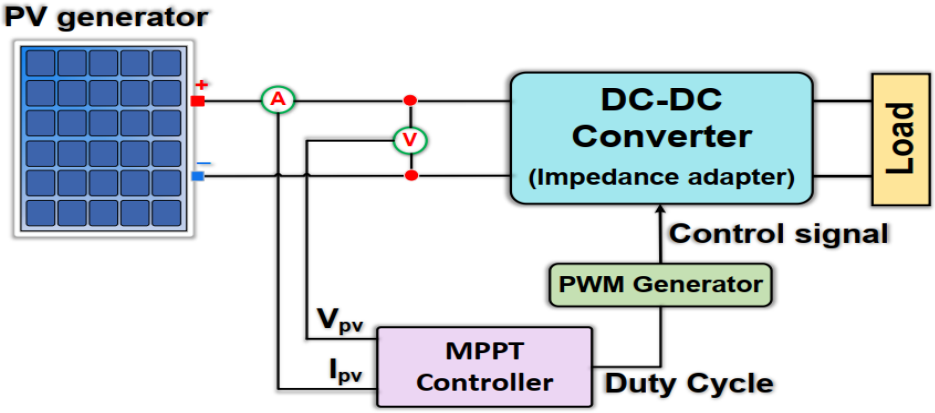

Figure 1.22 Block diagram of MPPT controller

3. Summary

In this chapter, the operation of a PV solar cell has been described and explained. We investigated the modeling of a PV cell and observed its power-voltage and current-voltage characteristics. In order to get the desired output voltage, series-parallel connections must also be made while designing a PV module. Partial shade has a significant impact on the output power of a PV array. This aspect causes a HOT SPOT problem, which leads to irreversible PV module damage. In order to avoid degradation when they are subjected to partial shading, bypass diodes must be used to protect PV modules. Moreover, the PVG and Load adaption phases was discussed in this chapter. This adaption serves as an interface between the PV generator and the load, ensuring that the maximum power generated by the generator is transferred via a control action. The maximum power point tracking (MPPT) controllers provide the optimal operation of a PVG in this situation. This is a device that tracks the voltage (or current) where the most power is generated.

Chapter 2

State of the art of the MPPT algorithms

1. Introduction

Due to the non-linear characteristics I–V of the PV curve, the tracking of the maximum power point (MPP) at various environmental conditions can sometimes be a challenging task. The issue becomes more complicated when the entire PV array is subjected to partial shading. The drawback with the conventional MPPT is that for the majority of the cases, the algorithm is likely to trap at the local peak, simply because it could not differentiate between the local and the global peak. Consequently, it oscillates around the vicinity of the local peak and will remain in that location indefinitely. As a result, significant output power is reduced.

The problem can be overcome by employing improved MPPT methods that can deal with partial shading conditions. Due to its ability to handle multi-modal, non-linear functions, metaheuristics techniques are envisaged to be very effective to deal with such a problem. In recent years, several MPPT algorithms have been proposed to track the maximum power of PV systems operating under partial shading conditions. Even if these algorithms are designed for the same aim, they differ markedly in terms of efficiency, tracking speed, complexity, and cost of the PV systems. Moreover, each method may work best in certain conditions while not in others. For instance, some GMPPT methods yield better performance under simple partial shading conditions (PSCs) but under dynamic change of PSCs, the results are found to be unsatisfactory.

This chapter presents a strategic review of MPPT algorithms that have been prominently used in PV systems. The objective of the review is to provide an overview of various MPPT methods: describing their principles of operations and highlighting their advantages and limitations. This would be useful for a reader who requires a comprehensive background of MPPT methods, as well as keeping abreast with the latest development in this area. Hence, the ultimate goal of this literature review is to search for the gap in the existing methods. This gap shall be the basis for the research that will be conducted in this thesis.

2. Maximum Power Point Tracking: Literature review

MPPT algorithms can be classified into four groups. The first group is the traditional or conventional techniques, which includes Perturb and Observe (P&O), Hill Climbing (HC) and Incremental Conductance (INC) methods, etc. The second group is categorized by MPPT that exploits the characteristics of PV model such as curve fitting, fractional open-circuit voltage, fractional short-circuit current, and numerical calculation-based technique. This is also called as the indirect control methods. The third group is soft computing techniques, which is subdivided into artificial

intelligence, and metaheuristics techniques. The last group is hybrid techniques, which combine soft computing approaches with traditional techniques.

2.1. Group 1: Conventional Techniques

2.1.1. Perturb and observe (P&O)

The P&O method is the most common in the literature due to their simplicity. This approach measures dP/dV while perturbing the operating voltage in the desired direction. If dP/dV is positive, the algorithm gradually increases the voltage towards the MPP until dP/dV is negative. This iteration process is repeated until the algorithm reaches the MPP. When the variation in solar irradiation is considerable, this approach is ineffective. The voltage never reaches an exact value, but fluctuates with a fixed step around the maximum power point (MPP). The downside of this approach is that it oscillates around MPP in the region of MPP, resulting in a steady-state inaccuracy [39]. Low perturbation size values lower steady-state error at the expense of tracking speed. In [40], perturbation size is reduced during the tracking process to mitigate this shortcoming of the P&O approach. The initial perturbation size is 10% of the open-circuit voltage, and it is halved for each perturbation. The steady-state oscillations near MPP are reduced in this way. In addition to [41], updated versions of P&O have been produced in various other research works in an attempt to offset the shortcomings of the original P&O. The flowchart of P&O MPPT algorithm is depicted in Figure 2.1.

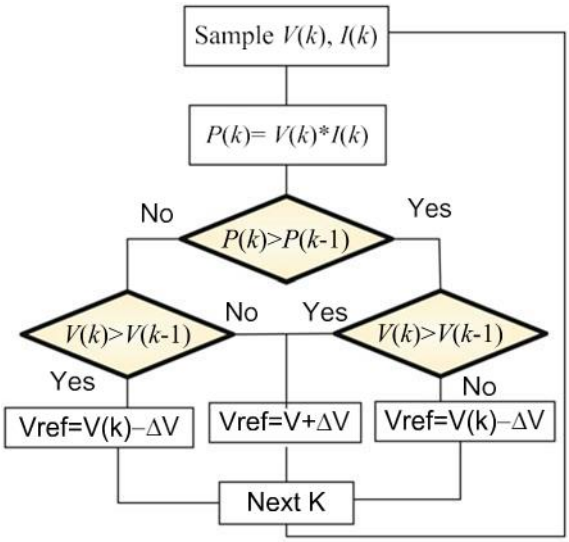

Figure 2.1 Flowchart of conventional Perturb and Observe (P&O) method.

2.1.2. Incremental Conductance (INC)

As previously stated, the P&O approach has two fundamental drawbacks [42]. A minor power fluctuation around the MPP is always present due to a constant amount of disturbance at the steady-

state, which adds to some power losses. In the presence of fast environmental variations, the operating point is most likely to deviate from the true MPP. To overcome the drawback described above, the INC approach was introduced [43-45]. The INC is based on the fact that at MPP, the derivative of (dP/dV) is equal to zero, which can be expressed mathematically by the following equation:

$$\frac{dP}{dV} = \frac{d(IV)}{dV} = V\frac{dI}{dV} + I = 0 \tag{2.1}$$

Where ΔV and ΔI are the increments of PV voltage and current, respectively.

Equation (2.2) can be rewritten as follows:

$$-\frac{I}{V} = \frac{dI}{dV} \cong \frac{\Delta I}{\Delta V} \tag{2.2}$$

The basic idea of INC method is to progressively compare instantaneous conductance with the ratio of derivative of conductance [46]. The working principle of this method can then be derived from the P-V curve, as shown in Figure 2.2 and can be expressed as follows:

$$\frac{dI}{dV} = -\frac{I}{V} \text{ at MPP} \tag{2.3}$$

$$\frac{dI}{dV} > -\frac{I}{V} \text{ at left to MPP} \tag{2.4}$$

$$\frac{dI}{dV} < -\frac{I}{V} \text{ at right to MPP} \tag{2.5}$$

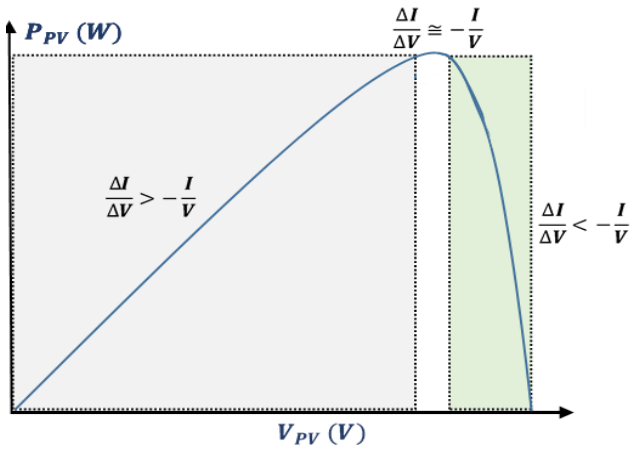

Figure 2.2 P-V characteristics for the basis of INC method.

Hence, the fundamental flow chart of the INC technique is represented in Figure 2.3 using the rules mentioned in equations (2.3)-(2.5).

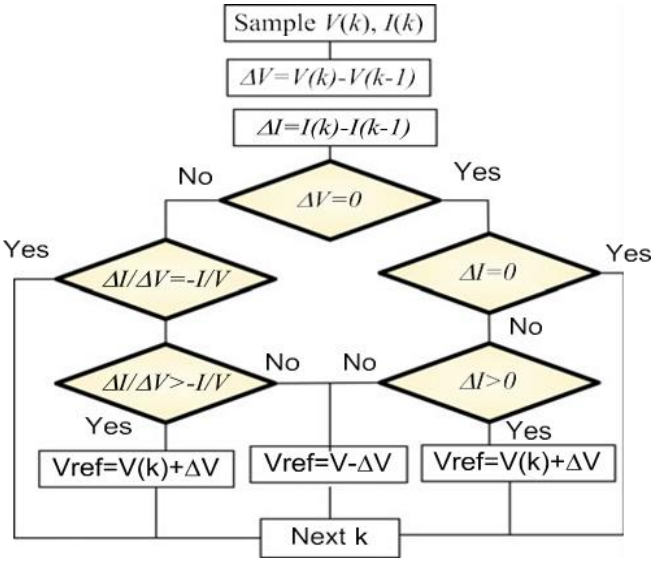

Figure 2.3 The basic flow chart of the voltage based INC method.

INC, like the P&O method, is affected by the perturbation value 'ΔV'. A big 'ΔV' value will result in fast-tracking, although the system may fluctuate at MPP. The incremental conductance ($\Delta I / \Delta V$) is not equivalent to the instantaneous inductance (I/V). A smaller 'ΔV' value, on the other hand, can circumvent this issue, but tracking will become slower. As a result, the trade-off remains, as in the case of the P&O approach. Similarly, the INC technique may be distinguished depending on the fixed and adaptive value of 'ΔV'.

These two methods (P&O and INC) each have their own set of benefits and drawbacks. The choice of the algorithm to use must be determined based on the algorithm's necessity and the operating conditions. P&O is useful, for example, if the needed algorithm is simple and little effort is put into reducing the voltage ripple. The INC technique is acceptable if the algorithm is to produce a defined operating point and the voltage fluctuation around the MPP is to be decreased, but this would make the procedure more difficult and costly. Although traditional approaches are simple to apply, they do not track the true MPP when the partial shading occurs [47].

2.2. Group 2: MPPT based on PV model and PV characteristics

2.2.1. Fractional Open-Circuit Voltage (FOCV)

This technique is based on the relationship between the open circuit voltage (V_{oc}) and the maximum power point voltage (V_{mpp}) as can be seen in equation (2.6).

$$V_{mpp} = K_v \times V_{oc} \tag{2.6}$$

Where K_v is a proportionality that must be determined using the relationship between V_{oc} and V_{mpp} at different levels of insolation and temperature. Generally, the value of K_v has reported to be between 0.71 and 0.84. Thus the open circuit voltage is obtained experimentally and the operating voltage is adjusted to 76% of this value.

2.2.2. Fractional Short-Circuit Current (FSCC)

Similar to FOCV method, this technique is based on the relationship between the open circuit current (I_{sc}) and the maximum power point current (I_{mpp}) as can be seen in equation (2.7).

$$I_{mpp} = K_i \times I_{sc} \tag{2.7}$$

Like K_v, the constant K_i also needs to be determined using the relationship between I_{sc} and I_{mp} at different levels of insolation and temperature. Most of the cases, K_i has been found to be between 0.78 and 0.96.

The main problem of these methods resides in the measurement of I_{sc} or V_{oc} during the MPP operation. An extra switch is added to the power converter which periodically shorts or open the PV module terminal so that I_{sc} or V_{oc} can be measured. However, this additional circuitry increases the components and thus the cost. To avoid extra circuitry, authors in [48] used a boost converter, in which the switch of the converter itself was used to short the PV panel. Despite these efforts, the extracted power is reduced while finding the value of I_{sc} as well as owing to the approximate value of K_i. To address this problem, authors in [49] proposed a compensation approach for K_i that allows the MPP to be better tracked under various environmental conditions.

There is another method which is based on the FOCV or FSCC algorithm called pilot cell. These are discussed in the following subsections [50].

2.2.3. MPPT based curve fitting

The curve fitting method is based on the characteristic curves of the PV module under different conditions in order to find the equivalent polynomial of curve fitting [51, 52]. In general, the curve-based fitting (y=$f(\rho)$) for any curve can be expressed as follows:

$$y\big(f(\rho_N)\big) = \sum_{i=1}^{N+1} C_i x^{N+1-i} \tag{2.8}$$

Where x is the input variable of the system, $Y(\rho_N)$ is the output and $N+1$ is order of the polynomial, and C_i are the coefficient of the polynomial.

To apply the curve-based fitting in MPPT problem to find the MPP [53], power of the PV is described as follows:

$$P = \sum_{i=1}^{N+1} C_i V^{N+1-i} \tag{2.9}$$

For example, where N=3, then the equation is expressed as:

$$P = C_1 V^3 + C_2 V^2 + C_3 V + C_4 \tag{2.10}$$

$$\frac{dP}{dV} = 3C_1 V^2 + 2C_2 V^1 + C_3 \tag{2.11}$$

At MPP the value of $\frac{dP}{dV}$ is equal to zero. The solution of the equation $\frac{dP}{dV} = 0$

$$V = V_{mpp} = \frac{-2C_2 \mp \sqrt{4C_2^2 - 12C_1C_3}}{6C_1} \tag{2.12}$$

Where V_{mpp} is the voltage at Maximum power point, and C_1, C_2, C_3 are the coefficient of the third order polynomial.

This method suffers from many problems such as reducing the convergence time and having low accuracy due to the high mathematical burden. Moreover, under PSC, the P-V characteristic of the PV array becomes more complicated. So, it requires have many weather sensors near to each PV module and it will need too much mathematical operation to get the global peak in the case of PSC, which makes the implementation more complex.

2.3. Group 3: Soft computing Approach

2.3.1. Fuzzy Logic Control (FLC)

One of the soft computing approaches is fuzzy logic control (FLC). The system model is not required while using FLC. This is a significant benefit since it allows for effective handling of variations in operating point, non-linearities, and uncertainties such as unmodeled physical

parameters. Nonetheless, the designer must have some prior knowledge of how the output responds to the inputs qualitatively [54].

Figure 2.4 depicts the process of a typical FLC controller. It involves three main phases: fuzzification, rules inferences and defuzzification. The inputs of the FLC are the error (E) and the error variation (ΔE), defined by equations (2.13) and (2.14), while the output is the duty cycle (D).

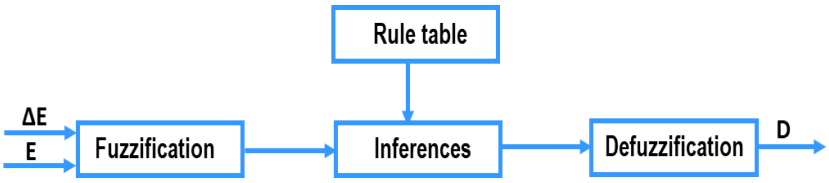

Figure 2.4 Block diagram of Fuzzy logic control (FLC)

$$E(k) = \frac{P(k)-P(k-1)}{V(k)-V(k-1)} \quad Or \quad E(k) = \frac{P(k)-P(k-1)}{I(k)-I(k-1)} \tag{2.13}$$

$$\Delta E = E(k) - E(k-1) \tag{2.14}$$

A. Fuzzification

According to the fuzzy process, each variable utilized in the description of the control rules must be represented in terms of fuzzy set notations with linguistic variables. The membership functions of the input variables E (k) and ΔE (k) and the output variable D (K) are shown in Figure 2.5. As shown in this figure, each of the membership functions can be assigned to five fuzzy sets, namely PB (Positive Big), PS (Positive Small), ZE (Zero), NS (Negative Small) and NB (Negative Big).

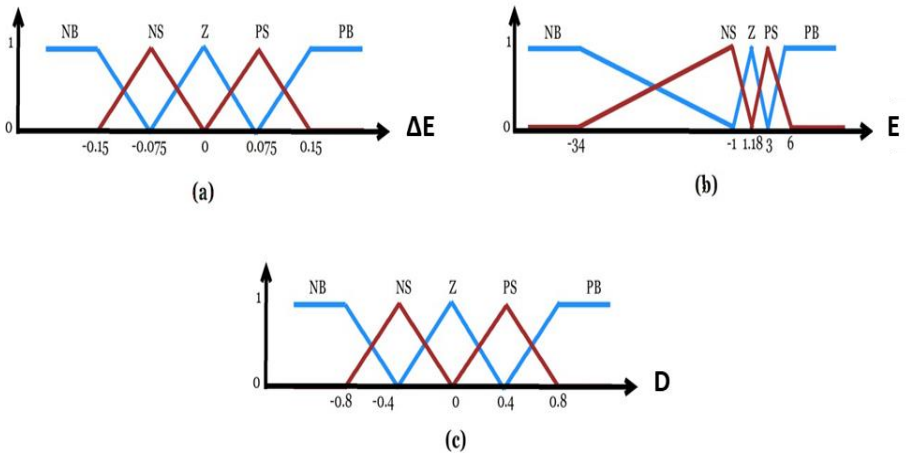

Figure 2.5 Fuzzy membership functions (a) of the error variation CE, (b) of the error C, (c) of the duty cycle D.

B. Rules inferences and rule table

Fuzzy inference is the mapping process of a given input to an output based on the truth table shown in Table 2.1. The error E and error variation ΔE are generally the inputs to the FLC-based MPPT controller and can be calculated using equations (2.13) and (2.14).

Table 2-1 Fuzzy rule table.

		Error (E)				
		NB	***NS***	***ZE***	***PS***	***PB***
Error variation (CE)	***NB***	***PB***	***PB***	***PS***	***PB***	***PB***
	NS	***PB***	***PS***	***PS***	***PS***	***PB***
	ZE	***NS***	***NS***	***ZE***	***PS***	***PS***
	PS	***NB***	***NS***	***NS***	***NS***	***NB***
	PB	***NB***	***NB***	***NS***	***NB***	***NB***

C. Defuzzification

In the defuzzification process, the linguistic variable is re-converted to a numerical variable. The output variable is linguistically defined in terms of the duty cycle, as shown in Figure 2.5. There are many defuzzification methods, such as Bisector of Area (BoA), Mean of Maxima (MoM), Centre of Gravity (CoG) and Centre of Gravity for Singleton (CoGS), and they differ in accuracy and computational intensity [55]. The center of gravity (CoG) is the most commonly used method and is represented by the following equation:

$$\mu = \frac{\sum_{i=1}^{n} \mu(x_i).x_i}{\sum_{i=1}^{n} x_i} \tag{2.15}$$

Where n is the number of output membership function, $\mu(x_i)$ is the degree of membership function and x_i is the peak location of the membership function.

The dynamic performance of FLC is particularly efficient when compared to previous MPPT algorithms [56]. Furthermore, FLC provides a wide range of control parameter tuning options. This enables simple adjustments, making it compatible with many linear and non-linear controllers [57].

2.3.2. Artificial Neural Network (ANN) based MPPT

An artificial neural network (ANN) is a set of processing units called neurons. ANNs are increasingly used in various fields to solve real-life engineering problems. They have the advantage of handling engineering problems with a greater degree of complexity thanks to interrelated parameters and acting as a black box, requiring no particular information about the system's performance. As shown in Figure 2.6, the operating principle of this method is based on establishing relationships between input and output variables by analyzing previously stored data.

The ANN structure can be divided into three layers as follows:

- ✓ **Input layer**: The input variables of this layer are the irradiation G and temperature T.
- ✓ **Hidden layer**: This layer constitutes the heart of the neural network. In this layer, the output of the first layer goes through a non-linear function, called the activation function of the neuron, to generate the final output.
- ✓ **Output layer**: In this layer, the output of the second layer is mapped into a duty cycle D using a linear activation function.

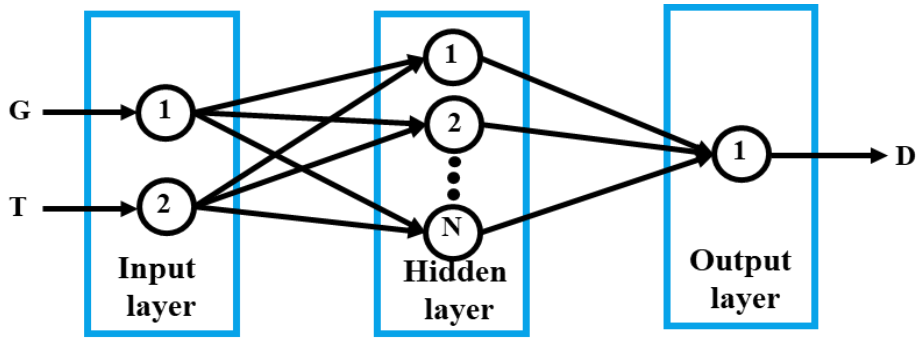

Figure 2.6 A typical three layer feed-forward ANN structure.

The ANN method has an excellent performance in the identification and prediction of unknown parameters, which has strongly encouraged researchers to use it for MPPT controllers. Irradiation and temperature can be used as inputs to the ANN-based MPPT controller, and the duty cycle is the controller output. The MPPT's tracking performance (accuracy and speed) is determined by the used hidden layer approach and the ANN's suitable training method [58, 59].

To effectively track the MPP, the weights assigned in the ANN method must be carefully calculated through a comprehensive learning process. As a result, the PV array must be rigorously evaluated over several months or even years. The resultant patterns between the ANN's inputs and outputs are then saved. Once the ANN is fully trained, it can estimate the MPP and provide the MPPT controller with a reference value (duty cycle).

2.3.3. Metaheuristic approach (Evolutionary computation)

Metaheuristic approaches have been widely used because of their potential to handle nonlinear functions without the need for derivative information. They are stochastic optimization methods that seem to be very effective in optimizing multimodal real-valued objective functions [60, 61]. With these advantages, a meta-heuristic algorithm is considered to be very efficient in dealing with the MPPT issue. Because this approach is based on search optimization, it should be able to find the suitable MPP for any type of P-V characteristics regardless of environmental variations.

Particle swarm optimization (PSO), Artificial Bee Colony (ABC), Whales Optimization Algorithm (WOA), Grey wolf optimization (GWO), and Ant Colony Optimization (ACO) are examples of metaheuristic methods that have been identified in the literature. The most widely used meta-heuristic method in the MPPT problem is PSO and this is owing to its simple structure, easy implementation and high response time [62-64].

A. Particle Swarm Optimization based MPPT

PSO is the most widely used metaheuristic optimization technique in PV systems for MPPT operating under PSCs. It is based on the flocking behavior of birds [65]. It uses NP particles to search within the search space. The particles are seeded at random. Each particle's best location is referred to as its personal best. The position vector of personal best is indicated by P_i for the ith particle, and its associated objective value is denoted by P_{best}. The best position reached by the whole swarm is referred to as the global best. It is represented by G_{best}, while the related objective value is represented by G_{best}. PSO remembers all particles' personal bests as well as the global best [66]. The velocities and locations of all particles are updated at each iteration t. The general idea of particles movement in PSO is shown in Figure 2.7.

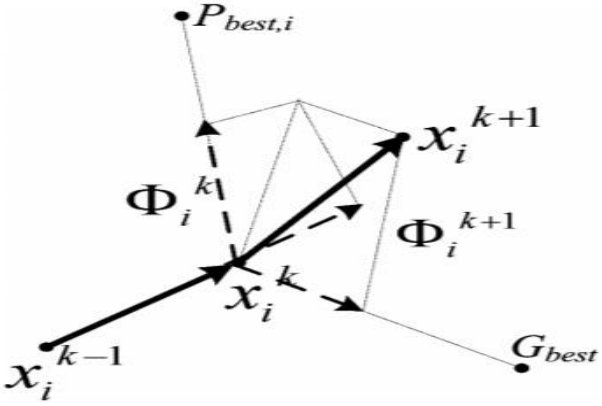

Figure 2.7 The particles movement in PSO.

The individual particles position is defined by:

$$x_i^{k+1} = x_i^k + \emptyset_i^{k+1} \tag{2.16}$$

where the velocity component Φ_i is the step size and is calculated as follows:

$$\emptyset_i^{k+1} = \omega\emptyset_i^k + C_1 rand(0,1)\left(P_{best,i} - x_i^k\right) + C_1 rand(0,1)\left(G_{best} - x_i^k\right) \tag{2.17}$$

where C_1 and C_2 are the acceleration coefficients, $P_{best,i}$ is the best own position of the particle i, G_{best} is the neighborhood best position of particle *i* and ω is the inertia weight. The latter has an important role in the balance between global and local search, where a large makes the global search easier while a small one improves local search. It can be a positive constant or a positive decreasing linear function of iteration index *K*.

To apply the PSO algorithm in MPPT problem to find the global MPP, parameters of the PSO algorithm need to be specified. These parameters include the inertia weight, acceleration coefficients, swarm size and maximum iterations. The algorithm then initializes a solution vector of duty cycles and transmits duty cycles to the power converter. In the first iteration, these duty cycles act as the initial particles. Particles are all moving towards P_{best}, their local best position. One of these particles is the global best G_{best}, which provides the best fitness value. A new position of the duty cycle is obtained after computing the velocity, which acts as a perturbation to the duty cycle. All particles advance towards the global best position with each iteration. Here is the detailed pseudo-code of the PSO algorithm:

Begin

Step1: Setting values of the control parameters of PSO algorithm inertia weight ω; acceleration coefficients C_1 and C_2; swarm size *N*; and maximum iterations number Max_generation.

Initialization

Step2: Set the generation number cycle =0; Initialize a population of N particles; Initialize ϕ_i^k of the particles.

Repeat

Step3: Calculate $P_{best,i}$ and G_{best}

Step4: Evaluate the fitness of particles.

Step5: For each particles {

Calculate its new velocity by (equation (2.17))
Update its position by using (equation (2.16)))

}

Step6: Increase the generation count : cycle = cycle +1

Until

Step7: The stopping criterion is satisfied.
And

The flowchart of the PSO algorithm is show in figure (2.8)

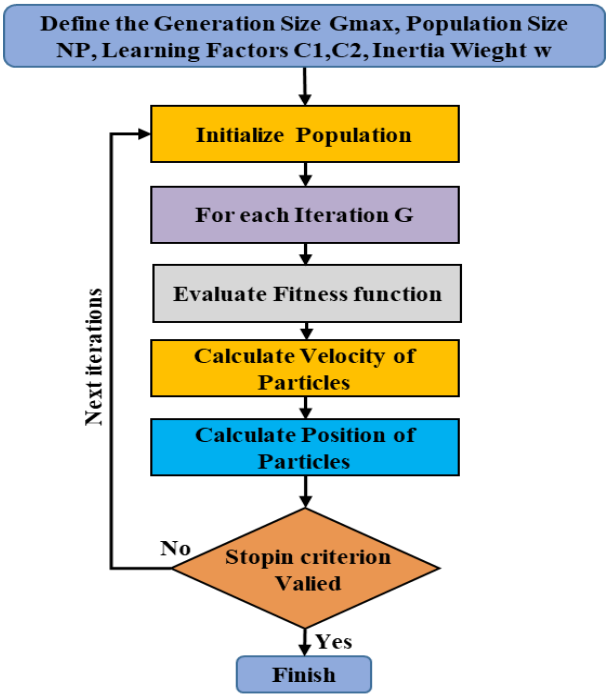

Figure 2.8 Flowchart of the PSO algorithm.

Despite its strengths such as simplicity, great exploitation capacity, and a limited number of control parameters, PSO has limited exploration capacity to find the global optimum in complex multimodal optimization tasks with multiple local optima. [67]. As a result, for MPPT under partial shading circumstances, traditional PSO cannot provide a global optimum and is seldom employed to address this issue. Therefore, many research efforts are being made to improve the exploration capabilities of PSO and enable it to successfully handle MPPT in partial shading situations. Many improved variants have been proposed in the literature, such as improved particle swarm optimization (IPSO) [68], leader particle swarm optimization (L-PSO) [69], deterministic particle swarm optimization (DPSO) [70], and modified particle velocity-based particle swarm optimization (MPV-PSO) [71].

B. Artificial Bee Colony (ABC) based MPPT

The ABC algorithm is a swarm-based algorithm that was developed to solve multidimensional and multimodal optimization issues. It is based on Tereshko and Loengarov's model for the foraging behavior of bee colonies [72, 73]. In the ABC algorithm, the artificial bees are divided into three

groups: employed bees, onlooker bees and scouts. An employed bee is one that is currently looking for food or exploiting a food source. An onlooker bee is one that is waiting in the hive to make a decision to choose a food source. Employed bees that cannot enhance their food sources via a predefined number of trials become scouts, and their food sources are abandoned. The number of food sources is the same as the number of employed bees and also the same as the number of onlooker bees. Similarly, in the optimization context, the position of a food source is a candidate solution to the optimization issue, and the nectar amount of a food source represents the quality (fitness) of the associated solution.

During the initialization phase, the ABC algorithm creates a randomly distributed initial population of SN solutions. According to the equation below, each solution is generated within its parameters:

$$x_i^j = x_{min}^j + rand(0,1)\left(x_{max}^j - x_{min}^j\right) \; ; \; i = 1, 2, \dots, SN \; and \; j = 1, 2, \dots, D \qquad (2.18)$$

where SN represents the number of candidate solutions and D is the number of optimization parameters.

After the initialization phase, the population of the solutions is subjected to repeated cycles from 1 to a maximum cycle number (MCN), of the search processes of the employed bees, the onlooker bees, and the scout bees. For every cycle, each employed bee produces a new solution V_{ij} using the equation (2.19) and then evaluates its fitness:

$$v_{ij} = x_{ij} + \emptyset_{ij} \, (x_{ij} - x_{kj}) \qquad (2.19)$$

Where Φ_{ij} is a random number between [-1, 1], and k ϵ{1, 2, …SN} are j ϵ{1, 2, …D} randomly chosen index. *K* has to be different from.

Once the information is shared by the employed bees, each onlooker finds a new solution v_{ij} in the neighborhood of x_i according to equation (2.20) and by using the probability P_i which is defined by the following equation:

$$P_i = \frac{fit_i}{\sum_{n=1}^{SN} fit_n} \qquad (2.20)$$

where fit_i represents the fitness value of the solution x_i.

Each produced candidate solution V_{ij} whose value is beyond the bounds of the allowable search space is updated to be inside these bounds. Each newly created candidate solution is compared to its previous one in terms of fitness. If the new solution is as good as or better than the previous one in terms of fitness, it takes its position in the memory. If not, the old solution is kept in memory. In other words, in the selection procedure between the old and the candidate, a greedy selection mechanism is used. If the fitness of a solution cannot be improved after each search cycle, and the preset number of trials, known as the "limit," has been reached, the solution will be abandoned by the scout bee, and a new solution will be randomly found. The equation (2.14) will be used to get the new solution x_{ij}. From the above, it is clear that the fundamental ABC algorithm has three control parameters: SN, "limit," and MCN. The basic flowchart of the ABC algorithm is shown in Figure 2.9.

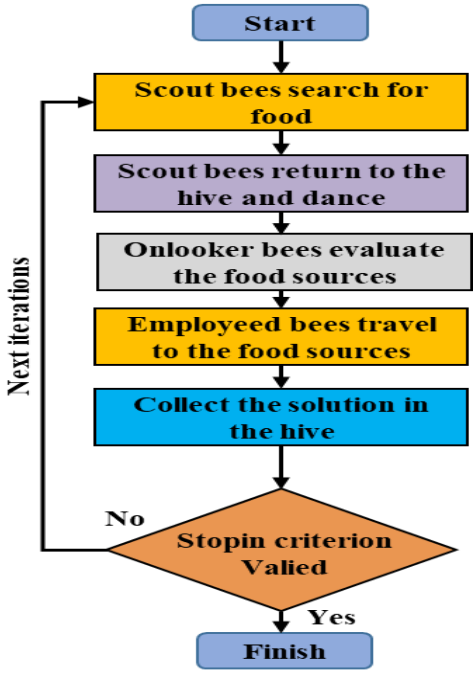

Figure 2.9 Flowchart of the ABC algorithm.

In this paper [74], the authors have proposed an ABC-based MPPT by using a direct duty cycle control method for PV systems operating under partially shaded. This algorithm has been compared with the PSO-based MPPT algorithm. It was mentioned that the convergence of the PSO-based MPPT algorithm is dependent on the initial condition of the particles. For this reason, an ABC-based MPPT algorithm is introduced to avoid this limitation of the PSO algorithm.

C. Whales Optimization Algorithm (WOA) based MPPT

WOA is a new meta-heuristic optimization algorithm that imitates the hunting process of humpback whales, which is also known as bubble-net feeding method [75, 76]. The research agents (whales) follow the prey at random in relation to each research agent's position. As shown in

Equations (2.21)–(2.23), this behavior is based on a shrinking encircling approach and a spiral updating position [77].

$$X(T+1) = \begin{cases} X(T) - \vec{A}\vec{D} & if \quad p < 0.5 \\ D.e^{al}.\cos(2\pi l) + X(T) & if \quad P \geq 0.5 \end{cases} \tag{2.21}$$

$$\vec{D} = \left|\vec{C}\vec{X}(T) - \vec{X}(T)\right| \tag{2.22}$$

$$\vec{A} = \vec{a}\vec{C} - \vec{a} \tag{2.23}$$

Where x^* is the best solution position, D is the distance between whale and prey, A and C are Coefficient vectors, a is a random vector, l is a random number and T is the iteration.

Figure 2.10 depicts the basic flowchart for the WOA.

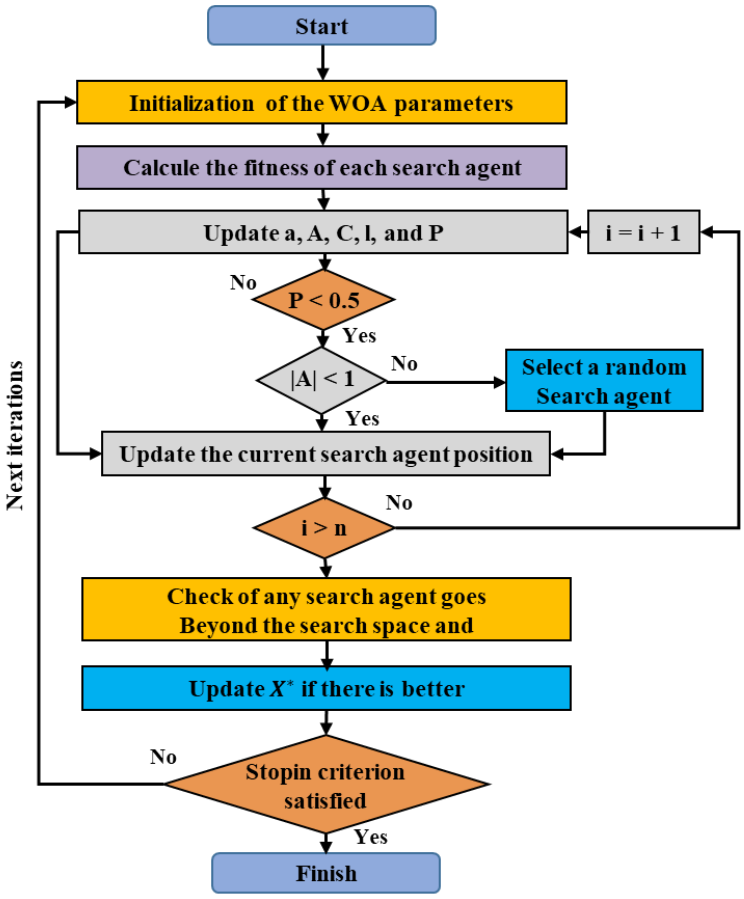

Figure 2.10 Flowchart of the WOA algorithm.

In [78], a new WOA-based MPPT system has been designed with the purpose of analytically modeling PV systems with series and parallel resistors tracked by MPP under PSC. According to the results obtained under different shading patterns, the WOA has shown satisfactory accuracy and tracking speed in tracking the MPP.

D. Grey Wolf Optimization (GWO) based MPPT

GWO is a bio-inspired optimization technique proposed by Mirjalili et al in [79]. This technique is designed according to the social behaviour of grey wolves to attack preys for hunting process in nature, as shown in Figure 2.11. A swarm is a group of grey wolves that can effectively attack preys by establishing a dominant social hierarchy. There are four levels of wolves in the GWO algorithm: alpha wolves, beta wolves, delta wolves, and omega wolves. The alpha wolves are the leaders (consider as the fittest solution). The beta and delta wolves represent the second-best and third-best solution, respectively. While, the remainder of the solutions are named omega. The candidate solutions represented by alpha, beta and delta wolves has not been changed. Contrariwise, the value of the omega wolves must be submitted to all the other dominant wolves.

The main steps of GWO algorithm consists of three phases:

- ✓ **Encircling prey**: the grey wolves encircle prey. This phase can be described by the following equations [80]:

$$\vec{D} = \left|\vec{C}\,\overrightarrow{X_p}(t) - \vec{X}(t)\right| \tag{2.24}$$

$$\vec{X}(t+1) = \overrightarrow{X_p}(t) - \vec{A}\,\vec{D} \tag{2.25}$$

Where,

$$\vec{A} = 2\vec{a}\,\overrightarrow{r_1} - \vec{a} \tag{2.26}$$

$$\vec{C} = 2\overrightarrow{r_2} \tag{2.27}$$

- ✓ **Hunting**: this operation is guided by alpha (α), beta (β) and delta (δ), as they have a better knowledge of the likely location of the optimal solution. The value of the omega wolves are must submit to all the other dominant wolves. The following equation is used to determine the search agent's updated position [80]:

$$\overrightarrow{D_\alpha} = \left|\overrightarrow{C_1}\,\overrightarrow{X_\alpha} - \vec{X}\right|, \overrightarrow{D_\beta} = \left|\overrightarrow{C_2}\,\overrightarrow{X_\beta} - \vec{X}\right|, \overrightarrow{D_\delta} = \left|\overrightarrow{C_3}\,\overrightarrow{X_\delta} - \vec{X}\right| \tag{2.28}$$

$$\overrightarrow{X_1} = \overrightarrow{X_\alpha} - \overrightarrow{A_1}\,\overrightarrow{D_\alpha}\ , \overrightarrow{X_2} = \overrightarrow{X_\beta} - \overrightarrow{A_2}\,\overrightarrow{D_\beta}\ , \overrightarrow{X_3} = \overrightarrow{X_\delta} - \overrightarrow{A_3}\,\overrightarrow{D_\delta} \tag{2.29}$$

$$\vec{X}(t+1) = \frac{\overrightarrow{X_1} + \overrightarrow{X_2} + \overrightarrow{X_3}}{3} \tag{2.30}$$

- ✓ **Searching for prey and attacking prey**: The GWO algorithm ensures a correct balance of exploration and exploitation. During exploration, the GOW algorithm must satisfy the condition |A| > 1, move in the direction of the best Neighbors (diverge from the prey). When |A| < 1 the GWO devoted to exploitation (converge to the prey).

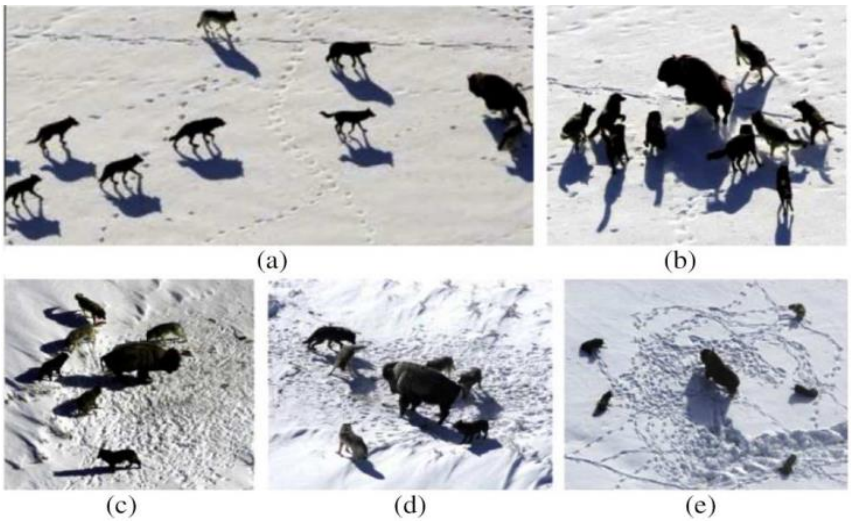

Figure 2.11 Hunting behavior of grey wolves: (a)–(c) chasing and tracking prey; (d) encircling prey; and (e) attacking prey method.

The flowchart of the GWO algorithm is shown in Figure 2.12.

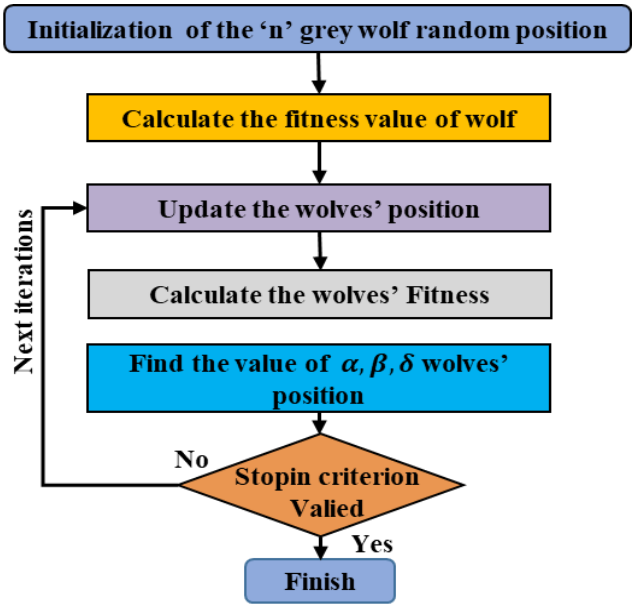

Figure 2.12 Flowchart of GOW algorithm.

Figure 2.13 shows the block diagram of the GWO based MPPT. For number of grey wolves, i.e., duty ratios, the controller measures V_{PV} and I_{PV} using voltage and current sensors and then calculates the output power. During partial shading, the P–V curve is characterized by multiple peaks with many local peaks (LPs) and one as a global peak (GP). It's worth noting that after the wolves locate the MPP, which is the GP, their associated coefficient vectors approach zero [81]. In this method, an attempt is made to combine GWO with direct control of the duty cycle, i.e., the duty cycle is held constant at the MPP, which reduces the steady-state oscillations that exist in traditional MPPT algorithms and, as a result, the power loss due to oscillation is reduced, improving the system's efficiency.

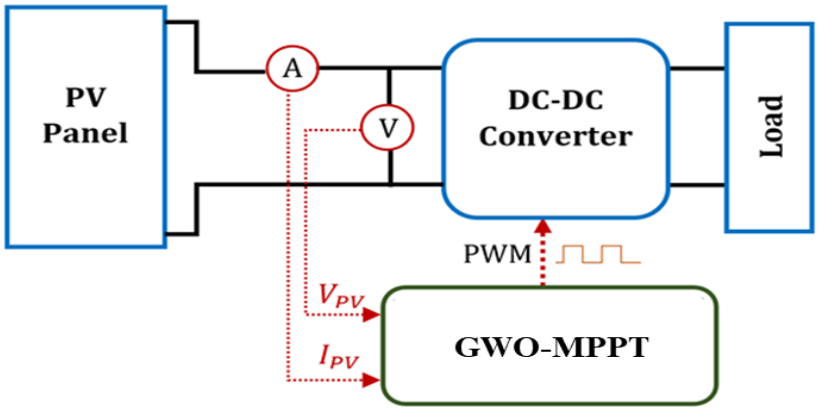

Figure 2.13 Block diagram of the GWO-MPPT method.

The new duty cycle is specified as a grey wolf. As a result, equation (2.31) can be modified as follows:

$$D_i(K+1) = D_i(k) - A.D \tag{2.31}$$

Accordingly, the fitness function of the GWO algorithm can be expressed as:

$$P\left(d_i^k\right) > P(d_i^{k-1}) \tag{2.32}$$

Where P is the output power, d is duty cycle, i is the number of current grey wolves, and k is the number iterations.

E. Ant Colony Optimization (ACO) based MPPT

The ACO algorithm mimics the foraging behaviour of ants to locate the optimum in the search space, and it can update the command value instantly in response to changing environmental variables [82]. Furthermore, as compared to PSO, ACO can reduce the number of LMPPs on the current-voltage (I-V) curve, making it ideal for both centralized and distributed MPPT controllers. Another benefit of ACO is that its convergence does not depend on the primary location of the samples [83]. It is worth noting, however, that when ants are created away from GMPP, the likelihood of being

caught at LMPPs is increased. ACO's global search ability is greater than that of certain clever algorithms such as PSO, but it still has a few flaws such as a weak local search ability and a lack of an effective acceleration mechanism.

2.4. Group 4: Soft computing Approach

2.4.1. Hybrid DEPSO method

The DEPSO is a hybrid method that combines PSO and Differential evolution (DE), in which a sequential mathematical model is used to explain the behaviors of PV systems under PSC [84]. It combines solution operators with the PSO algorithm to improve solution diversity, allowing it to avoid getting stuck at a local optimal solution. According to Equation (2.33), the following criteria must be met for the algorithm to be re-initialized:

$$\left|\frac{P(t+1)-P(t)}{P(t)}\right| > \Delta P \tag{2.33}$$

This performance of this method is unaffected by the initial value. But, it is extremely dependent on the parameters of PSO algorithm.

2.4.2. Artificial Bee Colony and P&O algorithm

The authors of [85] propose a hybrid algorithm for MPPT of PV systems under PSC that uses the ABC and P&O algorithms. In the hybrid ABC-P&O , the ABC algorithm is first used to track GMPP, and then the P&O algorithm is used to track LMPP, which successfully combines the P&O algorithm's high local searching ability with the ABC algorithm's global searching ability to provide the best duty cycle for the boost converter [86]. Figure 2.14 shows the flowchart of the ABC-P&O algorithm. The ABC- P&O algorithm can achieve accurate tracking performance while also being efficient and fast.

2.4.3. Hybrid GWO and FLC method

The hybrid GWO and FLC method is an intelligent computing method that may prevent confusion in the transfer of uniform to non-uniform insolation [87]. The FLC is used to attenuate oscillations around the GMPP and GWO is utilized to catch it. When compared to traditional GWO and P&O methods, the hybrid method has higher tracking capability, faster convergence speed, and higher efficiency. Although this approach has a higher tracking accuracy, it is more sophisticated and requires more computational time.

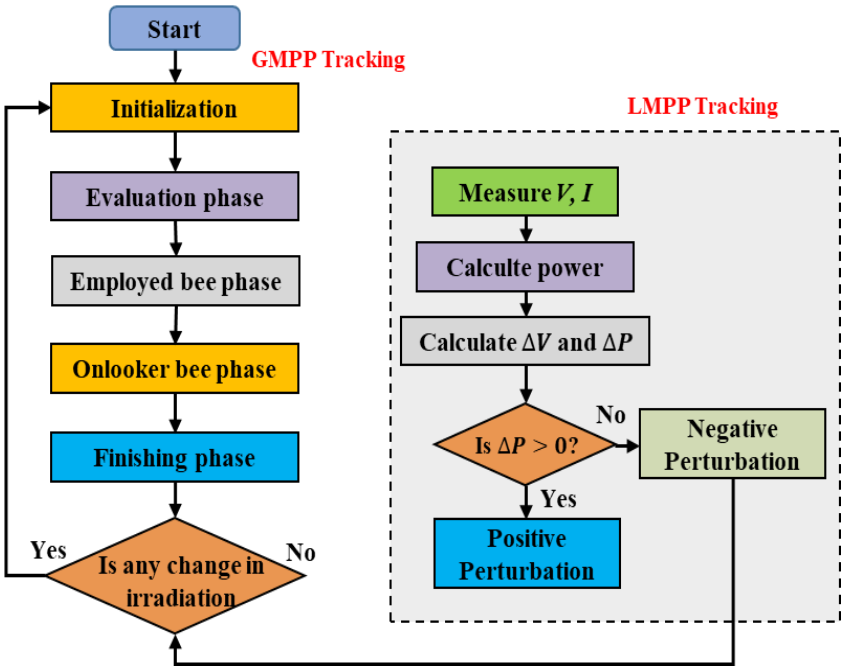

Figure 2.14 Flowchart of ABC-P&O algorithm.

3. Recapitulation

As a reminder, the soft computing methods such as Artificial Neural Networks (ANN), Fuzzy Logic Control (FLC), and evolutionary computation (EC) have emerged as powerful optimization algorithms for solving complex problems and providing optimal solutions. Parallel, dynamic, decentralized, asynchronous and self-organizing behaviour of the soft computing algorithms are best suited for optimization applications [88, 89]. The effectiveness of soft computing methods in handling nonlinear problems, such that encountered in PV array behaviour, and their implementation simplicity make them very attractive to solve the MPPT problem of PV systems, especially in the case of partial shading and module mismatches [90]. Artificial Neural Networks, is one of the soft computing methods that was used in MPPT algorithms. Typically, they were used to estimate the MPP with respect to the randomly changing weather conditions [91], and to improve the P&O and IC algorithms [92]. It is known that using ANN with larger number of hidden nodes leads to more accurate results, but at the expense of longer computational time and complex hardware implementation. Evolutionary computation techniques such as Differential Evolution (DE) [93], has been also proposed to deal with the MPPT problem. However, EC techniques might present a poor convergence rate and slow convergence time [94, 95]. The metaheuristics techniques have a good convergence rate and fast convergence compared to EC techniques, although they may have more parameters to determine, which makes them inflexible and complex [96]. At last, in this chapter a comparative assessment of

the most MPPT used has been done on the following criteria: GMPP tracking ability (The MPPT method can operate at MPP or not under PSC), tracking Speed, sensors used, Steady state oscillations level, algorithm complexity and efficiency. Comparison of MPPT methods according to these criteria is presented in Table 2.2

Table 2-2 Review of the most used MPPT algorithms.

Category of MPPT	MPPT algorithms	Convergence speed	Tracking Efficiency	Steady-state oscillations	No of Sensors	Implementation Complexity	GMPP tracking ability
Group 1: Conventional Techniques	**P&O method**	Low	Low	High	2	Low	No
	Incremental conductance method	High	High	Low	2	Moderate	No
Group 2: MPPT based on PV model and PV characteristics	**Fractional open circuit voltage**	High	Low	Low	3	Low	No
	Fractional Short Circuit Current	High	Low	Low	3	High	No
	Curve-Based fitting MPPT	Moderate	Low	Low	4	Moderate	No
Group 3: Soft Computing Approach	**Fuzzy logic**	High	High	Low	2	High	No
	Neural network	High	Moderate	Low	3	High	No
	PSO based MPPT	High	High	Low	2	High	Yes
	ABC based MPPT	Moderate	High	Low	2	High	Yes
	WOA based MPPT	Moderate	High	Moderate	2	High	Yes
	GWO based MPPT	High	High	Moderate	2	Moderate	Yes
	ACO based MPPT	Moderate	Moderate	Low	2	Moderate	Yes
Group 4: Hybrid MPPT algorithms	**Hybrid DEPSO method**	High	Very High	Moderate	2	High	yes
	ABC and P&O algorithm	Moderate	High	Moderate	2	High	yes
	Hybrid GWO and FLC method	High	Very High	Low	2	High	Yes

4. Summary

In this chapter, a state of the art of the most MPPT algorithms used for tracking the MPP of PV system systems has been given and discussed. These techniques can be classified into four groups. The first group is the traditional or conventional techniques. The second group is categorized by MPPT which exploits the characteristics of the PV model. This is also called as the indirect control method. The third group is soft computing techniques, which are subdivided into artificial intelligence, and metaheuristics techniques. The last group is hybrid techniques, which combine soft

computing approaches with traditional techniques. Based on the review, all methods have their own advantages and disadvantages. Some of the methods show very effective results such as hybrid techniques but the methodologies used were complicated. The methods which are simple in implementation such as P&O and INC method. But, under PSCs these conventional method fail to differentiate between a GMPP and a LMPP, as they converge on the MPP that makes contact first, which in most cases is one of the LMPPs. This results in considerable energy loss. To overcome this problem, many metaheuristic techniques have been proposed. The most popular technique is the Particle Swarm Optimization (PSO) technique. The main problem of PSO technique is that the improvement of convergence time will increase the failure rate and oscillations at steady state. Therefore, in this thesis, an improved scanning method is proposed, the latter overcome reduce and limit the scan interval and memorizes all the peaks to get the global peak which is the GMPP. This modification improves the response time of the PV system compared to the conventional scanning method. Also, the simple structure used in this proposed method will ensure reduced complexity of implementation, which reduces the cost of the PV system.

On the other side, if minimizing the cost is not more important than guaranteeing a very high level of robustness and efficiency of the PV system, it is required to use a powerful method. Therefore, this thesis introduces a new SOA-based metaheuristic MPPT method for tracking the GMPP to maximize the PV power output in PV systems operating under both uniform and partial shading conditions. This method is considered best suited for real engineering problems compared to another metaheuristic algorithm. The MPPT's speed and efficiency will be considerably improved.

Chapter 3

Development of an improved GMPPT based on Scanning method for PV system operating under a dynamic partial shading condition

1. Introduction

As presented in chapter 2, the partial shading of the PV array is a major problem for the PV systems [4]. Therefore, the P-V characteristic of a PV array becomes more complicated due to the presence of more than one power peak in contrast to normal conditions (without shading) where there is only one peak named Maximum Power Point (MPP) [97]. Conventional methods are unable to find the global MPP (GMPP) under partial shading conditions (PSCs) due to multi-peaks exhibited in the P-V curve. Furthermore, due to the inability to track the real MPP (GMPP) under PSC, the power output of the PV array can be reduced by 10-70% [98]. To address this problem, many GMPPT algorithms have been introduced in chapter 2 to solve the complexity of the nonlinear behavior of PV characteristics and providing optimal solutions under partial or full shading conditions. Where we find most of them belong to soft computing, metaheuristic techniques, and hybrid techniques [99]. Even if these algorithms are designed for the same aim, they differ markedly in terms of efficiency, tracking speed, steady state oscillations, complexity, cost and range of effectiveness. Moreover, each method may work best in certain conditions while not in others. For instance, the hybrid MPPT methods yield better performance under PSC. But, this methods requires hardware with high specifications, high on complexity.

In this chapter, we propose a simple method to find the GMPP. This method scans the P-V curve and memorizes all the peaks in order to get the global peak. Next, we control a boost DC-DC converter to extract the GMPP from the PV system. Yet, this method is simple and easy to implement in low-cost microcontrollers. But, under storing all the possible MPPs, this method takes a long processing time as the scan is started from the point of the short-circuit current (I_{CC}) to the open-circuit voltage (V_{OC}) of the P-V characteristic. Hence, this technique interrupts the system operation when scanning the entire control range between the V_{OC} and I_{CC}, which yields power losses. To address this problem, an improved scanning method to track the GMPP with good tracking speed is introduced also in this chapter. The objective of this method is to reduce the response time by limiting the search interval of scan points in the scanning method, which makes the tracking of GMPP fast and efficient under PSCs. The effectiveness of the improved scanning method is verified using a PV simulator. This PV system simulators contains a real microcontroller, as can be found in reality, so that same code for the MPPT algorithm used in the simulation can be used in real implementation.

2. Investigation of partial shading conditions on a photovoltaic array's characteristics

Figure 3.1 shows the configuration of the PV array under consideration, which was composed of six PV panels connected in series and having the same characteristics. The P-V characteristic of the PV array's for three different tests, including the uniform and non-uniform irradiance conditions for STC (all PV panels received the same solar irradiation of 1000 W/m²) and for two shading scenarios as shown in figure (3.2). The first test of the shading scenarios was performed with an irradiance value of 100 W/m^2 for five shaded PV panels and 300 W/m^2 for the remaining unshaded PV panel, while the second test was performed with an irradiance value of 100 W/m^2 for three shaded PV panels and 700 W/m^2 for the other unshaded PV panels. From this figure, the P-V curve showed only one peak point under STC, while it showed two peaks for both shading scenarios. Each of these peaks was characterized by its own voltage and power: Vmpp1 and Pmpp1 for the first peak and V_{mpp2} and Pmpp2 for the second one. While the largest value between Pmpp1 and P_{mpp2} represents the GMPP, which sometimes existed in area 1 and other times in area 2.

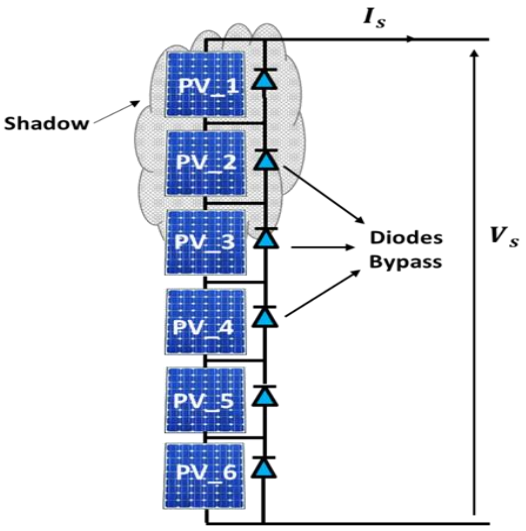

Figure 3.1 PV array with three PV panels exposed to shade.

To apprehend the current flow direction of the PV array under PSC, consider the PV array shown in Figure 3.3 consists of six PV panels, three of which are unshaded, while the others are shaded. In addition, as shown in Figure 3.2, the P-V curve of the PV array under PSC could be divided into two areas. In area 1, the bypass diode of each shaded PV panel is conducted as a short circuit. Figure 3.3(a) depicts the equivalence diagram of the current flow direction of the PV array when the load demanded more than the current value of the shaded PV panels.

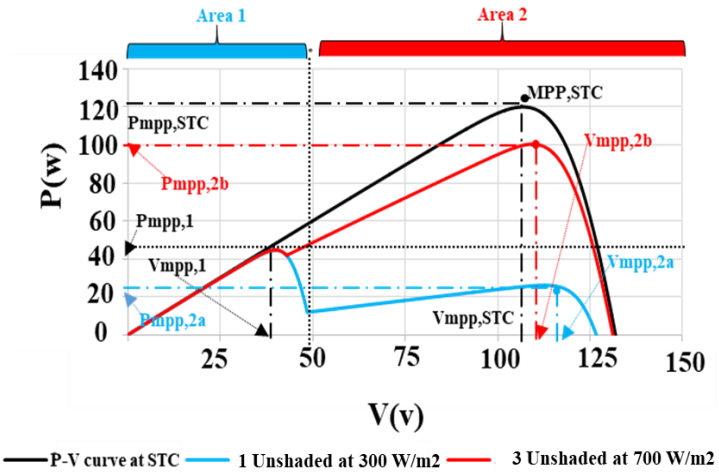

Figure 3.2 P-V curves of PV array for STC and for two shading scenarios.

Therefore, the equation of V_{mpp1} can be expressed mathematically as follows [100]:

$$V_{mpp1} = (N_s - N_{sh}) * V_{mpp,STC} - \Delta V_D * N_{sh} \quad (3.1)$$

where V_{mpp1} is the voltage at the first peak, N_s is the number of PV panels, N_{sh} is the number of shaded panels, and $V_{mpp,STC}$ is the voltage at the MPP of the PV array under STC. Concerning the forward voltage drop ΔV_D a typical value of 0.7-0.8 is sufficiently accurate.

By contrast, in area 2, the bypass diodes of all PV panels were not conducting. Figure 3.3(b) depicts the equivalence diagram of the current flow direction of the PV array when the load demanded less than the current value of the shaded PV panels. Therefore, the equation of V_{mpp2} can be expressed mathematically as follows:

$$V_{mpp2} = N_{sh} * V_{mpp,STC} \quad (3.2)$$

where V_{mpp2} is the voltage at the second peak. N_s is the number of PV panels.

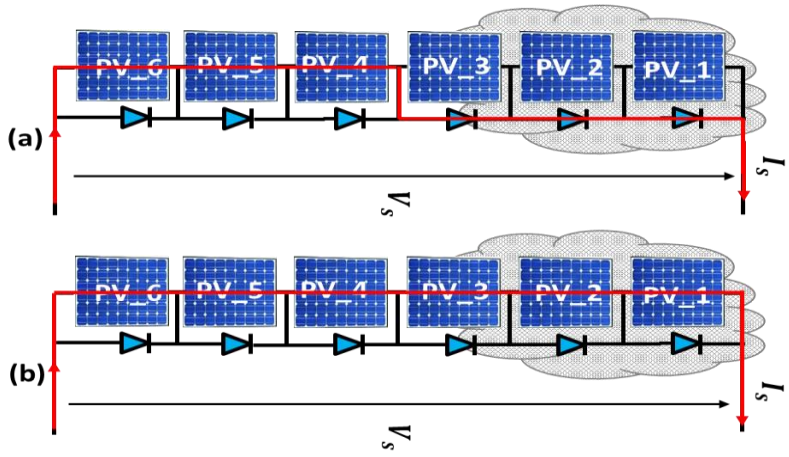

Figure 3.3 The current flow direction of the PV array (a) in area 1 and (b) in area 2.

To investigate the effects of partial shading on the PV array characteristics, multiple partial shading scenarios had to be simulated by changing the number of shaded panels and the incident irradiance value on the PV panels. An experimental test was conducted for this purpose in order to identify the irradiance value of the shaded panels that would be employed in all shading scenario simulations. Figure 3.4 presents the experimental set-up for this test, which included a PV panel and two pyrometers: one for measuring irradiance levels in an unshaded place and the other for measurements in a shaded place.

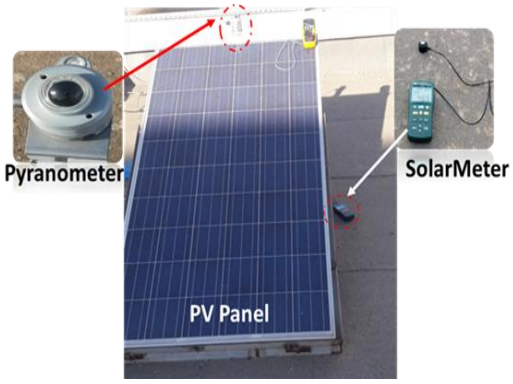

Figure 3.4 Experimental set-up of the measurement system.

Figure 3.5 illustrates the variation in irradiance levels in the shaded and sunny places across two days in two different months. As can be observed in this figure, the irradiance value in the sunny place varied over the course of the day from about 100 W/m^2 to 1000 W/m^2, while the irradiance value in the shaded place remained relatively constant at around 100 W/m^2. As a result, the irradiance value of the shaded panels would be set to 100 W/m^2 in all simulations of partial shading scenarios, whereas that of unshaded panels would vary between 100 and 1000 W/m^2.

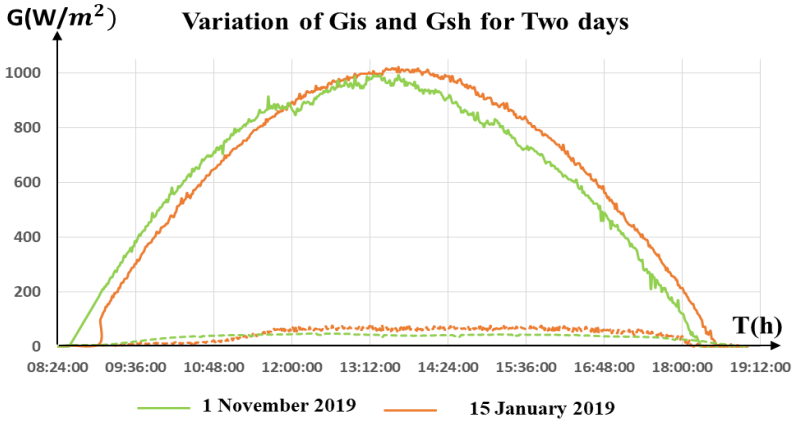

Figure 3.5 The variation in irradiance levels during a day in shaded and unshaded places.

Table 3.1 lists all the tests applied to the simulation of the PV array in the Matlab Simulink environment, and Figure 3.6 presents the P-V characteristic obtained in each test. As can be seen in this figure, the GMPP was sometimes located at V_{mpp1} and other times at V_{mpp2}, according to the

number of shaded panels and the irradiance value of the unshaded panel. In the case of tests 1 and 2, the GMPP appeared at Vmpp1 when the irradiance value varied between 200 and 1000 W/m^2 while it appeared at V_{mpp2} when the irradiance value varied between 0 and 200 W/m^2. In the case of test 3, the GMPP appeared at V_{mpp2} when the irradiance value of the unshaded panels was between 0 and 200 W/m^2 and appeared at V_{mpp2} when this value was between 200 and 1000 W/m^2. As for tests 4 and 5, analogous scenarios could be noted where the GMPP was located at Vmpp1 when the irradiance value of the unshaded panels was above a certain threshold, and it was located at V_{mpp2} when the irradiance value was below a certain threshold.

Table 3-1 Tests applied to the simulation set-up

	Number of Shaded Panels	The Unshaded Panel Irradiance (W/m^2)	The Shaded Panel Irradiance (W/m^2)
Test 1	1	200–1000	100
Test 2	2	200–1000	100
Test 3	3	200–1000	100
Test 4	4	200–1000	100
Test 5	5	200–1000	100

From these results, many critical observations can be extracted, such as the following:

(i) The first peak was created by the unshaded PV panels;

(ii) The second peak was affected by shading on the PV panels;

(iii) The localization of the GMPP was influenced by the irradiance value of the unshaded panels and the number of shaded panels.

As mentioned previous in this section that the GMPP sometimes existed in area 1 and other times in area 2, it was necessary to determine the critical point. It is observed that the critical point was influenced by the irradiance value of the shaded panel and the number of shaded panels. Furthermore, the critical point changed when the number of shaded panels and the irradiance value of the shaded panels changed, as shown in Figure 3.6. As a result, when the P-V characteristic of the PV array becomes more complicated, owing to the presence of many power peaks (more than two peaks). In this case, the previously study is not valeted. Therefore, a simple method to find the GMPP is proposed in the next section.

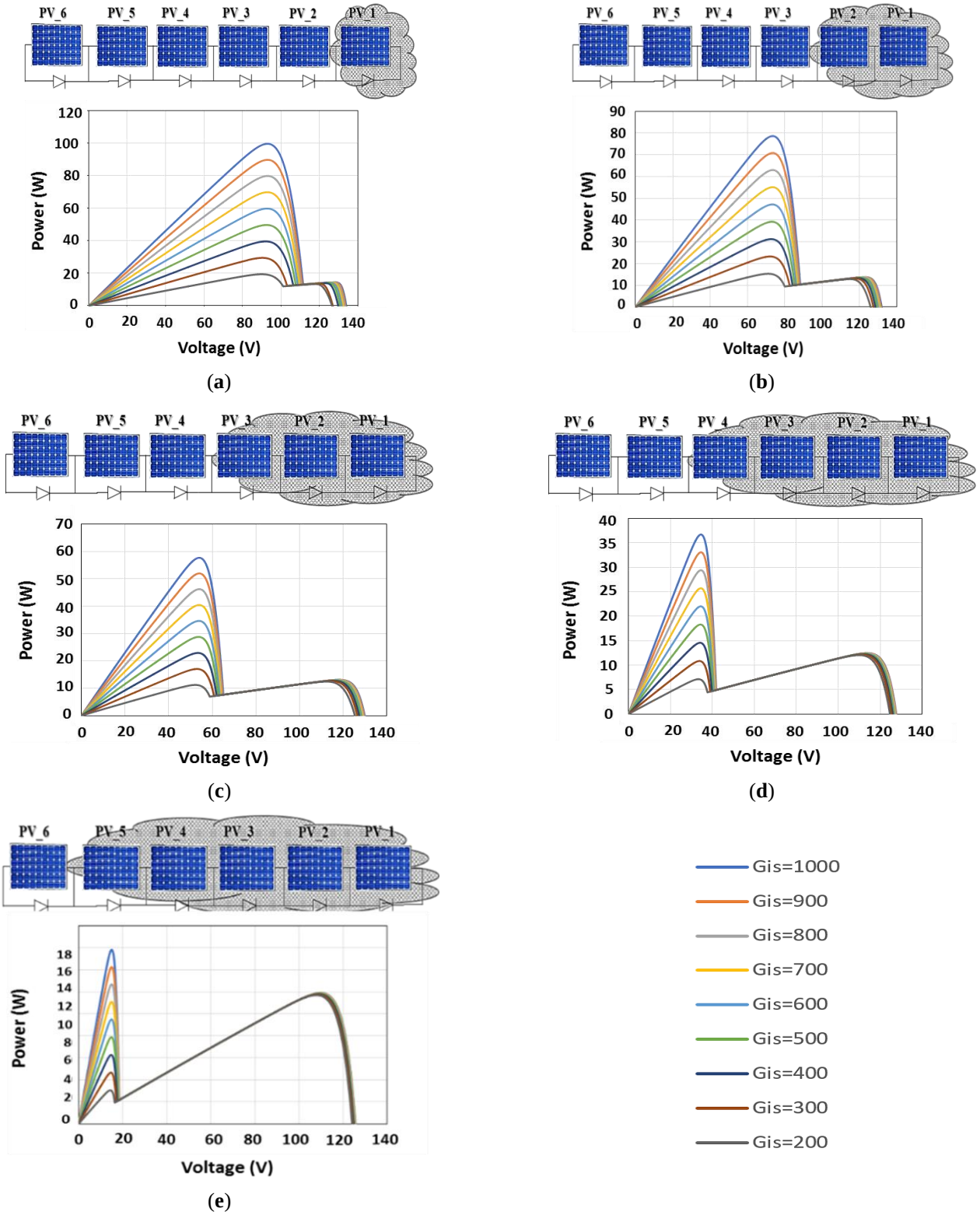

Figure 3.6 The P-V characteristic of the PV array for different shading scenario tests: (a) Test 1, (b) Test 2, (c) Test 3, (d) Test 4, (e) Test 5.

3. Scanning method based MPPT

3.1. Classical scanning method

The principle of the scanning method is based on the scan of the curve P-V characteristic in order to find the global power of the PV system using simple instructions. When the duty cycle is varied, the value of *V*, *I*, *P*, and *D* are stored in own vectors at each iteration. Next, it controls the converter by the corresponding value of the global duty cycle in order to maintain the out power of the PV system at the maximal value under various PSCs. Figure 3.7 presents the scan interval points on the P-V curve using the classical scanning method. It is observed that the scanning of the P-V characteristic starts from the point of the short-circuit current (I_{CC}) which corresponds to 0V and stops at 0.95*Voc*.

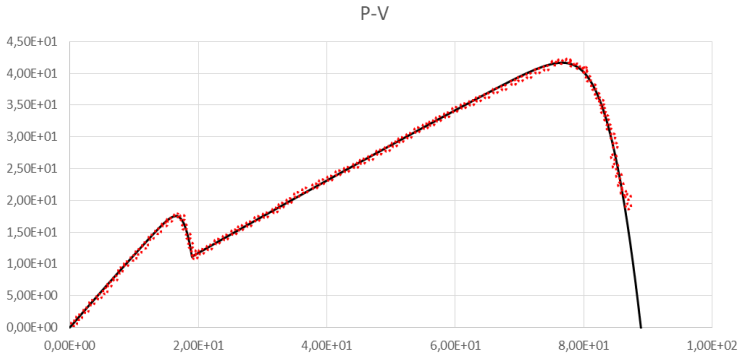

Figure 3.7 The scan points on the P-V curves under PSC3 using the scanning method.

Figure 3.8 depicts the proposed method's sequence, which consists of three steps. The first step is the scanning loop which contains the data backup of the vectors *D(i)*, *P(i)*, *V(i)*, *I(i)*, obtained in each iteration when the duty cycle is varied. Next, the second step consists of the determination of the GP using Equation (3.3). It is noted that GP of the P-V Characteristics is the maximum value among all the values of *P(i)* recorded. And the last step is the boucle of detection change PSC.

$$GMPP = Max(P_i) \tag{3.3}$$

Figure 3.9 presents the output power of the PV string under PSC3 by using the classical scanning method. From this first test, it is observed that the scanning method finds the GMPP with good efficiency and a response time is almost equal to 1.95 s. But, the drawback of this method is the short circuit of the PV string during the scan interval when each PSC change. This, of course, affects the efficiency of the PV array in long term.

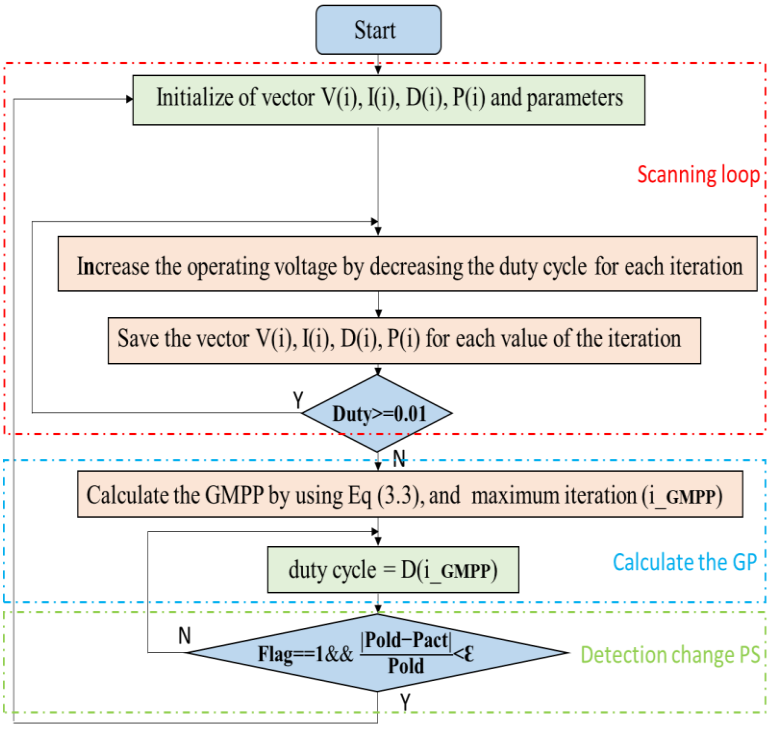

Figure 3.8 Diagram of the proposed scanning method.

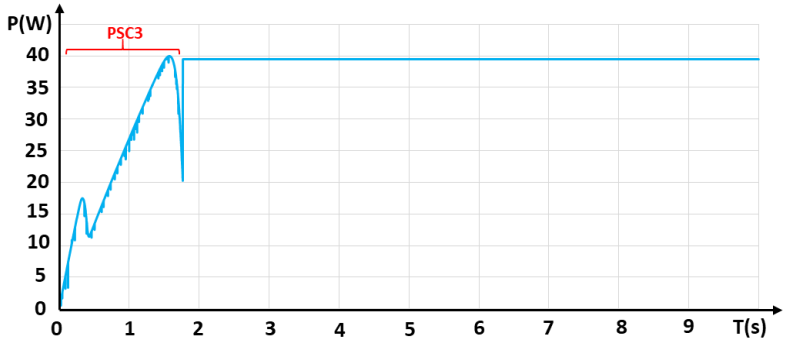

Figure 3.9 The output power of the PV string under PSC3 by using the classical scanning method.

3.2. Improved scanning method

Figure 3.10 presents the search interval of the scan points on the P-V curves under PSC3 using the classical and improved scanning methods. It is observed that the improved method has fewer scan intervals compared to the classical method. The idea of this method is to estimate the scan interval by limiting the search interval of the duty ratio. This limitation is giving by some analysis based on PV characteristics as mentioned in Figure 3.7. The first step does not start the scan with a short-circuit. In addition, the value of V_{mpp2} (voltage corresponding to the second peak) does not exceed the value 0.85×*Voc*. Therefore, we force the improved scanning method to stop at the value of 0.85×*Voc*. So, we will win time to extract the GMPP by limiting the search interval of the P-V curves.

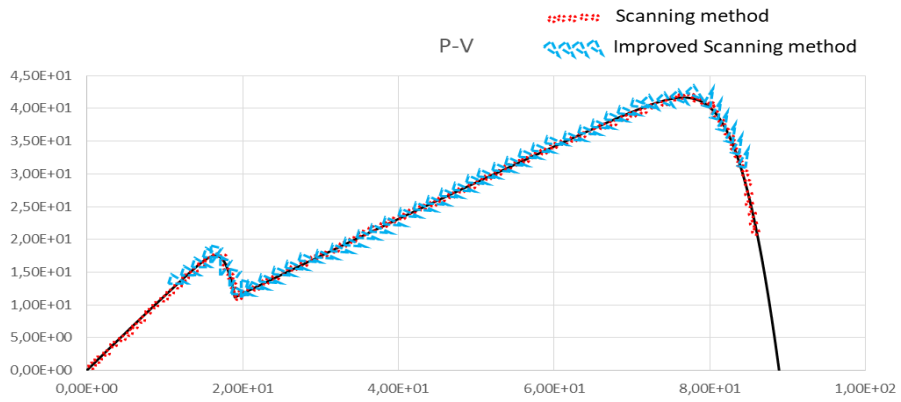

Figure 3.10 The scan points on the P-V curves under PSC3 using the classical and Improved scanning method.

Figure 3.11 illustrates the result of the simulation under PSC3. It is observed that the output power of the PV string is equal to the value of the GP. The irradiation value of each PV model is presented in Table 3-3. It can be observed that a scan of the P-V curve by the improved scanning method does not start with a short-circuit and stops at the value of 0.85×*Voc*. So, this modification improved the response time (1.4 s) compared to the classical scanning method (1.95 s).

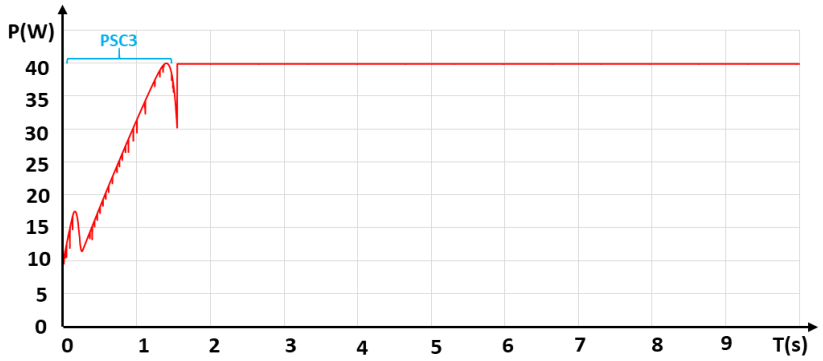

Figure 3.11 The output power of the PV string under PSC3 by using the improved scanning method.

4. Development of First PV simulator : Using Proteus software environment

It can be noticed that when using traditional design tools (such as Matlab/Simulink or PSIM) based on Figure 3.12, the software development and testing system cannot begin until a PCB or physical prototype is available. Thereafter, if something is wrong with the hardware design, the entire process must be repeated. However, using Proteus, software development can begin as soon as the schematic is drawn, and the combination of hardware and software can be thoroughly tested before physical prototyping [101].

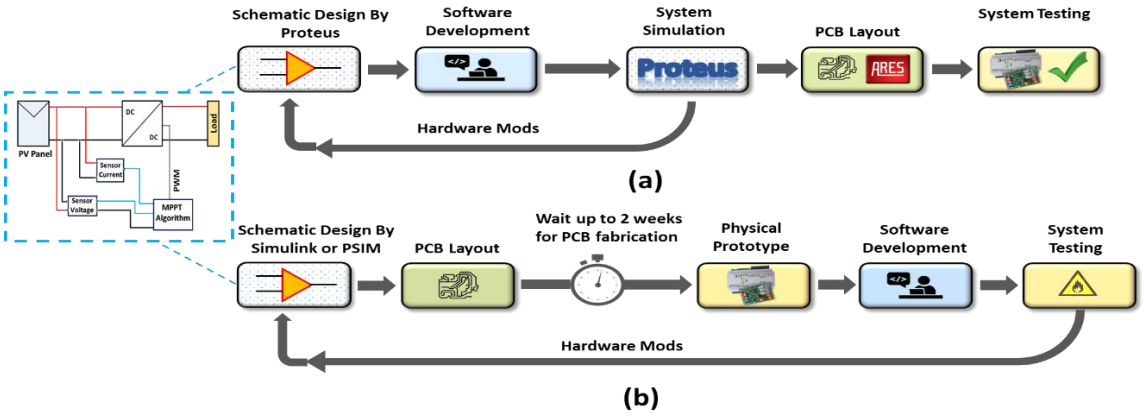

Figure 3.12 Steps to develop a circuit board in Proteus tool: (a) compared to those for developing it in traditional design tools, (b) such as Matlab/Simulink or PSIM.

4.1. Description of the Entire PV System

Figure 3.13 shows the schematic diagram of the entire PV system on Proteus. The latter is composed of a PV panel, a DC-DC converter, an MPPT controller, and a load. The PV panel is connected to the load via the boost converter. The MPPT controller implemented in the Arduino board uses the voltage and PV current data to control the boost converter to reach the MPP. The code of this controller is developed firstly in the Arduino software (IDE), and then its hexadecimal code is uploaded to the board on Proteus.

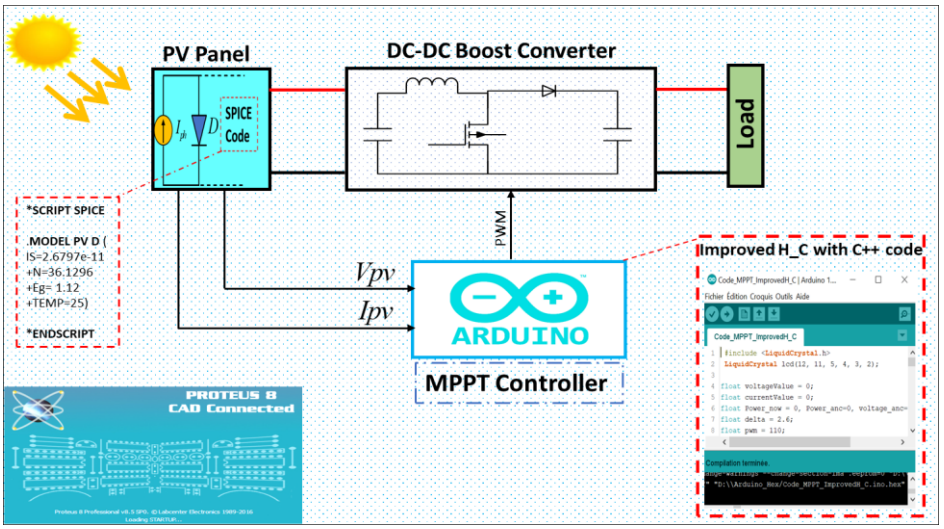

Figure 3.13 . Schematic diagram of the entire photovoltaic (PV) system.

4.2. Proteus PV panel model

The equivalent circuit for the most used solar cell model consists of a diode and a current source connected in parallel, as well as a shunt resistor R_{sh} and a series resistor R_s, as shown in Figure 3.14. Based on this circuit diagram, the output current is given by the following expression [25]:

$$I = I_{ph} - I_{s,o}\left(\exp\left(\frac{V + IR_s}{aV_t}\right) - 1\right) - \frac{V + IR_s}{R_{sh}} \quad (3.4)$$

where: I_{ph}: represents the photocurrent of the solar cell (A); $I_{s,0}$: represents the reverse saturation current of the solar cell (A); V: represents the output cell voltage of the solar cell (V); a: represents the diode ideality factor of the solar cell; V_t: represents the thermal voltage of the solar cell.

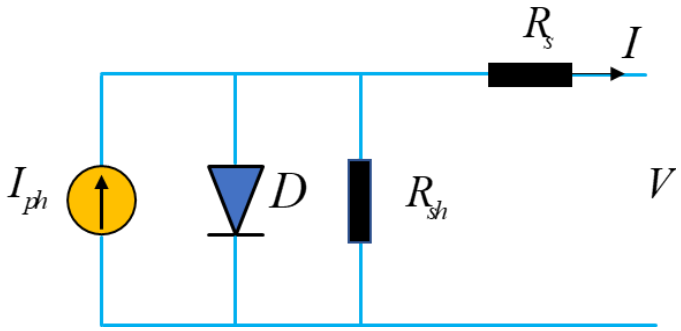

Figure 3.14 Equivalent circuit for single diode model of solar cell.

In this study, the TDC-M20-36 panel is used, and table 3-2 presents its specifications. Figure 3.15 presents the Proteus PV panel model with the Spice code. In this latter, the parameters of the used diode (saturation current, number of cells, ideality factor, and bandgap energy) according to the TDC-M20-36 panel's specification, must be introduced. Note that presented the PV panel model is already validated through simulation/ experimental results in our previous paper [101, 102].

Table 3-2 Characteristics of the used PV model at Standard Test Conditions (STC).

TDC-M20-36	
Pmax of PV panel	20 W
Vmpp at Pmax of PV panel	18.76 V
Impp at Pmax of the PV panel	1.07 A
Current Isc at Short-circuit (SC)	1.17 A
Voltage Voc at Open-circuit (OC)	22.70 V
Temperature coefficient Kv at OC	–0.35%/°C
Temperature coefficient Ki at SC	–0.043%/°C
Number of cells	36

Figure 3.16(a) presents a test bench used to validate the proteus model. It consists of a PV panel, a variable load, a Pyranometer to measure the solar radiation, a Multimeter to measure temperature, current and voltage sensors to measure PV current and voltage, and a computer to instrument the measured data by a virtual instrument made by LabVIEW tool. This model is published in [104]. In addition, Figure 3.16(b) shows the I-V and P-V curves of experimental and Proteus model at T=59 °C and G=920 W/m². And as shown, the simulated data is in accordance with the experimental data both in the current and the power curves.

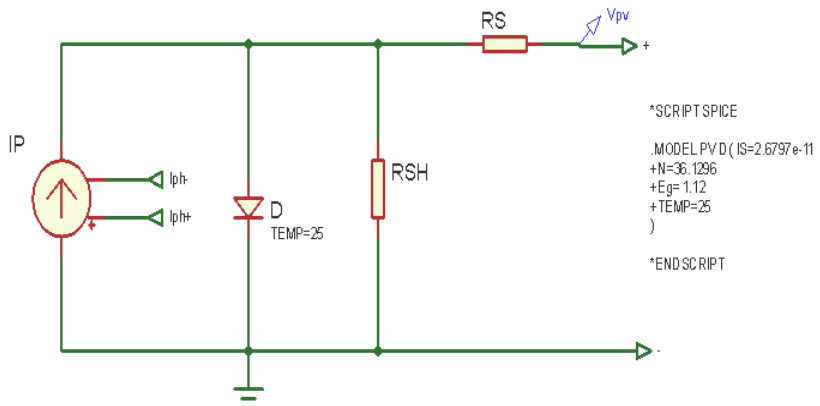

Figure 3.15 The equivalent circuit of panel model under Proteus [101].

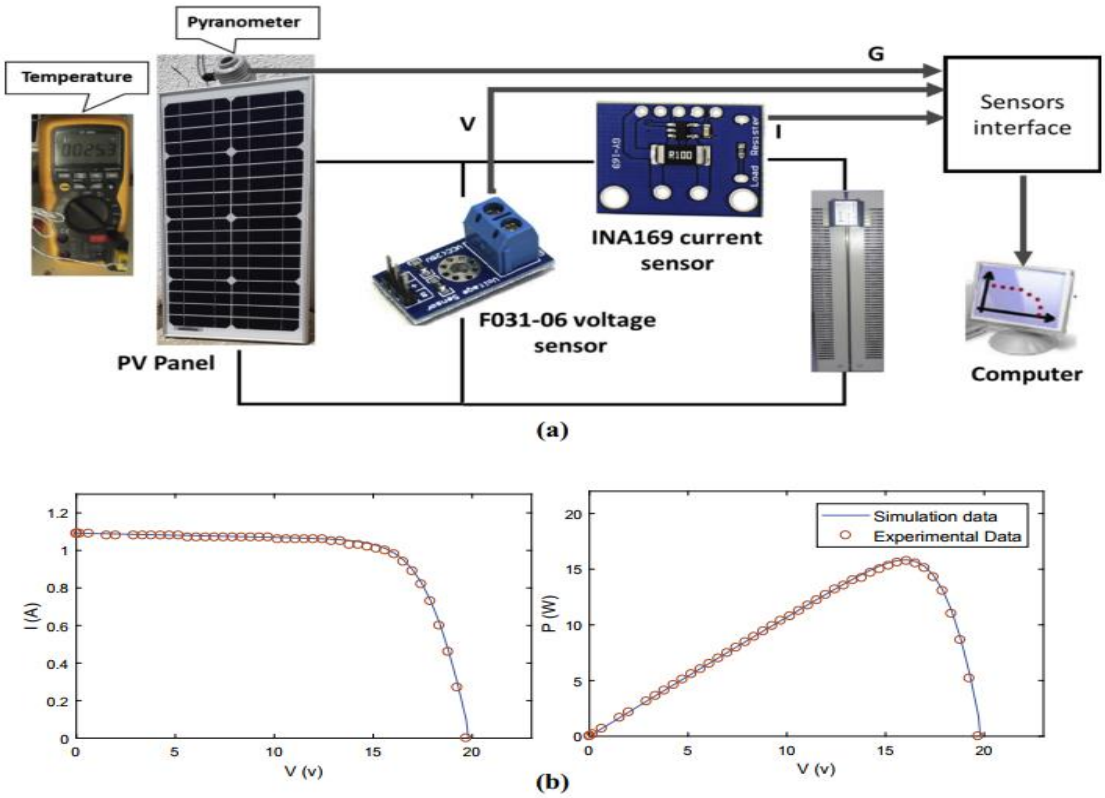

Figure 3.16 (a): Measurement setup, (b): I-V and P-V characteristics for simulation and experimental data [101].

4.3. PV system design in Proteus Software

Figure 3.17 presents the PV system design, made in Proteus [103]. As shown, this PV system can be divided into eight blocks as follows:

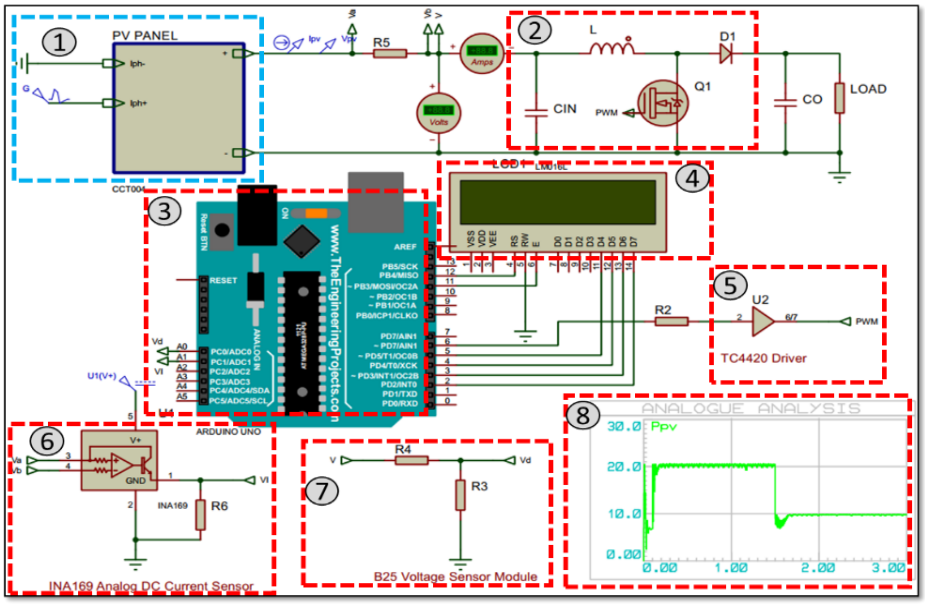

Figure 3.17 Schematic of PV system design in Proteus software.

- **Block (1):** presents the subcircuit of the PV panel model.
- **Block (2):** presents the boost converter.
- **Block (3)**: presents the embedded board (Arduino Uno).
- **Block (4)**: presents the LCD screen, which is used to display the values of PV voltage, current and power.
- **Block (5)**: presents the driver (TC4420), which is used to control the metal–oxide–semiconductor field-effect transistor (MOSFET) transistor of the Boost converter.
- **Block (6)**: presents the current sensor (INA169) used for measuring the PV current. The modelization of this sensor is based on the INA168, which is available in the Proteus Tool. In order to model this sensor, you will need to follow the next steps :
  - ✓ Launch the Proteus tool application.
  - ✓ Open the Pick Devices.
  - ✓ Select the INA168 component.
  - ✓ Add two resistances R_5 (0.1 Ω) and R_6 (50 KΩ). Where Rs is a shunt resistor placed in series between the output of the PV module and the Boost converter, and RL is a load resistor connected between the Pin 1 of the INA168 and the ground.
  - ✓ Set the power-supply voltage to 6 V in order to adapt it with that of INA169.

Then, the PV panel output current can be defined by the Equation (3.3) [104].

$$I_s = \frac{V_{out1}\,1k\Omega}{R_5 R_6} \tag{3.5}$$

- **Block (7)**: presents the module of the voltage sensor (B25 Voltage Sensor Module) used for measuring the PV voltage [105]. It is basically a voltage divider using two series resistances. The PV panel output voltage is defined by Equation (3.4):

$$V_{out2} = \frac{R_3}{R_3 + R_4} V_{in} \tag{3.6}$$

  - ✓ where $(R_3 = 25\text{K}\Omega)$ and $(R_4 = 100\text{K}\Omega)$

- **Block (8)**: presents the graph analysis, it is used to display the simulation results.

5. Results and discussions

The global schematic of the PV system designed in the proteus environment is presented in Figure 3.18. The PV string used is composed of four PV panels having the same characteristics. Next, the value of the load is designed by considering the value of the load optimal of the PV string. The DC-DC boost converter is used in order to implement the improved scanning GMPPT. The control of this converter is done through the TC4420 driver. The role of this driver is to boost the value of the duty cycle between a thresholds to attack the transistor. The results simulation of the proposed method is displayed in the graphic analysis.

In this section, the simulation results of the improved scanning method are shown in Figure 3.19 under various PSCs. The PV string is subjected to different PSCs (PSC1, PSC2, PSC3, and STC). The irradiation value of the PV module for each PCS is taken in Table 3-3. A comparison of results obtained by these two methods is done and a summary of the results is shown in Table 3-4.

Table 3-3 presents the values of the irradiation taken for all simulation tests. Under PSC1, the shading scenarios were performed with the irradiation value of three PV panels set to 1000 W/m2 and one PV panel set to 500 W/m^2. Thereafter, the shading of the other test is taken by varying the number of the shaded panels of the PV string. Otherwise, the temperature value of module PVs was fixed to 25 °C in all test simulations of PSCs.

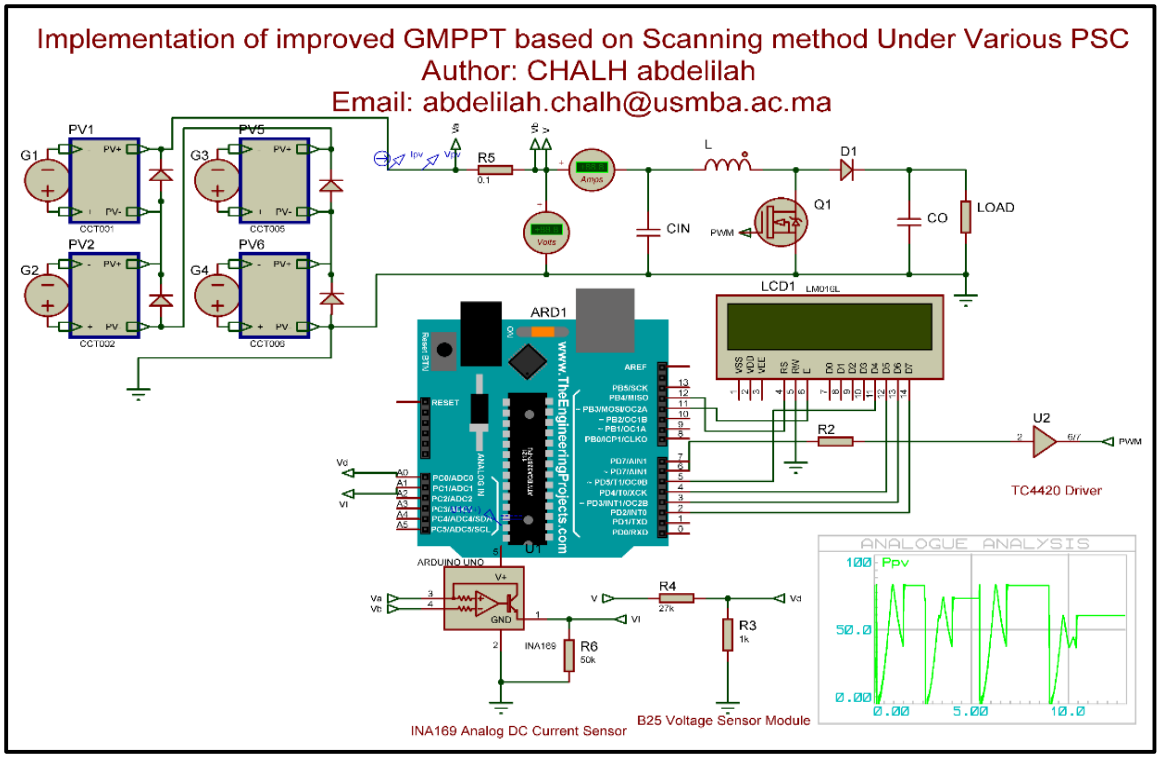

Figure 3.18 The global schematic of the PV system designed in the proteus environment.

Table 3-3 the value of the irradiation taken for all simulation tests.

	[G1…G4]	MPP1	MPP2	GMPP
STC	[1, 1, 1, 1]	80 W	N/A	80 W
PSC1	[1, 1, 1, 0.5]	59,4 W	44,01 W	59,4 W
PSC2	[1, 1, 0.5, 0.5]	38,4 W	41,8 W	41,8 W
PSC3	[1, 0.5, 0.5, 0.5]	17,5 W	39,9 W	39,9 W

N/A: not applicable.

Figure 3.19 presents the P-V characteristics under the various conditions of irradiation. During PSC, the P-V characteristic of a PV string mainly exhibits two peaks resulting from the presence of two irradiance levels, one is the global peak (GP) and represents the GMPP of the PV string and the other is the local peak. In addition, the first peak is delivered at V_{mpp1} (voltage corresponding to this peak) and the other at V_{mpp2}. It is assumed that the scan of the P-V characteristic under PSC3 is included a max search interval of search points. For that, the analysis of the classical and the improved scanning methods is based on the P-V characteristic under PSC3.

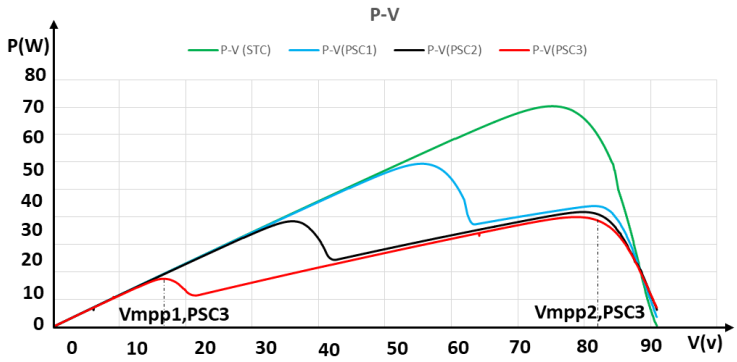

Figure 3.19 The P-V curves characteristics of a PV String under diverse irradiation.

5.1. Tests under a dynamic partial shading conditions

As mentioned in Figure 3.20, the tracking speed with the improved method is faster than that of the classical scanning algorithm. To clarify more, the proposed method only takes 1.4 s. Thus, the tracking speed of the improved method is 1.39 times faster than that of the classical scanning method. Also, the same conclusion can be observed under all PSCs with a fast response time than that of the classical scanning. Furthermore, a comparison between the classical and improved scanning algorithms is done in Table 3-4. The first test case under PSC1 presents a good efficiency (98.49%) and speed response time (1.4 s). In the other cases, the same response time (1.4 s) is obtained with a maximum efficiency of up to 98.50%. From this comparison, can be deduced in all test cases that the efficiency and the response time of the PV system are improved by 0.4% and 0.55 s respectively compared to the Scanning method [106].

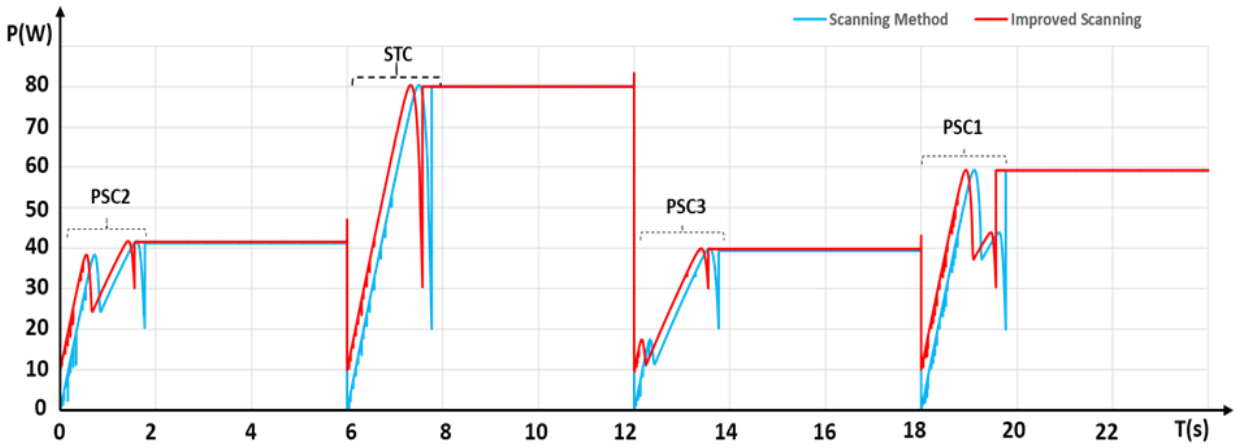

Figure 3.20 The output power of the PV string Under Various PSCs.

Table 3-4 Comparisons of classical and modified scanning methods under various PSCs

MPPT Algorithms	PSC1		PSC2		PSC3	
	Efficiency	Response Time	Efficiency	Response Time	Efficiency	Response Time
Scanning method[106]	98.29%	1.95 s	98.08%	1.95 s	98.24%	1.95 s
Modified Scanning	98.49%	1.4 s	98.18%	1.4 s	98.50%	1.4 s

5.2. Tests under a change of the solar irradiance value during the scanning loop

Although the proposed method is simple and easy to implement in low-cost microcontrollers. But, under a change of the insolation value during the scanning operation, this proposed method is unable to track a real GMMP as shown in the results obtained in Figure 3.21. On the other hand, when the PSCs change again on the outside of the scanning loop, this method is able to restart the scan in order to track the corresponding GMPP of the PV string.

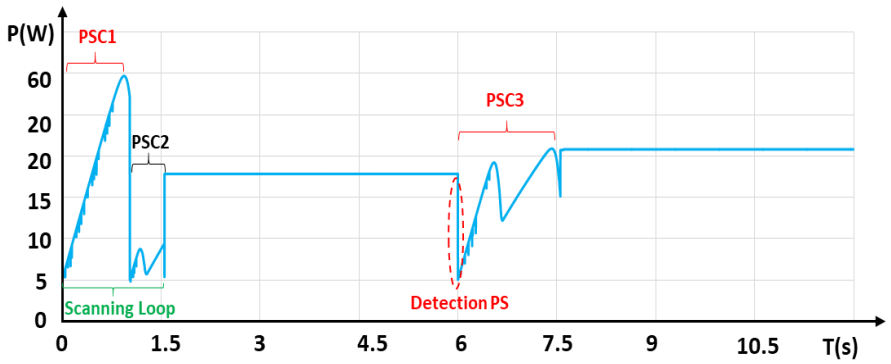

Figure 3.21 The output power under a change of the insolation value during the scanning loop.

Based on the results presented in this work, the problem of the proposed method's inability to track the actual GMMP during a change in the insolation value. Despite this, we can see that the proposed method presents better results than the conventional scanning algorithm. From the comparisons of conventional and modified scanning methods under various PSCs. we notice that the response time of the proposed method is improved by 0.55 s compared to the conventional scanning method. These results show that improved scanning method based MPPT presents a good efficiency (98.49%) and speed response time (1.4 s). Therefore, the latter can be considered as one of the simple and modest MPPT algorithms using under PSCs.

6. Summary

In this chapter, a simple GMPPT controller based on an improved scanning method is proposed. With the analysis based on PV characteristics, we could estimate the scan interval by limiting the search interval of the duty cycle. This limitation of the scan interval, eliminates the passage through the short-circuit point of the P-V characteristics. In addition, it avoided the open-circuit of the PV string during the scan interval in order to prevent disconnection of the PV system. The obtained results showed that the proposed method efficiently tracks the GMPPT under different PSCs and has a good response time (1.4 s), which improves the response time of the PV system by 0.55 s compared to the conventional scanning method. Thus, the simple structure used in this proposed method will significantly reduce the implementation complexity, which will lead to a reduction in the cost of the PV system. Therefore, this method can be used in the industrial PV system instead of the conventional P&O method in order to increase energy production under PSC. Although the proposed method is simple and easy to implement in low-cost microcontrollers, it has a limitation in terms of tracking the actual GMPP when a change in the insolation value during the scan operation occurs.

Chapter 4

Development of a Novel MPPT Design Based on the Seagull Optimization Algorithm for Photovoltaic Systems Operating Under Partial Shading

1. Introduction

A variety of metaheuristic MPPT approaches have been developed to handle partial shading effects such as grey wolf optimization (GWO) [81], ant colony (ACO) [11], and particle swarm (PSO) [68-71]. These algorithms have a significant influence on attaining the GMPP of PV panels in dynamic partial shading situations. However, PSO convergence is strongly influenced by the beginning of the agents' location, resulting in a low convergence rate in certain cases. Furthermore, both PSO and ACO need the determination of five parameters, making them rigid and complicated.

Recently, the authors of [12] established a comprehensive bio-inspired approach for addressing computationally costly issues called the seagull optimization algorithm (SOA), which mimics the search and attack behaviors of seagulls in nature. This algorithm is one of the latest effective optimization methods, which is gradient-free and applicable to optimize all engineering problems occurring in real life. Additionally, compared to other evolutionary algorithms, SOA requires fewer variables for adjustment and fewer operators, which is advantageous when considering a speedy design process [12]. However, to the best of the authors' knowledge, no research has been done on MPPT based on SOA, which motivates us to study this method and to enrich the scientific references with the developed version of the SOA for MPPT controllers. To this end, this chapter introduces a new SOA-based metaheuristic MPPT method for tracking the GMPP to maximize the PV power output in PV systems operating under both uniform and partial shading conditions. This method is considered simple and is best suited for real engineering problems. The MPPT's speed and efficiency will be considerably improved.

This chapter begins by describing the SOA's fundamentals and mathematical model. Then, the application of the seagull optimization algorithm to the MPPT. Thereafter, the SOA-based MPPT scheme is first proposed and then implemented for an 80 W PV system using the MATLAB/SIMULINK environment. Finally, the performance of the SOA based MPPT method is verified by comparing its performance with P&O and PSO (particle swarm optimization) based MPPT methods under different shading scenarios.

2. Seagull optimization algorithm (SOA)

2.1. The basics of the SOA

Seagulls are a type of coastal bird that has been around for roughly thirty million years. Their wings are large, and their rear legs have developed to enable them to travel on the water. Seagulls come in a range of sizes and shapes, and they may be found in practically every corner of the world.

Seagulls are capable of drinking both fresh and saltwater. Most animals are unable to do this. On the other hand, Seagulls have a unique set of drums covering their eyes that they use to clean the salt out of their system by opening their beaks. Seagulls inhabit in vast groups and use a variety of voices to communicate with one another. With their expertise, they can find and attack the prey. They steal food under the influence of other birds, animals, and even people, which is one of their strangest behaviours. Seagulls eat mostly fish, although they also eat insects, earthworms, and other insects. To discover and attack prey, seagulls use their intelligence. The most prominent characteristics of seagulls are their migratory and attacking habits. A group of seagulls migrated from one area to another using mathematical models of predator movement and attack. A seagull must satisfy the following requirements:

The migration behaviour is described as follows:

- They move in groups when migrating. To avoid accidents, their starting locations differ from one another.

- They use their swarm experience to their benefit that is they try to go in the way of the highest survival to acquire the lowest cost value.

Seagulls typically attack migratory birds over the sea. This procedure is influenced by the natural structure of the spiral's activity during the attack. Figure 4.1 depicts a conceptual model of these characteristics. The Seagull Model for the Seagull Optimization Algorithm (SOA) is explained more below.

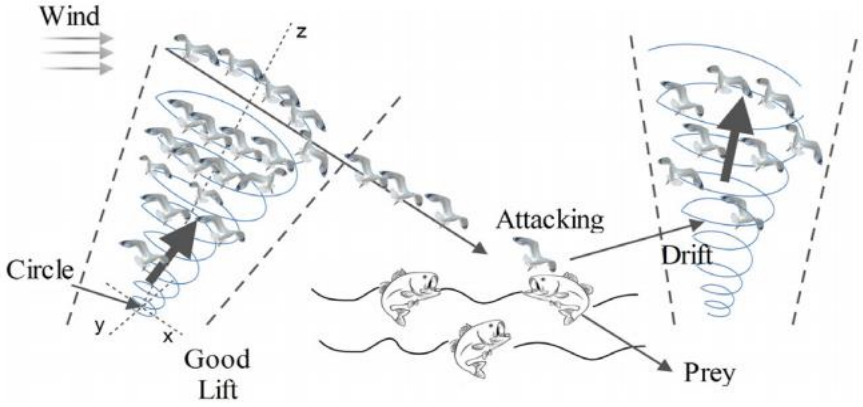

Figure 4.1 Migration and attacking behaviors of seagulls [12].

2.2. Mathematical model of SOA

Exploration (migration) and exploitation are the foundations of the SOA's mathematical model (attacking the prey).

During exploration, the algorithm must satisfy three conditions (avoiding collisions, move in the direction of the best neighbour, and stay close to the best search agent) to replicate how a group of seagulls moves from one place to another. The behaviour of the migration can be modelled by the following equation [12]:

$$\overrightarrow{D_s} = \left|A \times \overrightarrow{X_s}(t) + B \times (\overrightarrow{X_{bs}}(t) - \overrightarrow{X_s}(t)\right| \quad (4.1)$$

$$A = fc - \left(iter \times \left(\frac{fc}{Max\_iter}\right)\right) \quad (4.2)$$

$$B = 2 \times A^2 \times rand \quad (4.3)$$

Where the distance between the current search agent and the best-fit search agent is provided by $\vec{\mathrm{D}}_s$, $\vec{\mathrm{X}}_{\mathrm{s}}(t)$ denotes the current place of search agent, $\vec{\mathrm{X}}_{\mathrm{bs}}(t)$ denotes the best-fit search agent. t denotes the current iteration, A presents a linearly decreases from 2 to 0, B is a randomized variable that ensures a correct balance of exploration and exploitation.

During exploitation, seagulls seek to make use of the search process's history and experience. During migration, seagulls use their wings and weight to keep their height. During the iteration process, the search agents might update their locations about the best search agent. As a result, the following equation is used to determine the search agent's updated position [12]:

$$\overrightarrow{X_s}(t+1) = \left(\overrightarrow{D_s} \times X' \times Y' \times Z'\right) + \overrightarrow{X_{bs}}(t) \quad (4.4)$$

Where $\vec{\mathrm{X}}_s(t+1)$ represents the equation of updating the position of other search agents. X', Y' and Z' described the spiral movement that behavior produces in the air, and which are defined as follows [12]:

$$k = pi.\mathrm{rand} \quad (4.5)$$

$$r = u.e^{kv} \quad (4.6)$$

$$X' = r.\cos(k) \tag{4.7}$$

$$y' = r.\sin(k) \tag{4.8}$$

$$Z' = r.k \tag{4.9}$$

The radius of each spiral turn is r, while k is a random value in [0, 2π]. e is the natural logarithm's base, while u and v are constants that determine the spiral form.

Here is the detailed pseudo-code of the SOA algorithm:

Algorithm : seagull Optimization Algorithm
Input: seagull population $\overrightarrow{P_s}$
Output: Optimal search agent $\overrightarrow{P_{bs}}$
Procedure SOA
Initialize the parameters A, *fc*, and Max_iteration
  While (x < Max_iteration)
    $\overrightarrow{P_{bs}}$ ← **ComputeFitness**($\overrightarrow{P_s}$) /* Calculate the fitness values of each search agent using **ComputeFitness** Function */
    rd ← Rand (0,1) /* To generate the random number in range [0, 1] */
    k ← Rand (0, 2π) /* To generate the random number in range [0, 2π] */
  /* Attacking behavior */
    r ← u × e^{kv} /* To generate the spiral behavior during migration */
    Calculate the distance $\overrightarrow{D_s}$ using Eq. 4.1
    P ← x' × y' × z' /* Compute x', y', z' planes using Eqs 4.7-4.9 */
    $\overrightarrow{P_s}$(x) ← $\overrightarrow{(D_s} \times P) + \overrightarrow{P_{bs}}$
    x ← x + 1
  End while
Return $\overrightarrow{P_{bs}}$
End procedure
Procedure ComputeFitness($\overrightarrow{P_s}$)
  For i ← 1 to n do /* Here, n represents the dimension of a given problem */
    FITs[i] ← **FitnessFucntion**($\overrightarrow{P_s}(i,:)$) /* Calculate the fitness of each individual */
  End for
  FITsbest ← **BEST(FITs[])** /* Calculate the best value using BEST function */
return FITsbest
End procedure
Procedure BEST(FITs[])
  Best ← FITs[0]
  For i ← 1 to n **do**
    if (FITs[i] < Best) **then**
      Best ← FITs[i]
  end if
  end for
return Best /* Return the best fitness value */
End procedure

2.3. Application of SOA to the MPPT

Each seagull's solution is specified as the duty cycle value of the DC-DC converter to achieve the direct control SOA-based MPPT. In the first iteration, the duty cycle value can be generated using the following equation:

$$d_i = d_{min} + rand[0,1](d_{max} - d_{min})\ ;\ \ i = 1,2,\dots Nbr\_Seagulls) \tag{4.10}$$

where d_{min} and d_{max} represent the limit of the search band mechanism.
The distance D_s can be calculated using the following equation:

$$D_s = |A \times d_i(t) + B \times (d_{best}(t) - d_i(t))| \tag{4.11}$$

The new seagull's solution can then be generated using the following equation:

$$d_{new}(t+1) = d_{best}(t) + (D_s \times X' \times Y' \times Z') \tag{4.12}$$

Since the GMPP changes continuously as the weather conditions change, the SOA-MPPT algorithm must be restarted to search for the new GMPP. Therefore, to detect if ever a change in weather conditions takes place to restart the search, the following inequality is adopted in the algorithm:

$$\frac{\left|P_{Pv_{new}} - P_{Pv_{last}}\right|}{P_{Pv_{last}}} \geq \Delta P_{Pv}(\%) \tag{4.13}$$

Whenever the inequality indicated above is met, the process of finding a new MPP will be repeated to ensure that the algorithm can always identify the GPPM regardless of the operating condition.

Figure (4.2) depicts the principle working of the SOA based MPPT algorithm.

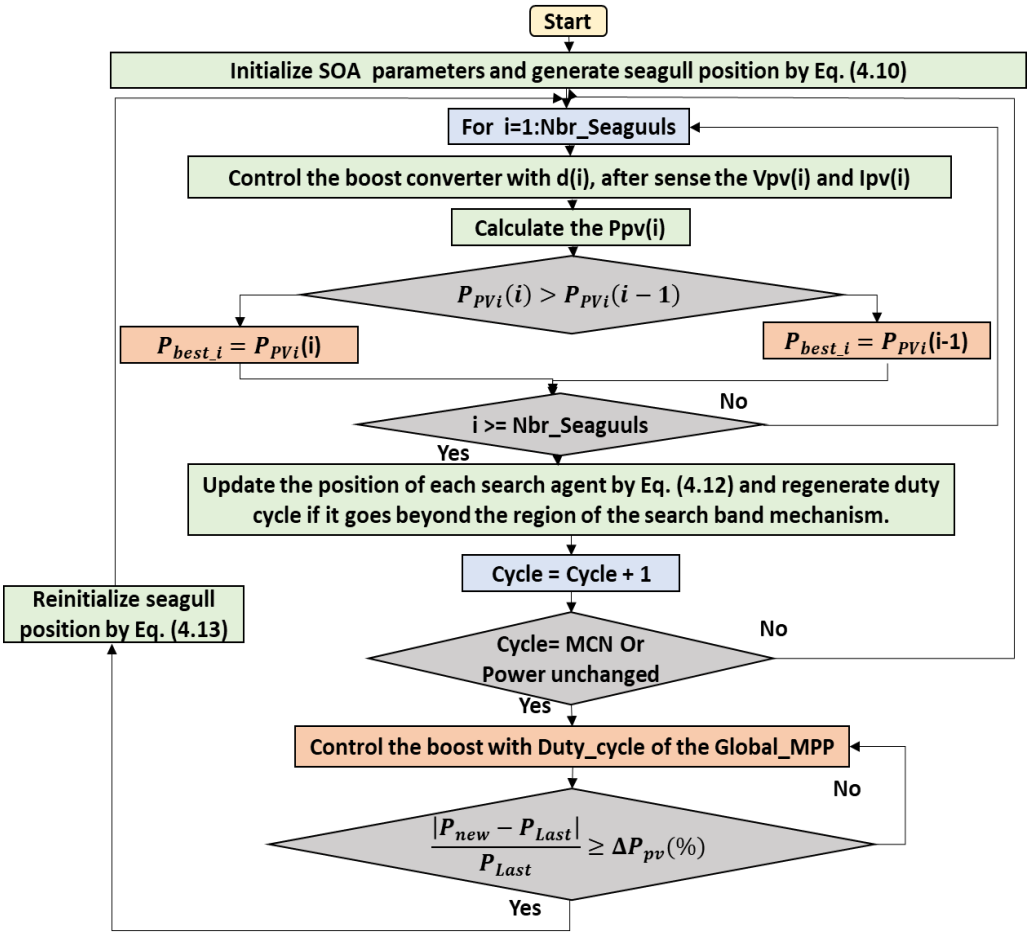

Figure 4.2 Flowchart of the SOA based MPPT algorithm

3. Results and discussions

To examine the performance of the SOA based MPPT method, the 20*4 (W) PV system depicted in Figure 4.3 is considered, which is designed under MATLAB/SIMULINK environment. This system is composed of a PV array formed by four PV modules (20 W) serially connected, a boost DC-DC converter, an MPPT controller and a DC load. The DC-DC converter is controlled, using a PWM generator, by the duty cycle "$\boldsymbol{\alpha}$" which is generated by the SOA based MPPT controller.

Table 4.2 shows the irradiation values considered in the simulation tests. The P-V characteristic obtained in each test is presented in Figure 4.4. As can be seen in this figure, the P-V curve shows multiple peaks under PSCs. Each of these peaks is characterized by its voltage and power. The peaks number is depending on the number of shaded panels. The key parameters of the implemented MPPT methods, namely SOA, PSO and P&O, are seated in Table 4.3.

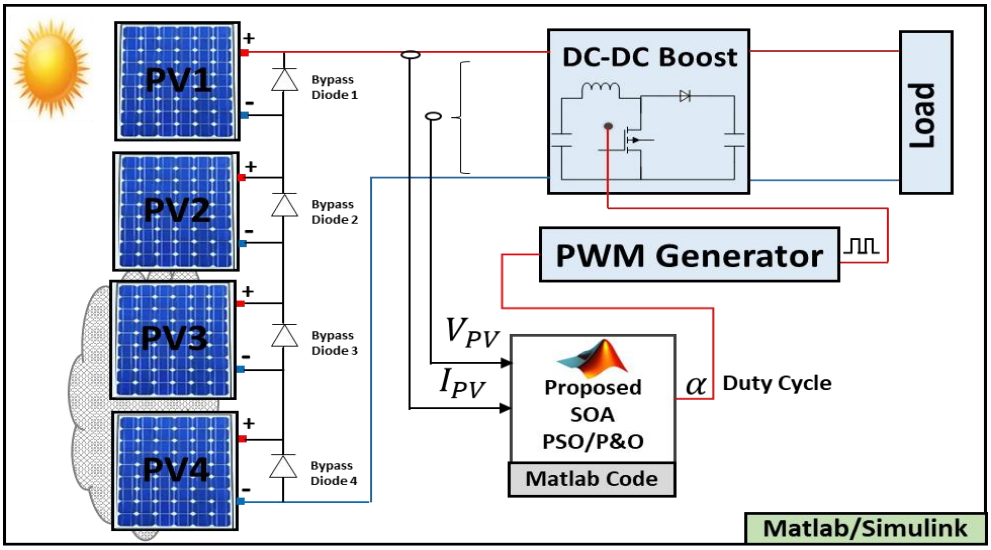

Figure 4.3 PV system configuration with the SOA based MPPT controller.

The electrical parameters of the used PV module are depicted in Table 4.1.

Table 4-1 The electrical parameters of the used PV system.

COMPONENTS	VALUES
PV MODULE	20W
INDUCTOR, **L**	15 mH
INPUT CAPACITOR, $\mathbf{C_{IN}}$	22 µF
OUTPUT CAPACITOR, $\mathbf{C_{OUT}}$	22 µF
SWITCHING FREQUENCY, **F**	10 KHZ
LOAD, $\mathbf{R_L}$	220Ω

Table 4-2 Irradiation values considered in the simulation tests.

Conditions	G_1 (W/m^2)	G_2 (W/m^2)	G_3 (W/m^2)	G_4 (W/m^2)
STC	1000	1000	1000	1000
PSC1	500	1000	1000	1000
PSC2	400	800	1000	1000
PSC3	800	1000	1000	1000

Table 4-3 Parameters of SOA, PSO and P&O based MPPT methods.

SOA		PSO		P&O	
Ts	0.05	*Ts*	0.05	*Ts*	0.01
ΔPpv	2%	ΔPpv	2%	ΔPpv	2%
N_{SOA}	6	*Np*	6	ΔD	0.01
Max_iter	30	*Max_iter*	30	-	-
A	[2-0]	w	0.4	-	-
fc	2	C1	1.6	-	-
-	-	C2	1.2	-	-

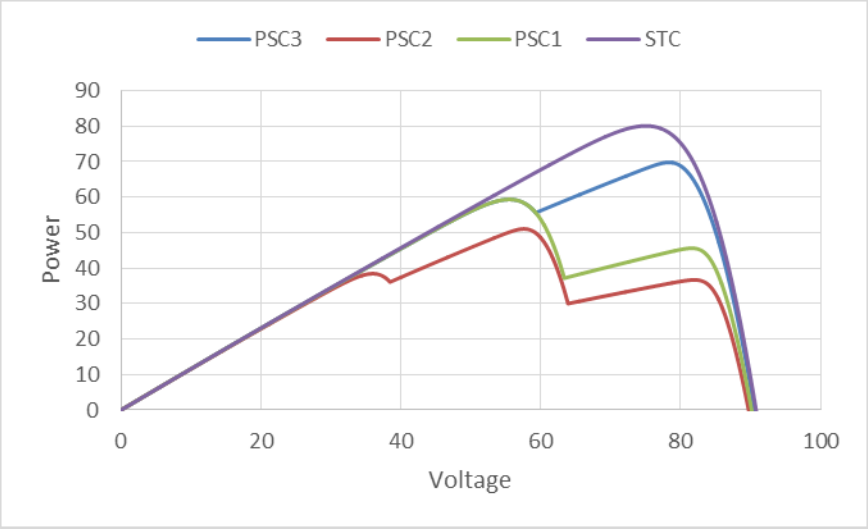

Figure 4.4 PV characteristics under different PSCs.

To verify the ability of the SOA-based MPPT method to track the GMPP, the PV system was simulated with various PSCs (PSC1, PSC2, and PSC3) in addition to the standard test condition (STC). The system was first started by testing it under STC, and then each PSC was applied every 7.5 s for a period between 0 and 30 s, as depicted in Figure 4.8. The obtained results are presented in Figure 4.5 - 4.8. Under PSC 1, the SOA meets the global peak (GP) of 59.35 W with a tracking speed of 1.10 s, PSO converges to the GP of 59.30 W with a tracking speed of 2.16 s, while the P&O algorithm only converges to a local peak (LP) of 44.71 W. Under PSC2, the SOA meets the GP of 51.06 W with 1.25 s, PSO meets the GP of 49.95 W with 4.13s, while the P&O converges to an LP of 36.32 W. Form this result, it's clear that P&O is unable to differentiate between LP and GP. In addition, when PCS3 is applied, the SOA meets the GP of 69.79 W with 1.05 s, PSO meets the GP of 69.36 W with 3.34 s, while the P&O meets this time to the GP of 69.21 W.

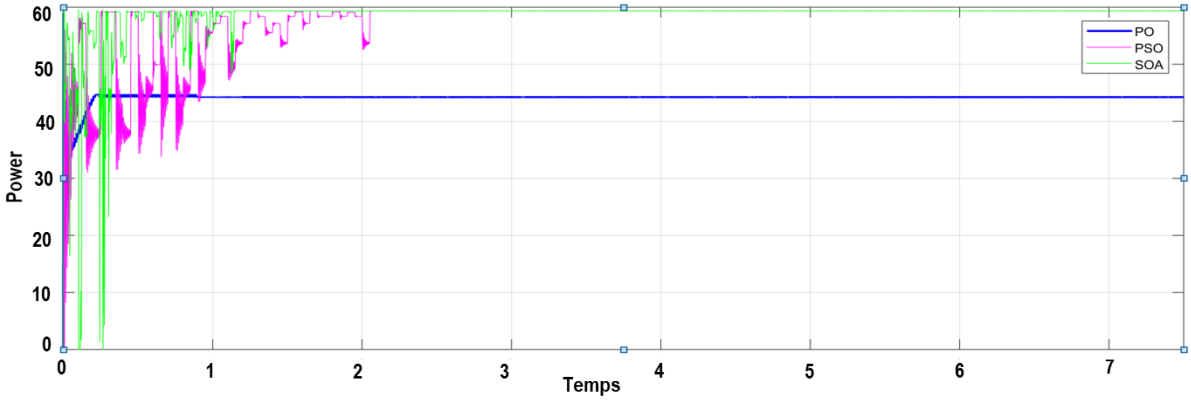

Figure 4.5 Output power under PSC1 using: P&O, PSO and SOA.

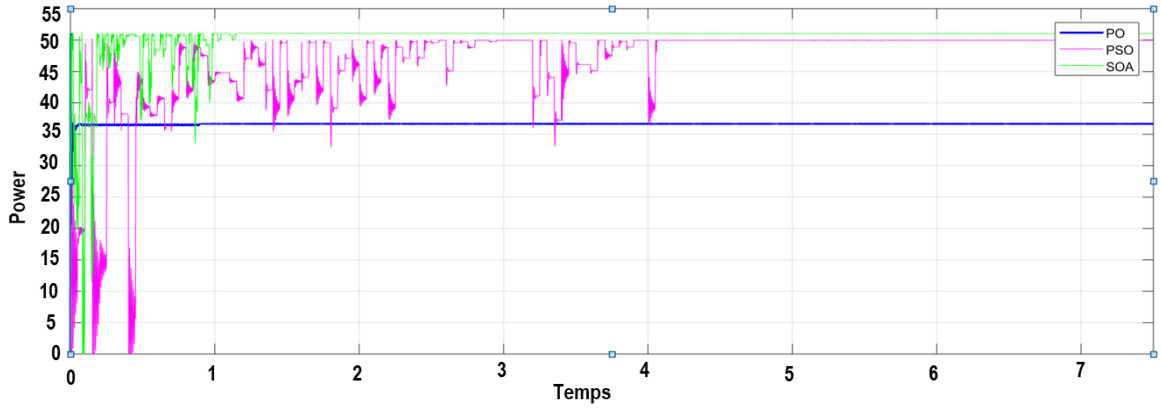

Figure 4.6 Output power obtained under PSC2 using: P&O, PSO and SOA.

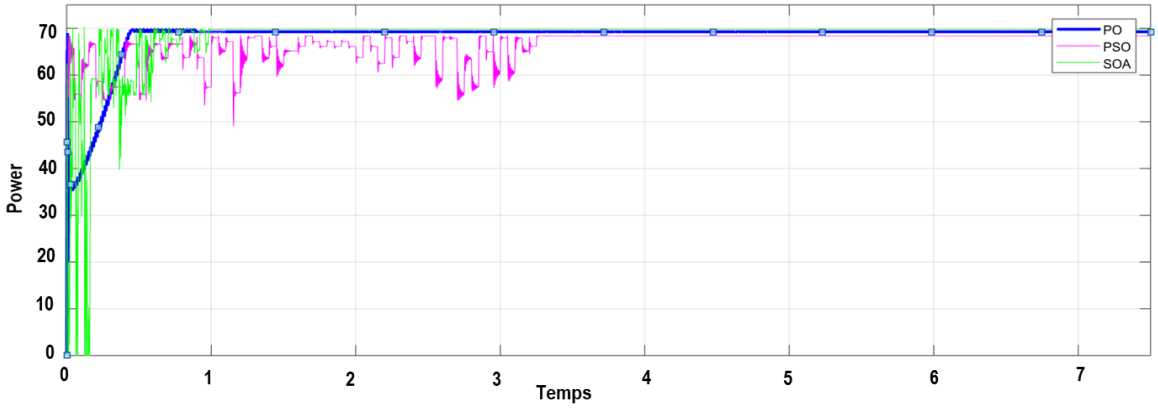

Figure 4.7 Output power obtained under PSC3 using: P&O, PSO and SOA.

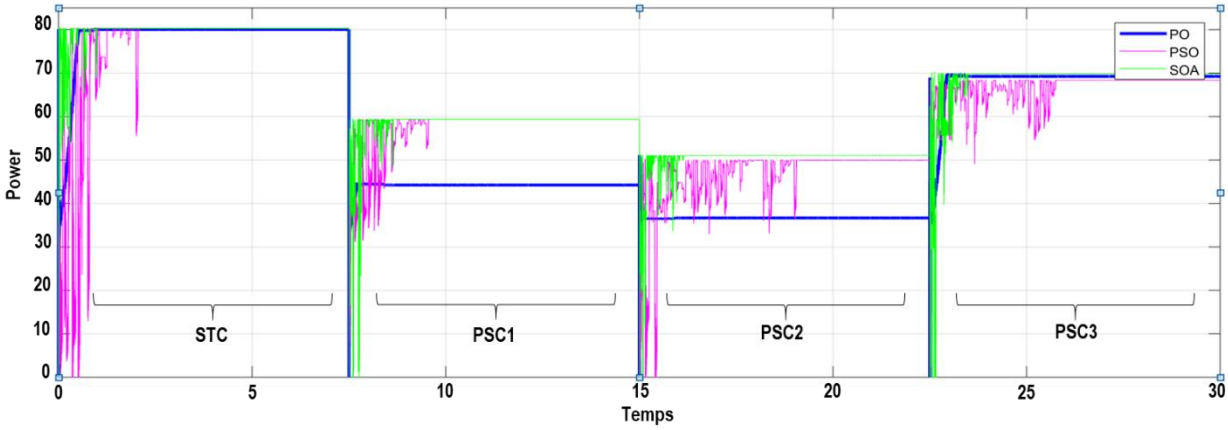

Figure 4.8 Output power obtained under STC to PSCs variations using: P&O, PSO and SOA.

4. Processor In the Loop (PIL) testing

The goal of this part is to put the MPPT controller model onto a real embedded processor and run a closed-loop simulation with the simulated plant model; this is known as the processor-in-the-loop (PIL) test. In this way, the SOA-MPPT controller is replaced by a PIL block that have the controller code running on the hardware. The PIL test will help us identify if the processor is capable of executing the developed MPPT controller to validate the proposed MPPT control strategy on an actual embedded board. Figure 4.9 shows the embedded board used to perform the PIL experimentation, which is the Arduino MKRZERO board. The microcontroller integrated in this board is the ATMEL SAMD21 from Microchip Technology. This microcontroller contains a 32-bit Arm® Cortex®-M4F processor with Floating Point Unit (FPU) running at up to 120MHz with 256kB flash memory, 32kB SRAM.

As presented in Figure 4.9, the PIL block is generated and connected to the plant model so as to acquire the PV output voltage and current, after that the PIL block will identify the required duty cycle by using the proposed algorithm and send it to the plant model. During the PIL process, the generated code is tested in real time while the plant model runs on a computer which allows to detect and correct possible errors. Figure 4.10 depicts the result from the PIL test. It can be observed that the results obtained using PIL test are similar to the simulation results obtained in MATLAB/Simulink. Therefore, the MPPT control algorithm proposed in this work is verified on a real microcontroller (or embedded board).

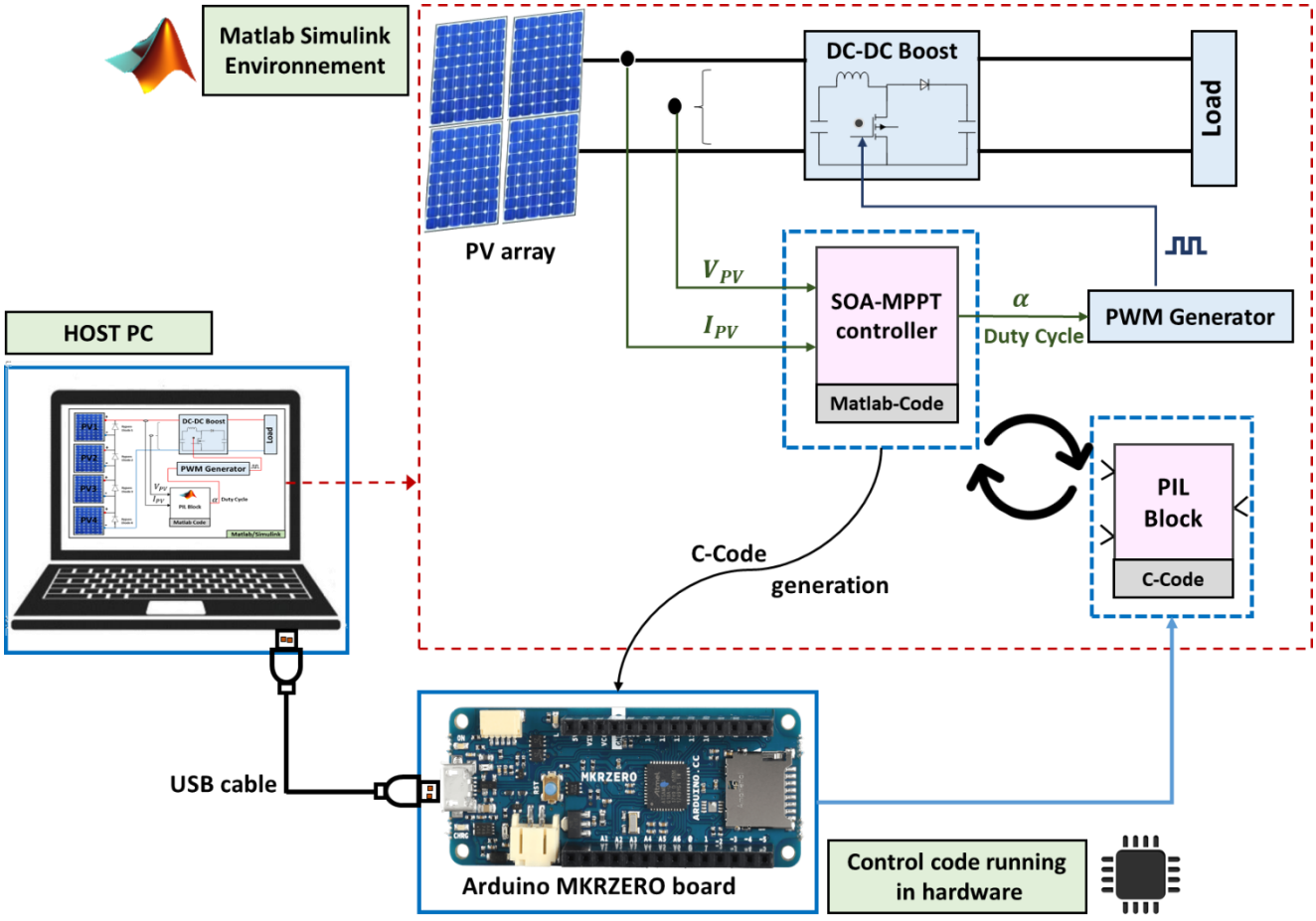

Figure 4.9 Diagram of PV generation using PIL block.

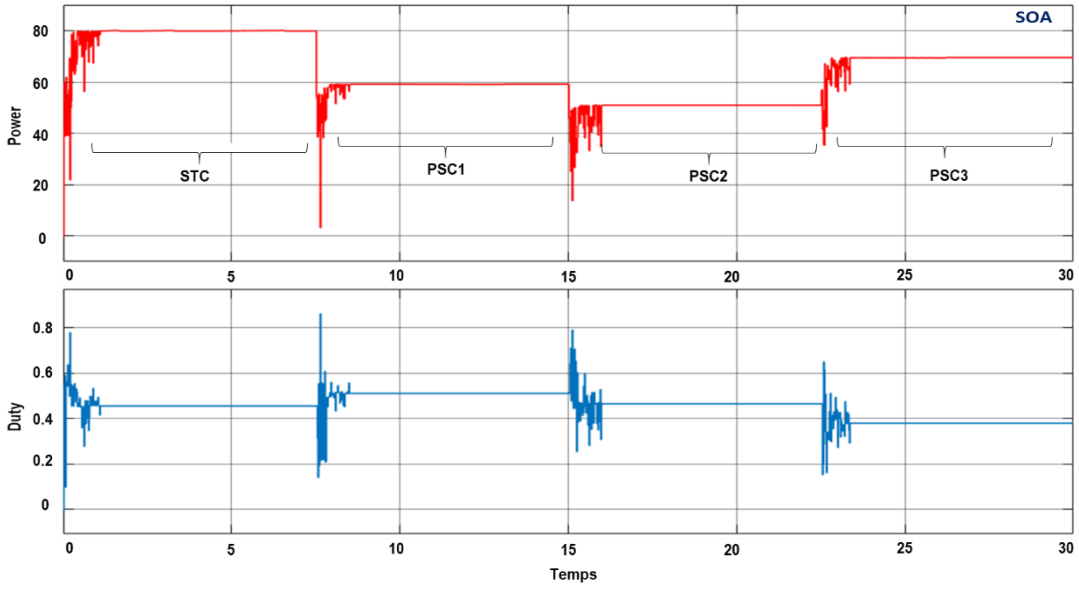

Figure 4.10 PIL results of output power obtained under STC to PSCs variation using SOA algorithms.

5. Recapitulation

The performance comparison between SOA, PSO and P&O based MPPT methods is presented in Table 4.4. The obtained power in the case of the SOA-based optimization method is significantly more than those of the PSO and P&O algorithms throughout the whole profile. Figure 4.11 presents the tracking efficiency of PV system output power under various PSCs using P&O, PSO and SOA methods. It can be concluded that the proposed SOA-MPPT is guaranteed the tracking of GMPP with high efficiency than P&O and PSO.

Table 4-4 Performance comparison of the SOA, PSO, and P&O based MPPT methods.

	Global Peak from P-V Curve (W)	MPPT algorithms	Maximum Power (W)	Tracking Time (s)	Tracking efficiency (%)
PSC1	59.86	P&O	44.71	0.85s	73.71
		PSO	59.30	2.16s	96.10
		Proposed MPPT-SOA	**59.35**	**1.10s**	**97.80**
PSC2	51.36	P&O	36.32	0.92s	71.35
		PSO	49.95	4.13s	90.60
		Proposed MPPT-SOA	**51.06**	**1.25s**	**98.85**
PSC3	69.95	P&O	69.21	0.75s	97.40
		PSO	69.36	3.34s	95.25
		Proposed MPPT-SOA	**69.79**	**1.05s**	**97.74**
STC	80.29	P&O	80.05	0.75s	95.80
		PSO	80.25	3.28s	94.11
		Proposed MPPT-SOA	**80.27**	**1.09s**	**99.25**

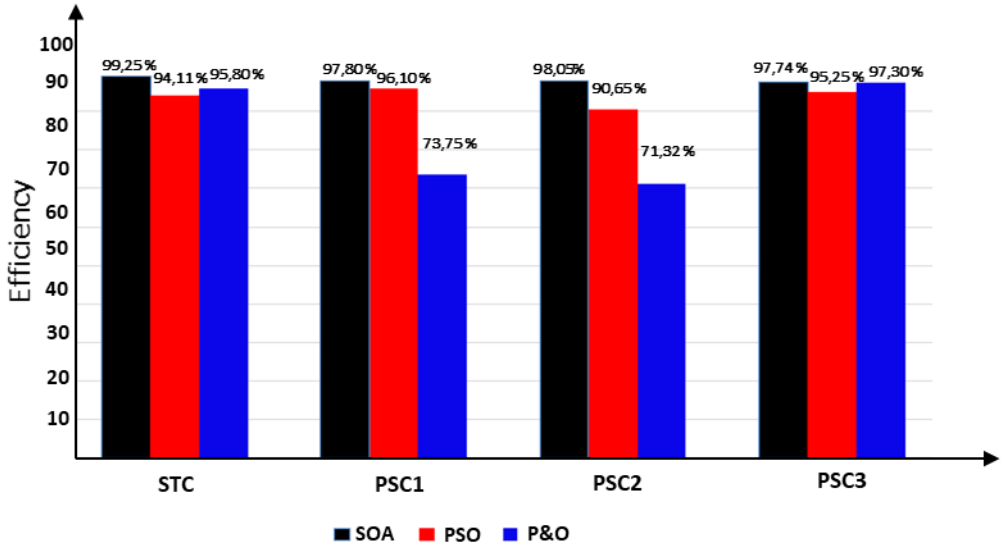

Figure 4.11 Comparison of the tracking efficiency between P&O, PSO and SOA methods.

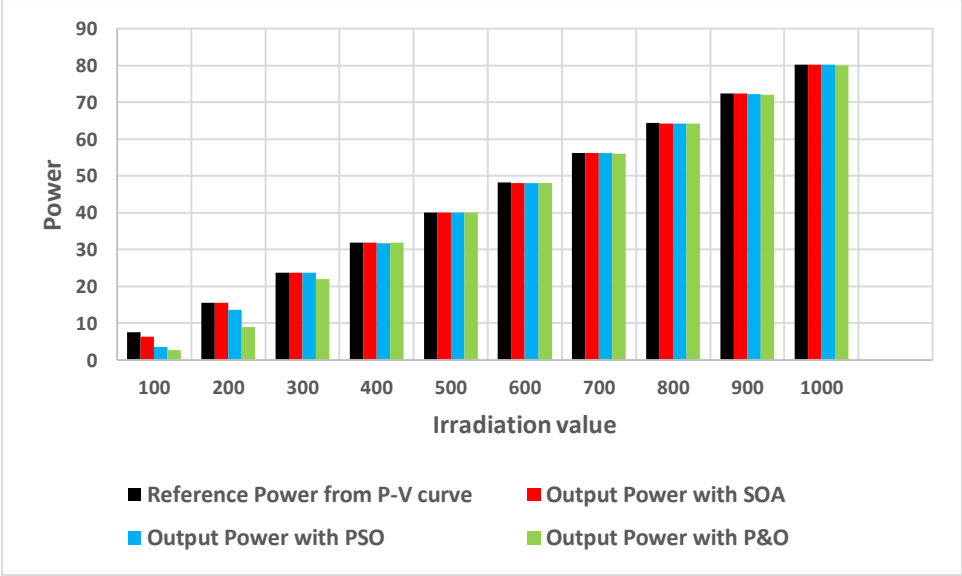

Figure 4.12 Extracted output power of PV system from different uniform irradiation using P&O, PSO and SOA.

In these tables, we compared the three methods based on two criteria which are:

(i) The response time: the time needed by the method to achieve the maximum power.

(ii) The efficiency: a factor that defines how close the results obtained to the ideal maximum power.

Based on the results obtained in this work and the criteria cited before, it can be observed that the proposed SOA-MPPT and PSO algorithms successfully converge to the GMPP corresponding to the different PSCs, with a noticeable superiority of the proposed SOA-MPPT in terms tracking speed. Although the tracking speed of the P&O algorithm is higher than that of SOA and PSO, it is not able

to track the GMPP in most case of PSCs and is trapped in the local MPP of the P-V curve (in the case of PSC1 and PSC2). In addition, we note that the P&O and PSO algorithm are not able to track the true MPP when the PV system operating under weak uniform conditions (see Figure 4.12). Otherwise, the proposed SOA-MPPT successfully converge to the MPP when the PV system is operating under weak uniform conditions. Finally, it can be interpreted that the SOA based MPPT converges with a good speed and zero oscillation around the GP compared to PSO and P&O based MPPT.

6. Summary

In this chapter, a new metaheuristic method based on MPPT has been proposed to track the maximum power point of a photovoltaic system. The effectiveness of the proposed SOA-based MPPT method was verified for an 80 (W) PV system using the MATLAB/SIMULINK environment. The simulation results were performed under various partial shading scenarios and weak uniform conditions. It proves the superiority of the proposed method in terms of tracking efficiency and fast response time, compared to other methods (P&O and PSO). We can conclude that SOA-based MPPT is better when it is used as MPPT than the PSO algorithm.

Finally, the design and implementation of a new MPPT method were carried out. Moreover, a Processor in the Loop (PIL) test was performed, using the Arduino MKRZERO board, to confirm the functionality of the proposed SOA-MPPT approach.

Conclusion and future work

The objective of this thesis was to improve the output of the PV system in order to mitigate power losses caused by partial shading. The main contributions of this thesis can be summarized as follows: (i) the first solution is to improve the scan-based GMPPT controller for PV systems operating under dynamic partial shading conditions. (ii) The second solution consists of developing a new MPPT design based on the seagull optimization algorithm for PV systems operating under partial shading and low uniform conditions.

In the first chapter, we discussed the operation of PV technology. We started with an overview on PV systems, including the principle of PV effect, PV cell and PV generator, and the mathematical model of PV generator. Then, the equations governing the PV generator were established by choosing the single diode equivalent electrical model which has good accuracy and low complexity. In this chapter, the bypass diode that protects the PV module in case of shading is also introduced.

The second chapter presented a detailed critical review of several maximum power point tracking (MPPT) techniques reported in the literature. They are classified into four groups, namely the traditional or conventional techniques, MPPT that exploits the characteristics of PV model, soft computing techniques and hybrid techniques. The advantages, limitations and disadvantages of each method have been highlighted.

In the third chapter, we proposed a simple GMPPT controller based on an improved scan method. To do this, we first presented a scan-interval point analysis on the P-V curve using a conventional scan method. Then, with the PV characteristics-based analysis, we were able to estimate the scan interval by limiting the search interval of the duty cycle. The efficiency of the improved scan method is verified using a PV simulator designed in the Proteus environment. According to the benchmarking results, the proposed method efficiently tracks the GMPPT under different PSCs and has a good response time (1.4 s), which improves the response time of the PV system by 0.55 s compared to the conventional scanning method. The simple structure used in this proposed method will significantly reduce the implementation complexity, which will result in a reduction in the cost of the PV system. Finally, this method can be used in the industrial PV system instead of the conventional P&O method to increase the power generation under PSCs.

It is worth mentioning that a Proteus PV panel model is developed in this work to verify the performance of the improved scanning method. This PV model as well as the electronic boards available in Proteus can be used as a low cost PV simulator to test the implementation of MPPT algorithms. This simulator makes future modifications to the system much easier to achieve.

In the fourth chapter, we designed a new MPPT algorithm based on the seagull optimization algorithm (SOA) to track the maximum power point of a PV system under various scenarios of partial shading and weak uniform conditions. The efficiency of the SOA-based MPPT method was verified for an 80 W PV system using the MATLAB/SIMULINK environment. It is noted that the average tracking efficiency of the proposed method is higher than 98.32%. The simulation results were performed under various scenarios of partial shading and weak uniform conditions. They prove the superiority of the proposed method in terms of tracking efficiency and fast response time compared to the other methods (P&O and PSO).

On the other hand, a PIL test is developed to validate the functionality and robustness of the proposed SOA-MPPT method, which was performed using the MKRZERO embedded board. The results show that the proposed method is superior in terms of tracking efficiency and fast response time compared to other methods (P&O and PSO). Therefore, the PIL test can be considered a low-cost solution to test the hardware implementation of the proposed SOA-MPPT method.

Within this thesis, two main solutions are proposed: the first one is for low cost applications with good performance using the improved scanning method, and the second one is for higher performance and critical applications using a new MPPT method based on the Seagull optimization algorithm.

Some contributions of MPPT control operating under partial shading have been addressed in this research. Nevertheless, there are still many interesting aspects and problems to be studied in the future. The following points have been identified for future work based on the results of this thesis:

- ✓ **Design an improved SOA MPPT method for tracking the GMPP under complex shading conditions**

Chapter 4 describes the design of a novel MPPT based on the seagull optimization algorithm for photovoltaic systems operating under partial shading. But the hardware implementation of this method is not made. Therefore, it would be interesting to implement this method in a microcontroller with experimentation to verify and validate our results. In addition, it would be interesting to design an improved SOA MPPT method for tracking the GMPP under complex shading conditions.

- ✓ **Design of the PV emulator to be suitable for testing shading conditions**

The high cost of commercial PV emulators requires finding new solutions to build a low-cost system with PV panel-like behavior. For this reason, we have proposed a low-cost PV emulator with which we replace a PV panel to test the real implementation of MPPT algorithms for PV applications. But, this emulator is used to test the performance of the MPPT algorithm under rapid variation of solar irradiance and temperature. In fact, improving the design of this PV emulator to be suitable for shading conditions is a challenge for users (researchers, engineers, students, etc.) to test and verify their MPPT algorithms under partial shading conditions.

- ✓ **Fault detection and isolation in PV systems.**

Photovoltaic (PV) arrays are constantly exposed to numerous potential faults, resulting in significant energy production losses. Accurate fault detection procedures are essential to ensure reliable operating conditions. These faults include: short circuit (SC) and open circuit (OC) faults, inverter disconnection (ID) and partial shading (PS). In addition, many other faults can occur in a PV system that cannot be easily detected. Research trends in PV system fault detection and diagnosis will focus on more complex methods such as machine learning methods and data mining.

REFERENCES

[1] PATEL, Hiren and AGARWAL, Vivek. MATLAB-based modeling to study the effects of partial shading on PV array characteristics. IEEE transactions on energy conversion, 2008, vol. 23, no 1, p. 302-310.

[2] ISHAQUE, Kashif and SALAM, Zainal. A review of maximum power point tracking techniques of PV system for uniform insolation and partial shading condition. Renewable and Sustainable Energy Reviews, 2013, vol. 19, p. 475-488.

[3] MOTAHHIR, Saad, EL HAMMOUMI, Aboubakr, and EL GHZIZAL, Abdelaziz. The most used MPPT algorithms: Review and the suitable low-cost embedded board for each algorithm. Journal of cleaner production, 2020, vol. 246, p. 118983.

[4] MÄKI, Anssi and VALKEALAHTI, Seppo. Power losses in long string and parallel-connected short strings of series-connected silicon-based photovoltaic modules due to partial shading conditions. IEEE Transactions on Energy Conversion, 2011, vol. 27, no 1, p. 173-183.

[5] SILVESTRE, Santiago, BORONAT, Alfredo, and CHOUDER, A. Study of bypass diodes configuration on PV modules. Applied energy, 2009, vol. 86, no 9, p. 1632-1640.

[6] BOZTEPE, Mutlu, GUINJOAN, Francesc, VELASCO-QUESADA, Guillermo, and al. Global MPPT scheme for photovoltaic string inverters based on restricted voltage window search algorithm. IEEE transactions on Industrial Electronics, 2013, vol. 61, no 7, p. 3302-3312.

[7] SUGANTHI, Leonel, INIYAN, S., and SAMUEL, Anand A. Applications of fuzzy logic in renewable energy systems–a review. Renewable and sustainable energy reviews, 2015, vol. 48, p. 585-607.

[8] SARVI, Mohammad, AHMADI, Saeedeh, and ABDI, Shirzad. A PSO-based maximum power point tracking for photovoltaic systems under environmental and partially shaded conditions. Progress in Photovoltaics: Research and Applications, 2015, vol. 23, no 2, p. 201-214.

[9] ISHAQUE, Kashif, SALAM, Zainal, AMJAD, Muhammad, et al. An improved particle swarm optimization (PSO)–based MPPT for PV with reduced steady-state oscillation. IEEE transactions on Power Electronics, 2012, vol. 27, no 8, p. 3627-3638.

[10] XU, Libin, CHENG, Ruofa, XIA, Zhen, and al. Improved particle swarm optimization (PSO)-based MPPT method for PV string under partially shading and uniform irradiance condition. In: 2020 Asia Energy and Electrical Engineering Symposium (AEEES). IEEE, 2020. p. 771-775.

[11] Jiang, Lian Lian, and Douglas L. Maskell. "A uniform implementation scheme for evolutionary optimization algorithms and the experimental implementation of an ACO based MPPT for PV systems under partial shading." 2014 IEEE symposium on computational intelligence applications in smart grid (CIASG). IEEE, 2014.

[12] Dhiman, Gaurav, and Vijay Kumar. "Seagull optimization algorithm: Theory and its applications for large-scale industrial engineering problems." Knowledge-Based Systems 165 (2019): 169-196.

[13] Sampaio, Priscila Gonçalves Vasconcelos, and Mario Orestes Aguirre González. "Photovoltaic solar energy: Conceptual framework." Renewable and Sustainable Energy Reviews 74 (2017): 590-601.

[14] Sampaio, Priscila Gonçalves Vasconcelos, and Mario Orestes Aguirre González. "Photovoltaic solar energy: Conceptual framework." Renewable and Sustainable Energy Reviews 74 (2017): 590-601.

[15] Mathieu, Henry, and Hervé Fanet. Physique des semiconducteurs et des composants électroniques-6ème édition: Cours et exercices corrigés. Dunod, 2009.

[16] Lorenzo, Eduardo. Solar electricity: engineering of photovoltaic systems. Earthscan/James & James, 1994.

[17] Markvart, Tomas, ed. Solar electricity. Vol. 6. John Wiley & Sons, 2000.

[18] NDIAYE, Ababacar, CHARKI, Abdérafi, KOBI, Abdessamad, et al. Degradations of silicon photovoltaic modules: A literature review. Solar Energy, 2013, vol. 96, p. 140-151.

[19] Restrepo, F., and C. E. Backus. "On black solar cells or the tetrahedral texturing of a silicon surface." IEEE Transactions on electron devices 23.10 (1976): 1195-1197.

[20] Nelson, Jenny. "Imperial College Press." The physics of solar cells (2003).

[21] Green, Martin A. "Photovoltaics: technology overview." Energy policy 28.14 (2000): 989-998.

[22] Green, Martin A. "Third generation photovoltaics." (2006).

[23] ISHAQUE, Kashif, SALAM, Zainal, TAHERI, Hamed, et al. Modeling and simulation of photovoltaic (PV) system during partial shading based on a two-diode model. Simulation Modelling Practice and Theory, 2011, vol. 19, no 7, p. 1613-1626.

[24] MARKVART, Tomas. Light harvesting for quantum solar energy conversion. Progress in quantum electronics, 2000, vol. 24, no 3-4, p. 107-186.

[25] Chenni, R., et al. "A detailed modeling method for photovoltaic cells." Energy 32.9 (2007): 1724-1730.

[26] Ishaque, Kashif, Zainal Salam, and Hamed Taheri. "Accurate MATLAB simulink PV system simulator based on a two-diode model." Journal of power electronics 11.2 (2011): 179-187.

[27] Rahman, Shah Arifur, Rajiv K. Varma, and Tim Vanderheide. "Generalised model of a photovoltaic panel." IET Renewable Power Generation 8.3 (2014): 217-229.

[28] TDC-M20-36 Solar Panel. 2018. Available online: https://tdcsolar.en.alibaba.com/product/60018196685-220763581/20w_mono_small_solar_panel_from_chinese_factory.html?spm=a2700.8304367.rect38f22d.16.47185198OcA XoD (accessed on 10 January 2018).

[29] R.Ramaprabha (Member IEEE) , Dr.B.L.Mathur, "Impact of Partial Shading on Solar PV Module Containing Series Connected Cells", International Journal of Recent Trends in Engineering, Vol 2, No. 7, November 2009.

[30] KIM, Katherine A. et KREIN, Philip T. Photovoltaic hot spot analysis for cells with various reverse-bias characteristics through electrical and thermal simulation. In : 2013 IEEE 14th Workshop on Control and Modeling for Power Electronics (COMPEL). IEEE, 2013. p. 1-8.

[31] Huiying Zheng , Shuhui Li , Rajab Challoo , Julio Proano, "Shading and bypass diode impacts to energy extraction of PV arrays under different converter configurations" , Volume 68, August 2014, Pages 58 – 66, Renewable Energy

[32] VEMURU, Srinivasa, SINGH, Priyanka, et NIAMAT, Mohammed. Modeling impact of bypass diodes on photovoltaic cell performance under partial shading. In : 2012 IEEE international conference on electro/information technology. IEEE, 2012. p. 1-5.

[33] CHUVYCHIN, Vladimir N., GUROV, N. S., VENKATA, S. S., and al. An adaptive approach to load shedding and spinning reserve control during under frequency conditions. IEEE Transactions on Power Systems, 1996, vol. 11, no 4, p. 1805-1810.

[34] ANDERSON, Philip M. and MIRHEYDAR, Mahmood. An adaptive method for setting under frequency load shedding relays. IEEE Transactions on Power Systems, 1992, vol. 7, no 2, p. 647-655.

[35] BAHARUDIN, Nor Hanisah, MANSUR, T. M. N. T., HAMID, Fairuz Abdul, and al. Topologies of DC-DC converter in solar PV applications. Indonesian Journal of Electrical Engineering and Computer Science, 2017, vol. 8, no 2, p. 368-374.

[36] RAGHAVENDRA, Kummara Venkat Guru, ZEB, Kamran, MUTHUSAMY, Anand, and al. A comprehensive review of DC–DC converter topologies and modulation strategies with recent advances in solar photovoltaic systems. Electronics, 2019, vol. 9, no 1, p. 31.

[37] FARAHAT, M. A., METWALLY, H. M. B., and MOHAMED, Ahmed Abd-Elfatah. Optimal choice and design of different topologies of DC–DC converter used in PV systems, at different climatic conditions in Egypt. Renewable Energy, 2012, vol. 43, p. 393-402.

[38] Mamur, Hayati, and Rasit Ahiska. "Application of a DC–DC boost converter with maximum power point tracking for low power thermoelectric generators." Energy conversion and management 97 (2015): 265-272.

[39] Ahmed, J. and Salam, Z., 2016. A modified P&O maximum power point tracking method with reduced steady-state oscillation and improved tracking efficiency. IEEE Transactions on Sustainable Energy, 7(4), pp.1506-1515.

[40] Salam, Zainal, Jubaer Ahmed, and Benny S. Merugu. "The application of soft computing methods for MPPT of PV system: A technological and status review." Applied energy 107 (2013): 135-148.

[41] Liu, X. and Lopes, L.A., 2004, June. An improved perturbation and observation maximum power point tracking algorithm for PV arrays. In 2004 IEEE 35th Annual Power Electronics Specialists Conference (IEEE Cat. No. 04CH37551) (Vol. 3, pp. 2005-2010). IEEE.

[42] Hohm, D.P. and Ropp, M.E., 2003. Comparative study of maximum power point tracking algorithms. Progress in photovoltaics: Research and Applications, 11(1), pp.47-62.

[43] Liu, Fangrui, et al. "A variable step size INC MPPT method for PV systems." IEEE Transactions on industrial electronics 55.7 (2008): 2622-2628.

[44] MOTAHHIR, Saad, EL GHZIZAL, Abdelaziz, SEBTI, Souad, et al. Modeling of photovoltaic system with modified incremental conductance algorithm for fast changes of irradiance. International Journal of Photoenergy, 2018, vol. 2018.

[45] MOTAHHIR, Saad. Contribution to the optimization of energy withdrawn from a PV panel using an Embedded System. 2018. Thèse de doctorat. Université Sidi Mohamed Ben Abdellah Fès (Maroc).

[46] Ishaque, K., Salam, Z. and Lauss, G., 2014. The performance of perturb and observe and incremental conductance maximum power point tracking method under dynamic weather conditions. Applied Energy, 119, pp.228-236.

[47] Patel, Hiren, and Vivek Agarwal. "Maximum power point tracking scheme for PV systems operating under partially shaded conditions." IEEE transactions on industrial electronics 55.4 (2008): 1689-1698.

[48] Yuvarajan, Subbaraya, and Shanguang Xu. "Photo-voltaic power converter with a simple maximum-power-point-tracker." Proceedings of the 2003 International Symposium on Circuits and Systems, 2003. ISCAS'03. Vol. 3. IEEE, 2003.

[49] Noguchi, Toshihiko, Shigenori Togashi, and Ryo Nakamoto. "Short-current-pulse based adaptive maximum-power-point tracking for photovoltaic power generation system." IEEJ Transactions on Industry Applications 121.1 (2001): 78-83.

[50] Hohm, D. P., and M. E_ Ropp. "Comparative study of maximum power point tracking algorithms." Progress in photovoltaics: Research and Applications 11.1 (2003): 47-62.

[51] Leedy, A.W. and Garcia, K.E., 2013, March. Approximation of PV characteristic curves for use in maximum power point tracking algorithms. In 45th southeastern symposium on system theory (pp. 88-93). IEEE.

[52] Ramos-Hernanz, J.A., Campayo, J.J., Zulueta, E., Barambones, O., Eguía, P. and Zamora, I., 2013. Obtaining the characteristics curves of a photocell by different methods. In International Conference on Renewable Energies and Power Quality (Vol. 11, pp. 1-6).

[53] González-Castaño, C., Lorente-Leyva, L.L., Muñoz, J., Restrepo, C. and Peluffo-Ordóñez, D.H., 2021. An MPPT strategy based on a surface-based polynomial fitting for solar photovoltaic systems using real-time hardware. Electronics, 10(2), p.206.

[54] KOTTAS, Theodoros L., BOUTALIS, Yiannis S., et KARLIS, Athanassios D. New maximum power point tracker for PV arrays using fuzzy controller in close cooperation with fuzzy cognitive networks. IEEE Transactions on Energy conversion, 2006, vol. 21, no 3, p. 793-803.

[55] Peng, Ya-Fu, Rong-Jong Wai, and Chih-Min Lin. "Implementation of LLCC-resonant driving circuit and adaptive CMAC neural network control for linear piezoelectric ceramic motor." IEEE Transactions on Industrial Electronics 51.1 (2004): 35-48.

[56] ISHAQUE, Kashif, ABDULLAH, Shahrum Shah, AYOB, Shahrin Md, et al. Single input fuzzy logic controller for unmanned underwater vehicle. Journal of Intelligent and Robotic Systems, 2010, vol. 59, no 1, p. 87-100.

[57] ISHAQUE, Kashif, ABDULLAH, Shahrum Shah, AYOB, S. M., et al. A simplified approach to design fuzzy logic controller for an underwater vehicle. Ocean Engineering, 2011, vol. 38, no 1, p. 271-284.

[58] Hiyama, T., Kouzuma, S. and Imakubo, T., 1995. Identification of optimal operating point of PV modules using neural network for real time maximum power tracking control. IEEE Transactions on Energy Conversion, 10(2), pp.360-367.

[59] Dzung, P.Q., Lee, H.H. and Vu, N.T.D., 2010, October. The new MPPT algorithm using ANN-based PV. In International Forum on Strategic Technology 2010 (pp. 402-407). IEEE.

[60] Ishaque, K. and Salam, Z., 2011. An improved modeling method to determine the model parameters of photovoltaic (PV) modules using differential evolution (DE). Solar energy, 85(9), pp.2349-2359.

[61] Ishaque, K., Salam, Z., Taheri, H. and Shamsudin, A., 2011. A critical evaluation of EA computational methods for Photovoltaic cell parameter extraction based on two diode model. Solar Energy, 85(9), pp.1768-1779.

[62] Yang, B., Wang, J., Zhang, X., Yu, T., Yao, W., Shu, H., Zeng, F. and Sun, L., 2020. Comprehensive overview of meta-heuristic algorithm applications on PV cell parameter identification. Energy Conversion and Management, 208, p.112595.

[63] Yang, B., Zhu, T., Wang, J., Shu, H., Yu, T., Zhang, X., Yao, W. and Sun, L., 2020. Comprehensive overview of maximum power point tracking algorithms of PV systems under partial shading condition. Journal of Cleaner Production, 268, p.121983.

[64] Pal, R.S. and Mukherjee, V., 2020. Metaheuristic based comparative MPPT methods for photovoltaic technology under partial shading condition. Energy, 212, p.118592.

[65] Fu, Q. and Tong, N., 2010, July. A complex-method-based PSO algorithm for the maximum power point tracking in photovoltaic system. In 2010 Second International Conference on Information Technology and Computer Science (pp. 134-137). IEEE.

[66] Ishaque, K., Salam, Z., Shamsudin, A. and Amjad, M., 2012. A direct control based maximum power point tracking method for photovoltaic system under partial shading conditions using particle swarm optimization algorithm. Applied Energy, 99, pp.414-422.

[67] Basha, C.H. and Rani, C., 2020. Different conventional and soft computing MPPT techniques for solar PV systems with high step-up boost converters: a comprehensive analysis. Energies, 13(2), p.371.

[68] Ishaque, K., Salam, Z., Amjad, M. and Mekhilef, S., 2012. An improved particle swarm optimization (PSO)–based MPPT for PV with reduced steady-state oscillation. IEEE transactions on Power Electronics, 27(8), pp.3627-3638.

[69] Chen, W.N., Zhang, J., Lin, Y., Chen, N., Zhan, Z.H., Chung, H.S.H., Li, Y. and Shi, Y.H., 2012. Particle swarm optimization with an aging leader and challengers. IEEE transactions on evolutionary computation, 17(2), pp.241-258.

[70] Ishaque, K. and Salam, Z., 2012. A deterministic particle swarm optimization maximum power point tracker for photovoltaic system under partial shading condition. IEEE transactions on industrial electronics, 60(8), pp.3195-3206.

[71] Sen, T., Pragallapati, N., Agarwal, V. and Kumar, R., 2018. Global maximum power point tracking of PV arrays under partial shading conditions using a modified particle velocity-based PSO technique. IET Renewable Power Generation, 12(5), pp.555-564.

[72] Karaboga, D., 2010. Artificial bee colony algorithm. scholarpedia, 5(3), p.6915.

[73] Karaboga, D. and Akay, B., 2009. A comparative study of artificial bee colony algorithm. Applied mathematics and computation, 214(1), pp.108-132.

[74] soufyane Benyoucef, A., Chouder, A., Kara, K. and Silvestre, S., 2015. Artificial bee colony based algorithm for maximum power point tracking (MPPT) for PV systems operating under partial shaded conditions. Applied Soft Computing, 32, pp.38-48.

[75] Mirjalili, S. and Lewis, A., 2016. The whale optimization algorithm. Advances in engineering software, 95, pp.51-67.

[76] Nasiri, J. and Khiyabani, F.M., 2018. A whale optimization algorithm (WOA) approach for clustering. Cogent Mathematics & Statistics, 5(1), p.1483565.

[77] Rana, N., Latiff, M.S.A., Abdulhamid, S.I.M. and Chiroma, H., 2020. Whale optimization algorithm: a systematic review of contemporary applications, modifications and developments. Neural Computing and Applications, 32(20), pp.16245-16277.

[78] Jegajothi, B. and Sudhakar, S., 2019. Maximum Power Generation in Grid-Connected Photovoltaic System using WOA based Embedded Controller. Journal of Electrical Engineering, 19(5), pp.19-19.

[79] Mirjalili, Seyedali, Seyed Mohammad Mirjalili, and Andrew Lewis. "Grey wolf optimizer." Advances in engineering software 69 (2014): 46-61.

[80] Mirjalili, S., Saremi, S., Mirjalili, S.M. and Coelho, L.D.S., 2016. Multi-objective grey wolf optimizer: a novel algorithm for multi-criterion optimization. Expert Systems with Applications, 47, pp.106-119.

[81] Mohanty, S., Subudhi, B. and Ray, P.K., 2015. A new MPPT design using grey wolf optimization technique for photovoltaic system under partial shading conditions. IEEE Transactions on Sustainable Energy, 7(1), pp.181-188.

[82] Kashef, S. and Nezamabadi-pour, H., 2015. An advanced ACO algorithm for feature subset selection. Neurocomputing, 147, pp.271-279.

[83] Ahmed, J. and Salam, Z., 2014. A Maximum Power Point Tracking (MPPT) for PV system using Cuckoo Search with partial shading capability. Applied energy, 119, pp.118-130.

[84] Sayah, S. and Hamouda, A., 2013. A hybrid differential evolution algorithm based on particle swarm optimization for nonconvex economic dispatch problems. Applied soft computing, 13(4), pp.1608-1619.

[85] Pilakkat, D. and Kanthalakshmi, S., 2020. Single phase PV system operating under Partially Shaded Conditions with ABC-PO as MPPT algorithm for grid connected applications. Energy Reports, 6, pp.1910-1921.

[86] Pilakkat, D. and Kanthalakshmi, S., 2019. An improved P&O algorithm integrated with artificial bee colony for photovoltaic systems under partial shading conditions. Solar Energy, 178, pp.37-47.

[87] Eltamaly, A.M. and Farh, H.M., 2019. Dynamic global maximum power point tracking of the PV systems under variant partial shading using hybrid GWO-FLC. Solar Energy, 177, pp.306-316.

[88] Pedemonte, M., Nesmachnow, S. and Cancela, H., 2011. A survey on parallel ant colony optimization. Applied Soft Computing, 11(8), pp.5181-5197.

[89] Gupta, S., Bhardwaj, S. and Bhatia, P.K., 2011. A reminiscent study of nature inspired computation. International Journal of Advances in Engineering & Technology, 1(2), p.117.

[90] Salam, Z., Ahmed, J. and Merugu, B.S., 2013. The application of soft computing methods for MPPT of PV system: A technological and status review. Applied energy, 107, pp.135-148.

[91] Veerachary, M. and Yadaiah, N., 2000. ANN based peak power tracking for PV supplied DC motors. Solar energy, 69(4), pp.343-350.

[92] Xu, J., Shen, A., Yang, C., Rao, W. and Yang, X., 2011, September. ANN based on IncCond algorithm for MPP tracker. In 2011 sixth international conference on bio-inspired computing: theories and applications (pp. 129-134). IEEE.

[93] Taheri, H., Salam, Z. and Ishaque, K., 2010, October. A novel maximum power point tracking control of photovoltaic system under partial and rapidly fluctuating shadow conditions using differential evolution. In 2010 IEEE symposium on industrial electronics and applications (ISIEA) (pp. 82-87). IEEE.

[94] Qin, A.K., Huang, V.L. and Suganthan, P.N., 2008. Differential evolution algorithm with strategy adaptation for global numerical optimization. IEEE transactions on Evolutionary Computation, 13(2), pp.398-417.

[95] Fan, Q., Wang, W. and Yan, X., 2019. Differential evolution algorithm with strategy adaptation and knowledge-based control parameters. Artificial Intelligence Review, 51(2), pp.219-253.

[96] Rehman, A.U., Islam, A. and Belhaouari, S.B., 2020. Multi-cluster jumping particle swarm optimization for fast convergence. IEEE Access, 8, pp.189382-189394.

[97] Chalh, A., El Hammoumi, A., Motahhir, S., El Ghzizal, A., Derouich, A., Masud, M. and AlZain, M.A., 2021. Investigation of Partial Shading Scenarios on a Photovoltaic Array's Characteristics. Electronics, 11(1), p.96.

[98] Maghami, M.R., Hizam, H., Gomes, C., Radzi, M.A., Rezadad, M.I. and Hajighorbani, S., 2016. Power loss due to soiling on solar panel: A review. Renewable and Sustainable Energy Reviews, 59, pp.1307-1316.

[99] Nalluri, M.S.R., Kannan, K., Gao, X.Z. and Roy, D.S., 2019. An efficient hybrid meta-heuristic approach for cell formation problem. Soft Computing, 23(19), pp.9189-9213.

[100] PARASKEVADAKI, Evagelia V. et PAPATHANASSIOU, Stavros A. Evaluation of MPP voltage and power of mc-Si PV modules in partial shading conditions. IEEE Transactions on Energy Conversion, 2011, vol. 26, no 3, p. 923-932.

[101] Motahhir, S., Chalh, A., Ghzizal, A., Sebti, S. and Derouich, A., 2017. Modeling of photovoltaic panel by using proteus. Journal of Engineering Science and Technology Review, 10, pp.8-13.

[102] Motahhir, S., Chalh, A., El Ghzizal, A. and Derouich, A., 2018. Development of a low-cost PV system using an improved INC algorithm and a PV panel Proteus model. Journal of Cleaner production, 204, pp.355-365.

[103] Chalh, A., El Hammoumi, A., Motahhir, S., El Ghzizal, A., Subramaniam, U. and Derouich, A., 2020. Trusted simulation using Proteus model for a PV system: test case of an improved HC MPPT algorithm. Energies, 13(8), p.1943.

[104] INA1x9 Datasheet [WWW Document]. 2017. Available online: www.ti.com (accessed on 8 January 2018).

[105] Voltage Sensor Module-Arduino Compatible [WWW Document], n.d. Available online: https://www.emartee.com/product/42082/VoltageSensor (accessed on 8 January 2018).

[106] Chalh, A., Motahhir, S., Ghzizal, A.E., Hammoumi, A.E. and Derouich, A., 2020. Global MPPT of photovoltaic system based on scanning method under partial shading condition. SN Applied Sciences, 2(4), pp.1-5.